hyBIRD: Design of a Four and Six Seater Hybrid-Electric Aircraft Family

Thesis · June 2018

DOI: 10.13140/RG.2.2.10008.88326

4 authors, including:

Amr Mousa
AVL LIST GMBH
7 PUBLICATIONS **6** CITATIONS

SEE PROFILE

AIAA
American Institute of
Aeronautics and Astronautics

hyBIRD

مدينة زويل
ZEWAIL CITY
ESTABLISHED 2000
INAUGURATED 2011

hyBIRD : Design of a Four and Six Seater Hybrid-Electric Aircraft Family

IN RESPONSE TO:
- Aerospace Engineering Senior Project - Zewail City
- AIAA Aircraft Design Competition 2018

Amr Mousa

Wessam Mohamed

Ahmed Hashem

Ahmed Samir

Team Member	*AIAA Number*	*University / Major*	*Contact*	*Signature*
Ahmed Hashem	608477	Aerospace Engineering, University of Science and Technology at Zewail City	a.a.a.hashem94@gmail.com +201122340050	
Ahmed Samir	922169		ahmedsamirewida@gmail.com +201095492822	
Amr Mousa	922560		amrmousa.m@gmail.com +201002810908	
Wessam Mohamed	922171		wessamelhakeem@yahoo.com +201004989996	
Team Advisors	*University/Major*		*Contact*	*Signature*
Dr. Mostafa Abdallah	Aerospace Major Coordinator, University of Science and Technology at Zewail City		moabdall@gmail.com	
Dr. Ahmed Altaweel	Associate Professor, University of Science and Technology at Zewail City		ahmed.t.eltaweel@gmail.com	

Acknowledgements:

We would like to extend our gratitude to our families, our mentors, advisors and industry consultants without whom we wouldn't be able to reach this point. We would like thank all of them for the time, effort and expertise they put in this project. It's has been a wonderful journey filled with many challenges, great experiences, learning lessons and unforgettable memories.

Zewail City of Science and Technolog

Dr. Mostafa Abdalla – Faculty Advisor

Dr. Ahmed Eltaweel

Dr. Nader Abu Elftouh

Nashaat Gad – Teaching Assistant

University of Kansas

Dr. Ron Barret

Marwan Dessouki, PhD student

DAR Coporation

Dr. Pierson B. Sargent

ICON Corporation

John Kim

Zewail City Description:

Zewail City of Science and Technology is a nonprofit, independent institution of learning, research and innovation. The concept of the City was proposed in 1999 and its cornerstone laid on January 1, 2000. After numerous delays, the project was revived by the Egyptian cabinet's decree on May 11, 2011 following the January 25 Revolution. The Cabinet proclaimed it a National Project for Scientific Renaissance and named it Zewail City of Science and Technology. On December 20, 2012, a special law for Zewail City was granted, allowing students to enroll at its university and Egypt to begin a new era of modern development in scientific research and technological production.

مدينة زويل
ZEWAIL CITY
ESTABLISHED 2000
INAUGURATED 2011

Zewail City of Science and Technology – with its five constituents: The University of Science and Technology, the Research Institutes, the Technology Pyramid, the Academy, and the Center for Strategic Studies – is designed to bring about effective participation in 21st century science, to elevate local technologies to an international level and to increase national productivity. We aim to contribute to building a knowledge-based society, founded on creative thinking through providing a merit-based education and engaging with the public at large, and integrating the challenge of a rigorous academic study, with the spirit of collaborative work and scientific discoveries.

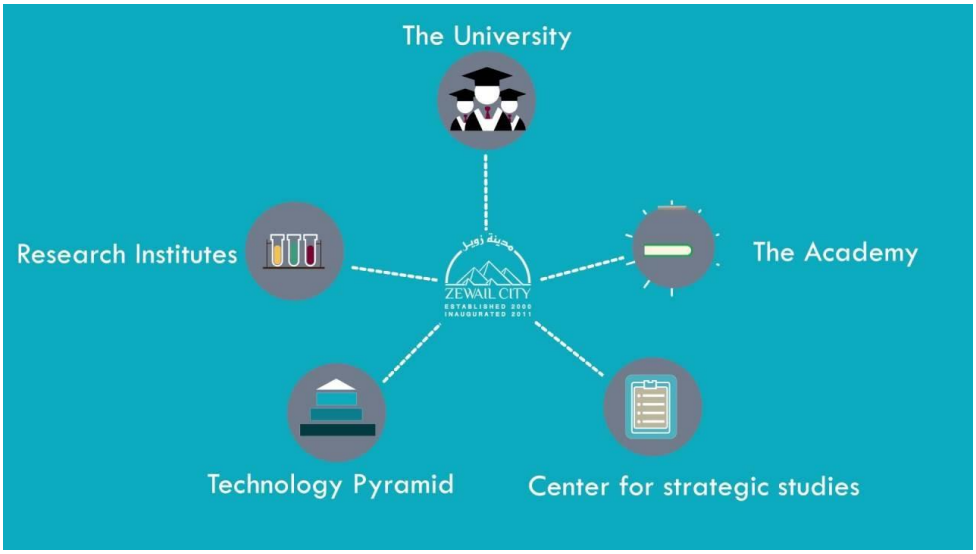

About the Founder, Ahmed Zewail (1946 –2016)

Dr. Ahmed Zewail is the Linus Pauling Chair Professor of Chemistry and Professor of Physics at the California Institute of Technology (Caltech), and the Director of the Moore Foundation's Center for Physical Biology at Caltech. He received his early education in Egypt and he completed his Ph.D. from the University of Pennsylvania and a postdoctoral (IBM) fellowship at the University of California, Berkeley, USA, before joining the faculty at Caltech. On April 27, 2009, President Barack Obama appointed him to the President's Council of Advisors of the White House, and in November of the same year, he was named the first United States Science Envoy to the Middle East.

Dr. Zewail was the sole recipient of the 1999 Nobel Prize for his pioneering developments in femtoscience, making possible observations of atomic motions during molecular transformations in femtosecond, a millionth of a billionth of a second. More recently, he and his group have developed the field of 4D Electron Microscopy for the direct visualization of matter's behavior, from atoms to biological cells, in the four dimensions of space and time. A significant effort is also devoted to giving public lectures on science and on the promotion of education and partnership for world peace, and he continues to serve on national and international boards for academic, cultural, and world affairs.

Table of Contents

1. Executive Summary

The aerospace industry is moving fast towards saving money, keeping the environment green, reducing noise and minimizing emissions. In response to AIAA aircraft design competition (undergraduate-team category) "Hybrid-Electric General Aviation (HEGAA) 2018", hyBIRD aircraft family is presented in this design report. hyBIRD is a team of four undergraduate students from the University of Science and Technology at Zewail City, Egypt. The team worked on designing a family of aircraft for an entry in service (EIS) in 2028 for the 4-seater aircraft and 2030 for the 6-seater based on the future technology. This required forecasting the technology trends for the powertrain components and studying the similar airplanes market, in the same category, which helped identifying our competitive edge and selling point.

Advanced design approaches were performed throughout the whole design process such as Integrated Reconfigurable Matrix of Alternatives (IRMA) for aircraft configuration selection, powertrain sizing optimization, Computational Fluid Dynamics (CFD) and composites FEA analysis.

hyBIRD aircraft is an all-composite airframe with serial hybrid propulsion system utilizing a turbo-normalized piston engine, a frontal electric motor and two smaller motors on the wing-tips. A tadpole-shaped fuselage with low-wing and V-tail was selected. Both airplanes are identical except for the flight controller, motors and batteries which results in an 83% part-commonality by weight and this can help achieve minimal development, certification, and manufacturing costs. Based on the aircraft weight, complexity, and performance, the Eastlake cost model estimates the aircraft to be highly competitively to various aircraft of similar performance in terms of initial and operational costs.

2. Design Objectives

Developments in electric motors, controllers, power generation and batteries have recently led to the development of both hybrid gas-electric and fully electric vehicles. The AIAA Request for Proposal (RFP) for the design of a two-member Hybrid-Electric General Aviation Aircraft (HEGAA) family listed the following main design driving objectives [22]:

- Create a product that can cover the largest number of missions and markets with a minimum of non-recurring development costs and changes to the design.
- The entry into service (EIS) is 2028 for a 4-seater model with 1000 nm of range and 2030 for the 6-seat model with 750 nm of range.
- To have energy storage for takeoff, climb, go-around and emergencies via batteries and electric motors with an engine providing additional power and/or direct propulsion.
- Minimize production cost by choosing materials and manufacturing methods appropriate for the annual production rate that is supported by the assessment of the potential market size.
- Make the aircraft visually appealing so it will be marketable and identify what features are important to the operators for different missions.
- Make the aircraft reliability equal or better than that of comparable aircraft.
- Make the aircraft maintenance equal or better than that of comparable aircraft.

3. Requirements Compliance

We took the NexGen 2015 flight pattern along with the RFP requirements into our consideration at the very early stage of the design process. All the following technical requirements have been met as shown in table (1 & 2):

Table 1 hyBIRD Performance Requirements

Parameter	Requirements / Target		Compliance	
No. of seats	Four	Six	Four	Six
Typical Empty Weight	Minimize		1185 kg	1173 kg
Maximum Takeoff Growth Weight (MTOW)	Minimize		2367 kg	
Takeoff field length	<1500 ft	<1800 ft	~ 1432 ft	~ 1432 ft
Climb Rate	1500 fpm	1300 fpm	1629 fpm	1573 fpm
	Both Electric and Fossil are operating		Met	
Target Cruise Speed	200 Knots		Met	
Minimum Cruise Speed	103 Knots		Met	

Table 2 hyBIRD Additional Requirements

Parameter	Requirements		Compliance	
No. of seats	Four	Six	Four	Six
Target Range Fully Loaded	1000 nm	750 nm	Met	Met
Acquisition Cost	Minimize		$390,000	$410,000
Operating Cost per flight hour	Minimize		$164.2	$165.4
Entry in Service (EIS)	2028	2030	Met	Met
Certification	FAA Part 23		Met	
Airframe and propulsion system commonality	at least 75% between the 4-seater and 6-seater by weight		83 %	

4. Market Research

General Aviation (GA) is a category of aviation that includes many different aircraft subcategories. It includes all kinds of aircraft except military and large commercial aircraft. It is a huge market that is evidently expanding fast. The total number of shipped GA aircraft doubled from 1,132 in 1994 to 2,262 unit in 2016 [1].. And the billings also jumped from $3,749 M in 1994 to $20,714 M in 2016. Figure (1) shows how the GA market is developing worldwide.

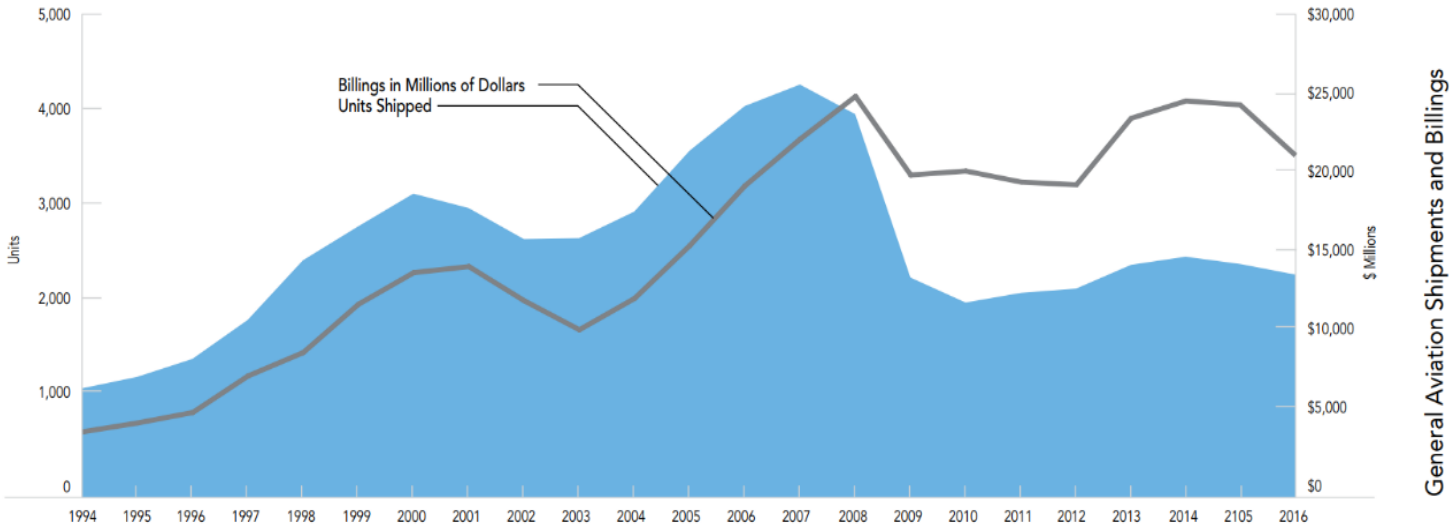

Figure 1: General Aviation Airplane Shipments and Billings Worldwide (1994-2016)

The total number of airports that have runways of length longer than 1,500 ft (paved and unpaved) was recorded in 2011 to be 13,746 in both Europe and the US only as per the CIA Factbook and GAMA Statistical Data book, 2016 [1]. This along with the fact that *hy*BIRD is capable of taking-off and landing on grass gives the family a great advantage over most of the other GA airplanes in the GA market since it gives the airplane access to most of the airports, which in turn helps solve the "first and last mile" transportation problem.

The hybrid-electric general aviation market is dramatically growing. Most of the aerospace industry's big players are now taking huge steps into aircraft electrification through introducing their hybrid-electric and fully electric aircraft. Airbus with E-Fan, Vahana and CityAirbus, Boeing and JetBlue through their shares in the electric airplane startup; Zunum Aero and tens of many other startups all over the world such as Wright Electric, Eviation, Pipistel, etc.

5. Technology Forecast

5.1 Internal Combustion Engine (ICE)

Although the GA aircraft is rapidly increasing, the new engine technology, on the other hand, has been very slow to come into the piston engine market since the certification and testing costs are very expensive. There are modernized engines on the market with electronic fuel injection, computerized engine management with turbo-control and single-level operation. Some manufacturers made progress in engine development such

as Rotax 915 and Lycoming O- 320-C1A with modern technology and improved performance which helped us to predict our engine performance in 2028. The future forecast shows that the power density will be 1.3 kW/kg in comparison with current power density of 1.26 kW/kg. Specific fuel consumption is also expected to be improved from a concurrent value of 0.27 Kg/kWh to 0.261 Kg/kWh in 2028 as shown in Figure (2).

Normally aspirated engines will be affected by the decrease in density of the air as the altitude increases which would cause the efficiency to decrease and increase the fuel consumption. However, piston engines with turbocharger will increase the pressure and temperature of the intake in all flight segments which will shift the engine power curve, and, consequently, cause the engine to reach the temperature limit in the sea level where the density and temperature are relatively high.

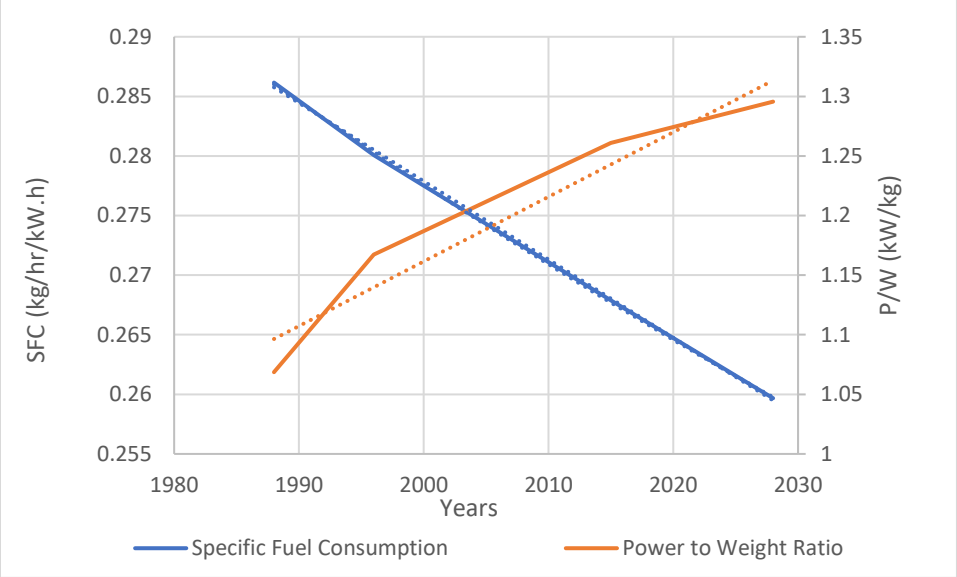

Figure 2: ICE Technology Forecast

We chose our engine to be a Turbo-normalized ICE which increases the pressure of the engine intake to maintain the sea level pressure at higher altitudes up to 20,000 ft and increases the overall efficiency of the engine. Its principle is to have a wastegate that is electrically controlled by a stepper motor with a sensor to sense the outside temperature and pressure then controls the intake of the turbocharger. The airflow that passes by the centrifugal compressor after increasing its pressure (density) will have a higher temperature, therefore it passes by an intercooler to decrease its temperature and then increases the thermal efficiency of the engine, in addition to normalizing the total efficiency at the maximum level at any altitude up to FL200.

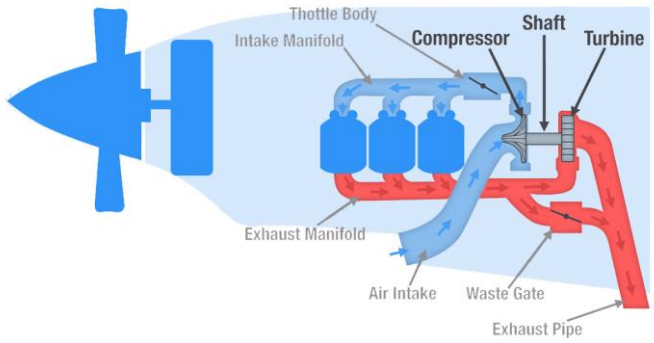

Figure 3 Part1) Turbonormalized Internal Combustion Engine

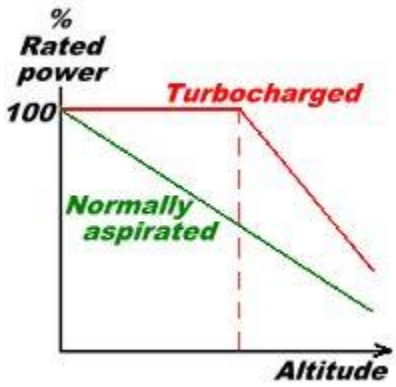

Figure 4 (Part2) Comparison between turbocharger and Turbonormalized

5.2 Electric Motor

A possible choice for the electric motor is Siemens SP260D - 260 kW that is already in the market and is being used in Extra 330LE, figure (5). It is a double winding motor with a 95% efficiency running at a low RPM of 2,500 with just 50Kg weight! The motor technology is projectable to our desired power values with current and future power densities of 5 and 10 kW/Kg respectively [23].

Figure 5 Extra 330 LE Electric Motor

5.3 Generator

Siemens Generator (100kW) used in Pipistrel Hypstair aircraft is a good example for a double winding, high-density generator with power density of 5.3 kW/Kg and is expected to reach 7.5 kW/Kg by 2028, Figures (6,7) [23].

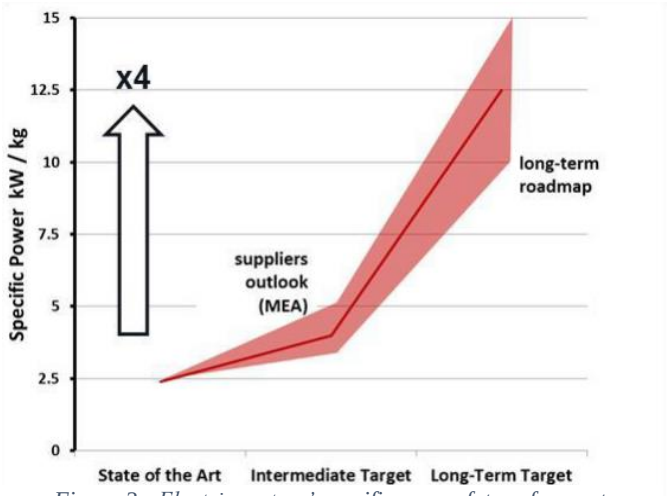

Figure 3: Electric motors' specific power future forecast

Figure 4: Pipistrel Hypstair Siemens Generator

5.4 Inverter

Pipistrel Hypstair used Siemens NexGen 100kVA with a power density of 10.5 kW/Kg and a 98% efficiency. This would be a great fit for *hy*BIRD, but no future forecast was available for this new developed technology [23].

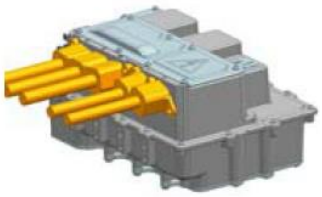

Figure 5: Pipistrel Hypstair Siemens NexGen Inverter

5.5 Batteries

If we go back to the introduction of the mass market lithium-ion cell in 1991 battery capacity has only improved about 5–6% per year (Lemkin, 2013; The Week Staff, 2013) [28]. Lithium-ion battery technology today offers only about 1/10th of the energy of gasoline or diesel fuel but projecting on 2028 given the data from the past three decades as shown in Figures 9 and 10, we will be able to get a battery energy density of 400 Whr/Kg as shown in Table (3). In addition to being green and more environmentally friendly, lithium ion battery (LIB) cost is declining with years where the fuel prices will still keep going up. On one hand, it's predicted that by 2028 the cost of the kWh of battery energy density will reach $84 as per Bloomberg New Energy Finance [24], Figure (11). On the other hand, the cost of the barrel of fuel is predicted to reach $70 in 2028 as per the World Bank.

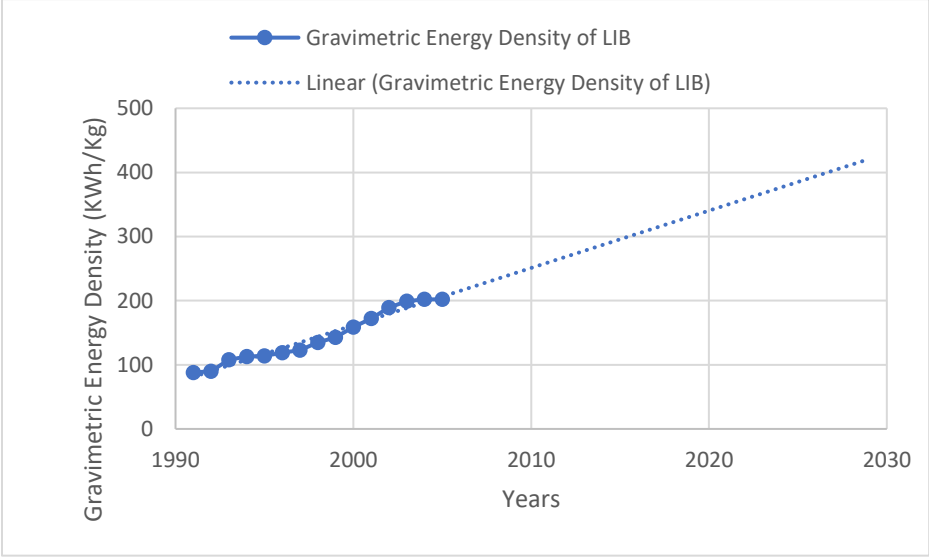

Figure 6:Gravimetric Energy Density of LIB Over Years

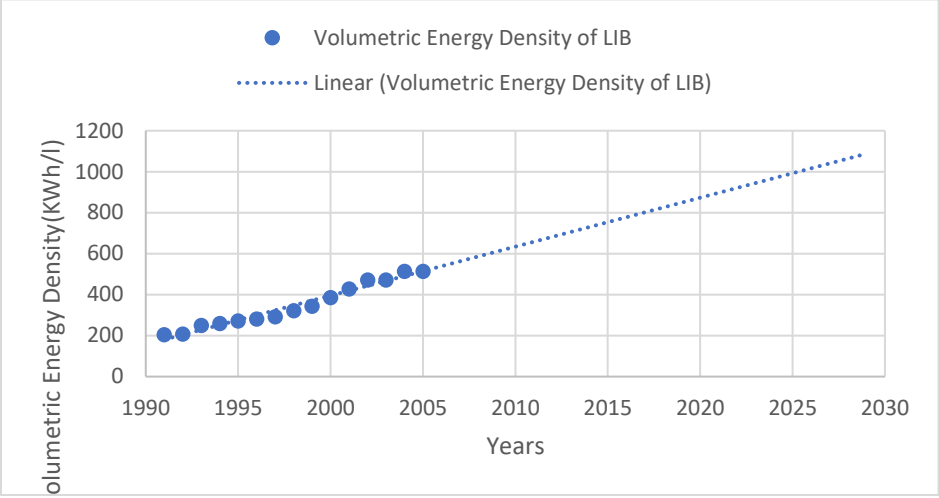

Figure 7: Volumetric Energy Density of LIB over Years

Table 3 Summary of LIB Current and Projected Energy and Cost

	Gravimetric Energy Density	Volumetric Energy Density	Cost of kWh
In 2017	320 Whr/Kg	800 Whr/I	$200/kWhr
In 2028	400 Whr/Kg	1100 Whr/I	$84/kWhr

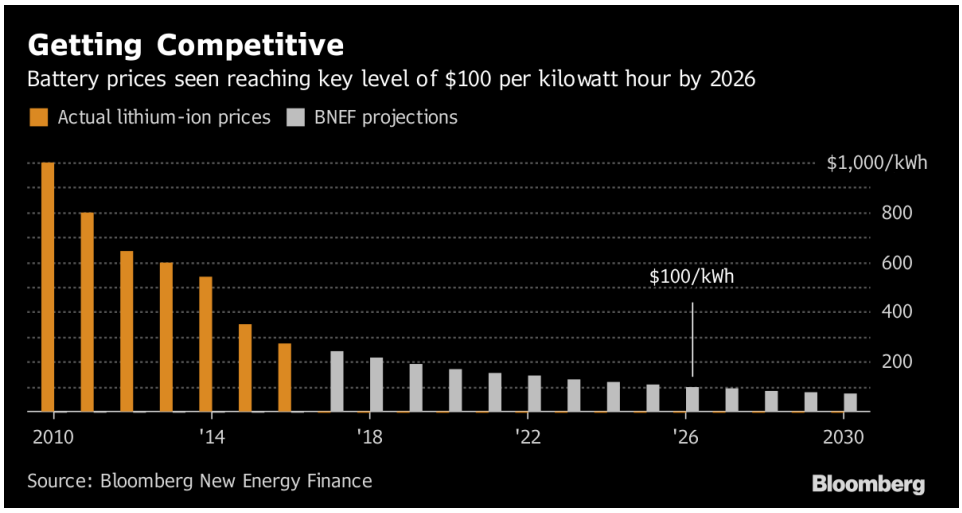

Figure 8: Cost per kWh of Lithium-Ion Battery over years

There are also many futuristic predictions that we will be able to have a battery of different chemistry (potentially Lithium Air or Solid-State) that can provide an energy density up to 1,000 kWh/Kg. But since we are designing an aircraft with an EIS in 2028, we have decided that we will be using a battery chemistry that's already is use.

6. Conceptual Design

6.1 Design Algorithm

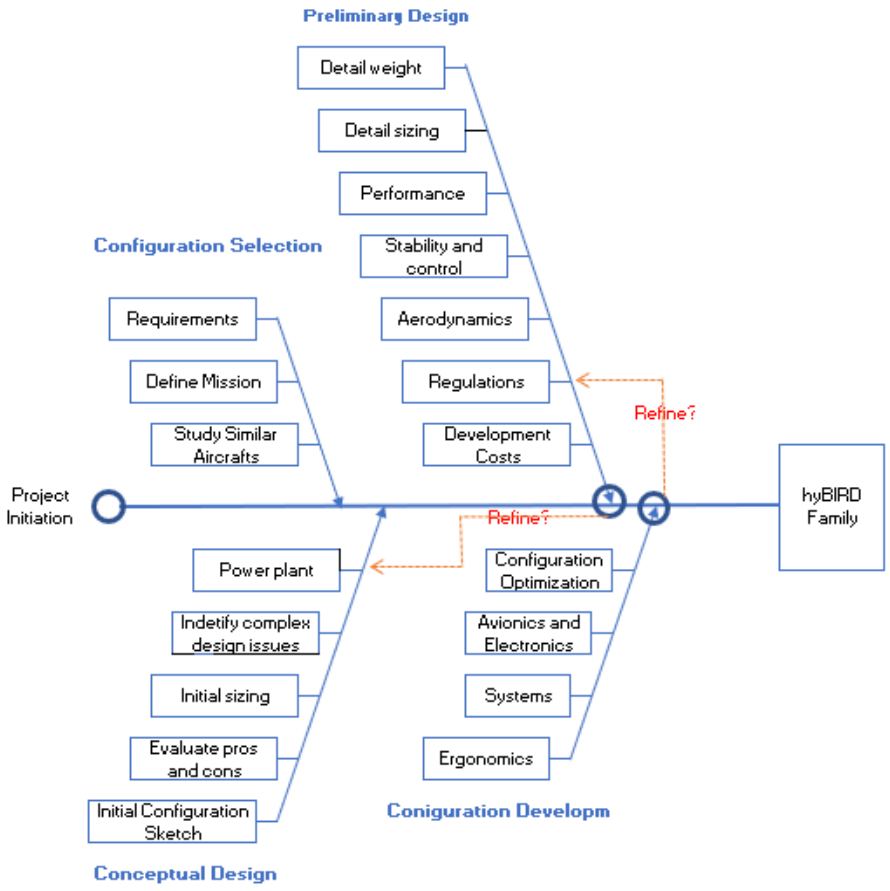

6.2 Survey and Reference Aircraft

The **Cessna 310 II** is a light, twin-piston engine aircraft designed and produced by Cessna Corporation and was introduced in 1954 as the first aircraft to put into production after World War II. It is a four-to-six-seater airplane with low wing and fuel tanks mounted on the wing tips and a conventional tail configuration, Figure (12).

Figure 9: Cessna 310 II Aircraft

Cessna 310 II has some innovative features such as the tip fuel tanks which were marketed as 'Stabile-tip' and engine exhaust thrust augmenter tubes. The wing tip fuel tanks were found to enhance the stability of the aircraft in flight and reduce the bending moments applied to the wing. The main specs we used while referring to this aircraft are summarized in Table (4) followed by a 3-views drawing, Figure (13) [25].

Table 4 Cessna 310 II Specs

Operating Weights			**Dimensions**	
Max T/O Weight	5500	lb	Exterior Height	10 ft 7 in
Max Landing Weight	5400	lb	Wing Span	36 ft 9 in
Operating Weight	3976	lb	Wing Area	175 ft^2
Empty Weight	3358	lb	Length	32 ft
Fuel Capacity	840	lb	Cabin width	4 ft
Payload W/Full Fuel	719	lb	Cabin height	8 ft 7 in
Max Payload	924	lb	External Baggage	65 cu ft
Performance				
Engine Model	IO-520-MB		Rate of Climb	1662 fpm
Engine power	2x 240 hp		Max Speed	207 kts
Service ceiling	20,000 ft		Cruise Speed	188 kts
TO distance	1700 ft		Cost per hour	449.4 $

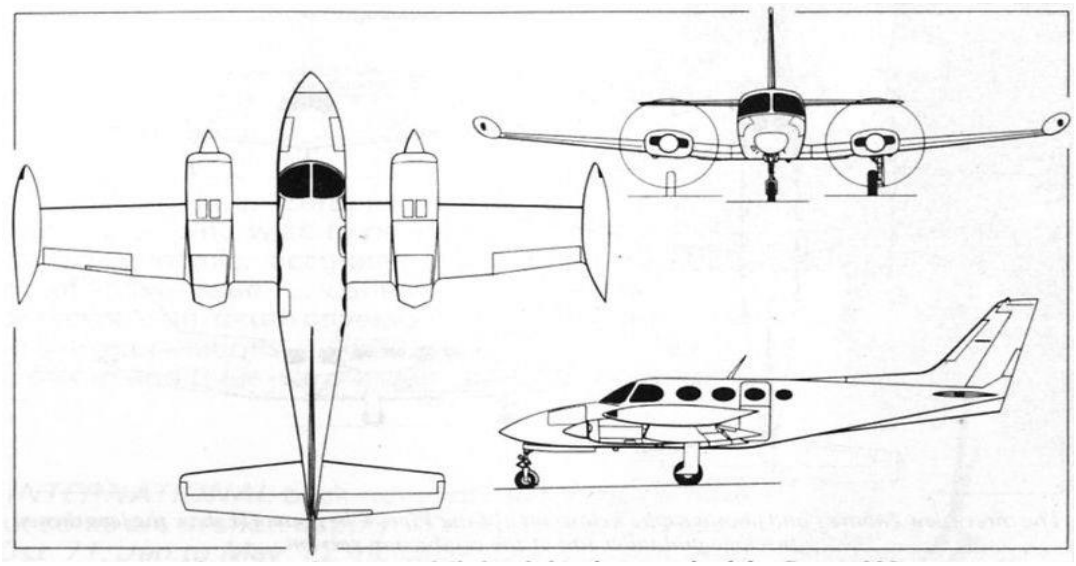

Figure 10:Different Views of Cessna 310 II

6.3 Weight Sizing (Class I)

After discussing the requirements and design potential choices, it was decided to start the sizing procedures for the six-seater variant first. Modification could be made after that to size the four-seater variant to guarantee the 75% commonality. In other words, it's assumed to have the same structure given that the increase in range will counter the decrease in passengers' weight. For class I sizing, it's assumed we have a conventional aircraft. Hybridization will be taken into consideration at a later stage.

Initial weight sizing was based on conventional Breguet and endurance equation, fuel fractions and performance parameters were chosen based on historical data from Roskam's Airplane Design part I [15]. Mass fuel fractions for cruise and loiter were estimated using the same reference knowing the airspeed, altitude, drag polar and lift to drag ratio. The major variable contributing to the sizing is payload weight which includes crew, passengers and their luggage as shown in Table (5).

Table 5 Payload Weight Break-down

Type	Quantity	Weight (lbs.)	Total Weight (Ibs.)
Crew	1	175	350
Passengers	5	175	875
Luggage	6	30	180
Total	-	-	1405

We started by estimating the relation between empty weight and maximum take-off weight. This was done by plotting the historical data of several aircraft which are similar or very close in range, speed and weight to our aircraft. It was also considered to involve recently-produced airplanes which were designed with modern materials such as composites. The regression line used for this analysis can be seen in Figure (14)**.**

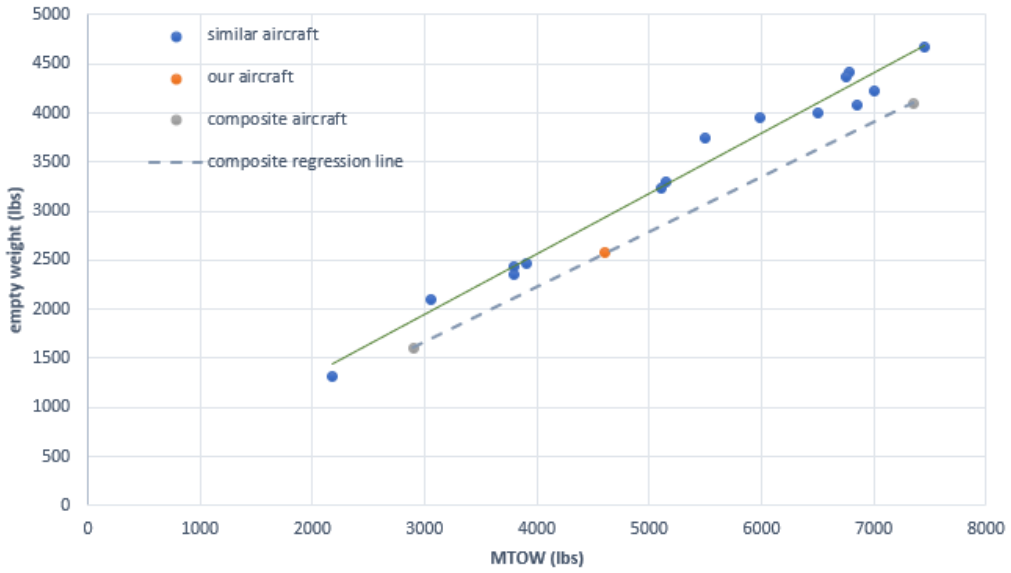

Figure 11: Historical empty weight vs Max takeoff weight (MTOW)

The figure has two regression lines, the solid line is for aircraft made through conventional manufacturing techniques such as sheet metal forming and the dotted one includes few airplanes, which are recently-produced and made from composite materials. The composites technology allows having lighter aircraft that can carry the same payload with similar performance.

Using the dotted regression line, we were able to get the equation describing the relation between the empty weight and the MTOW. We managed to solve for MTOW, empty weight and fuel weight which in turn would give us a good weight estimate for the aircraft we are designing. The results are summarized at the following Table (6):

Table 6 Six-seater class I weight estimation results

MTOW(lbs.)	Empty weight (lbs.)	Fuel weight (lbs.)
4599	2583	673

The estimated weights were plotted on a graph that has historical data of similar aircraft and they fitted on the regression line of the composite-made aircraft. Based on this result, we decided to manufacture most of the aircraft parts out of composite materials. Composites lead to lighter empty weight, which in turn reduces the required fuel for the same range and decrease the MTOW. This will increase the complexity and the cost but will increase the overall performance significantly.

6.4 Constraint Sizing

Based on the work of Roskam in Airplane Design part I [15], a constraint diagram was created to select the design point based on the constraints and top-level requirements (TLRs) for the aircraft design. First step was to breakdown the requirements to define the most constraining mission segment that will lead the design point upon. They were identified as following:

- Take off distance at different C_L (Different take off flaps positions)
- Climb performance at different C_L (Different climb flaps positions)
- Cruise Speed
- Landing performance at different C_L (Different landing flaps positions)

The assumed data at this stage of design were: the zero lift drag (C_{D0}), span efficiency and aspect ratio for minimum power which was derived in the same book. Different speeds were used based on the stall speed defined in FAR23 (61 knots) such as ($V_{lift-off}$, $V_{Take-off}$, $V_{landing}$)

The constraint analysis was done on the 4 and 6-seater versions of the aircraft but due to the commonality approach decided by the team that will be discussed later, only the 4-seater aircraft was considered for the design point selection.

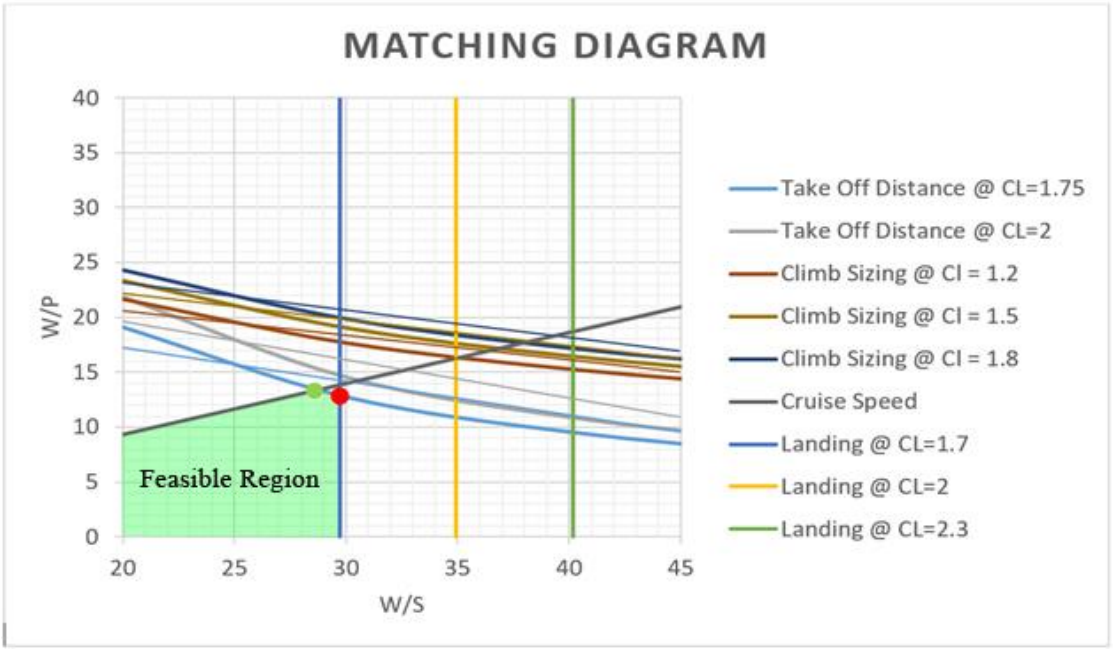

Figure 12:Matching diagram

The constraint diagram shown in figure (15) shows that the limiting factors for the aircraft design are landing with C_L = 1.7 (minimum landing flaps at max landing weight), take-off with C_L = 1.75 (minimum take-off flaps at maximum take-off weight) and cruise speed. The design point was selected to be the green point which is way better than the red one by the value of the power to weight ratio and wing loading. The analysis results were summarized in the following table (7):

Table 7 Summary of Design Constraints

W/S	**28.7**	**lbf/ft2**	**Power**	**356.5**	**hp**
W/P	13.6	lbf/hp	V_{Stall}	61	knots
AR min power	7.64		$V_{Lift\ off}$	67.1	knots
Wing Area	15.7	m2	$V_{Take\ off}$	73.2	knots
Span	10.95	m	V_{Cruise}	200	knots

6.5 Configuration Selection

The first step of conceptual design is to choose a configuration of the aircraft. Since this is an early stage of the design process, it's characterized with the greatest uncertainty in the process. Another challenge is that one configuration has to be chosen from almost infinite possibilities. This process can be time consuming and requires significant experience, and that's why a lot of the work in literature depended on industry and academic experts' opinions. But in our design, we wanted to adopt a rigorous procedure because options selected based on convenience, familiarity or aesthetics rather than objective information can lead to an inferior result. And that's why we use a method close to the concept of Interactive Reconfigurable Matrix of Alternatives or IRMA that was developed by William Engler et.al at Georgia institute of technology [8].

Based on Morphological Analysis, an IRMA is a concept development system engineering technique for functionally or physically decomposing an existing system into a set of components. An IRMA aids designer by bringing tacit knowledge and objective merits into a collaborative design tool. The idea, more detailed in [8], is to break down the system into its morphological components then tabulate the different alternatives for each component in a matrix. The evaluation of each option is based on what is called the Merit of Interest MOI. The latter is a list of objectives and design goals derived from mission requirements and analyses. Each MOI is given a weight depending on its priority and importance to the mission objective. Table (8) presents our weighted MOI list that was derived from the Request for Proposal RFP and technical requirements summary previously listed in Table (1).

Table 8: Merit of Interest (MOI)

Merit of interest		
Num	MOI	weight
1	takeoff and landing field length	10%
2	Energy comsumption	20%
3	noise	10%
4	cost	20%
5	Reliability	15%
6	maintenance	15%
7	Safety and redundancy	10%
Total		100%

The combination of the framework and the iterative process into an IRMA gives a better documented and understood family of solutions for more detailed analysis and design. It also allows scanning of scores of options in practical time cost. However, for practical reasons, the aircraft was decomposed into three main components only each of which is further divided into four to six elements. The number of considered alternatives was also restricted to a maximum of five significant candidates for each element. Figure (16) shows the layout of our matrix of alternatives.

	Matrix of Alternatives							
	Components	Alt 1	Alt 2	Alt 3	Alt 32	Alt 33	Alt 4	Alt 5
Wing	Number	0	1	2	3			
	Location	Low	Med	High				
	shape	Rectangular	Tapered	Elliptic	Delta Wing			
	Sturcture support	Cantilevered	Strut					
	Wing-tips	Shark winglets	Blended	Wingtip-mounted motors	Wing Fence	Upswept	Spiroid	Wing Grid
Structure	Tail	T-Tail	V-Tail	Conv-Tail	H-Tail	No-Tail	U-Tail	Canard and vertical tail
	Fuselage No	0	1					
	Primary Material	Aluminum	Steel	Titanium	Composite			
	Landing Gear	Retractable						
Thurst Devices	Power generation	ICE	Fuel Cell	Brayton Cycle				
	Energy Storage	Electric	Fuel	Hybrid				
	Number	1	2	3				
	Location	Nose	tail	Centre				
	Thrust generation	Ducted Fan	Open Rotor	Turbojet	DEP			
	Number	1	2	3	Mult			
	Location	Nose	Aft-Fuselage	Up-Wing	Low-Wing	Tail	Wingtips	

Figure 13: Matrix of Alternatives

The scoring scale of different proposed configurations was defined from -4 to +4, 0 being neutral, -4 being very bad for the subject MOI and +4 being very good for that MOI. An example of configuration scoring scheme is presented in Figure (17).

			MOI							
	Components	Configuration	#TFL	#Energy	#Noise	#Cost	#Reliability	#Maintenance	#Safety	#TOT#
Wing	Number	1	3	4	0	2	3	4	2	2.75
	Location	Low	3	3	0	1	3	4	1	2.25
	shape	Tapered	0	3	0	-2	0	0	0	0.2
	type	Cantilevered	0	3	0	-1	-1	-1	1	0.2
	Wing-tips	Shark winglets	3	4	1	-2	-1	0	1	0.75
Structure	Tail	T-tail	3	4	0	-1	-1	1	2	1.1
	Fuselage No	1	4	3	0	4	-2	-1	2	1.55
	Primary Material	Composite	3	4	0	-2	1	-1	3	1
	Landing Gear	Retractable	0	3	0	-1	-1	-1	-1	1.1102E-16
Thurst Devices	Power generation	Turbo-normalized IC	3	1	-2	2	-2	-1	0	0.25
	Number	1	0	3	1	3	2	2	1	2
	Location	Nose	0	2	-1	1	0	2	0	0.8
	Thrust generation	E-Motors & open rotor	3	3	-3	4	3	3	1	2.4
	Number	1	1	2	0	4	3	3	0	2.2
	Location	Nose	3	2	-1	1	2	4	3	2
										1.29666667

Figure 14:Example of configuration scoring scheme

The scoring was based on our literature review, research of the pros and cons of each alternative on the MOI and was reviewed and consulted by professors and some industry experts.

6.6 Accepted designs

The down selection process produced four candidate configurations to choose from. The tables below present each configuration and its unique or significant pros and cons.

- **Fuselage-mounted motor/engine nacelles**

Pros	Cons
+ Enhanced thrust extraction + Redundant motor increase safety + Clean wing flow + Reduced noise	- Nacelle drag - Fuselage structure and internal cargo space - Wing wakes fed into motor - Tail flow affected by motor wakes - Engine Maintenance and accessibility

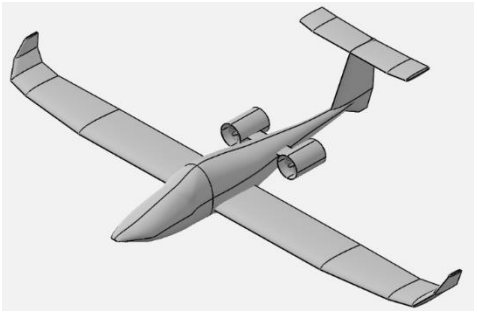

Figure 15:Fuselage-mounted motor/engine

- **Single nose engine/motor**

Pros	Cons
+ Simple and standard configuration	- Not unique or new to the market
+ High reliability and low maintenance cost	- Low redundancy and safety level
+ Compacted engine compartment	- Expected long takeoff field length

Figure 16 Single nose engine/motor

- **Pusher and tip-motors**

Pros	Cons
+ High redundancy and safety	- Very new to the market and hard to certify
+ Clear wing and tail flow	- High complexity and low reliability
+ Tip-motors enhance wing lift and reduce downwash	- High maintenance cost
+ Reduced cabin noise	- Very low ground clearance at tail which places high probability of the props striking the ground at takeoff.

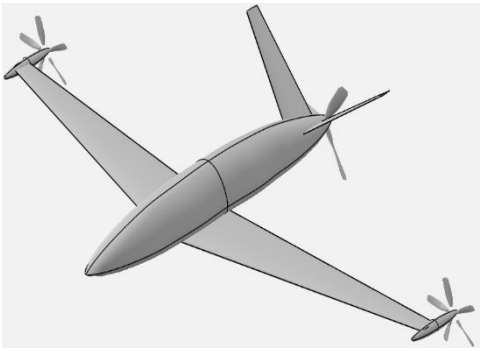

Figure 17 Pusher and tip-motors

- **Nose and tip-motors**

Pros	Cons
+ High redundancy and safety	- High cost
+ Clear wing and tail flow	- Complexity
+ Tip-motors enhance wing lift and reduce downwash	
+ Reduced cabin noise	
+ Unique but not strange & not hard to certify	
+ Compacted main-engine compartment	

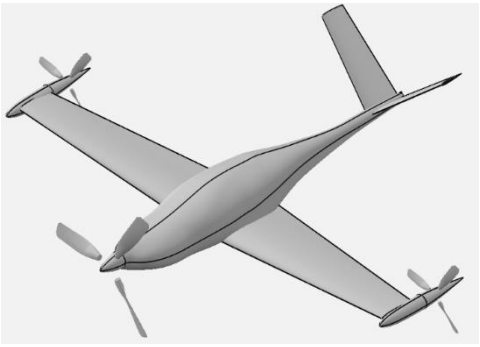

Figure 18 Nose and tip-motors configuration

After scrutineering each of the accepted designs and including the opinions of professors and industry experts, the last configuration was found superior and reliable. It is also adequate to our mission goals and objectives. Although the pusher tip-motors are new and unique feature of our design, a study has been conducted at the Langley Research Center to determine the effect of a wing-tip-mounted pusher turboprop on the aerodynamic characteristics. The study

> "Throughout the design process, always make sure to put reliability as your first criterion"
>
> Prof. Mostafa M. Abdallla
> Zewail City of Science and Technology

concluded that the performance of a propeller located just behind the wing tip is increased as a result of the influence of the wing tip vortex flow. Not only the tip vortex increases the propeller performance, the propeller wake itself reduces the drag due to left of the wing as well. And further reduction was found by having -3 degrees incident angle for the motor with the incoming flow [15]. Furthermore, a series of studies on Vought V-173, more commonly known as the "Flying Pancakes", to investigate the effect of tip motors on wing lift distribution. It was found that wings with tip-mounted motors exhibit almost rectangular lift or pressure distribution along the wing span. Additionally, the tip-motors can be utilized as stability augmentation system or attitude control system by applying differential thrust on each side. Finally, a bonus utility for these motors is as brakes by reversing their rotation and hence the thrust vector. This will alleviate the need for spoilers. An even more feature of these tip-motors is presented in the safety section.

One possible setback of the tip motors though, which was noted by professor Ron Barret from KU, is that if the motor's center of mass is behind the wing's mean quarter chord or aerodynamic center, this may introduce structural instability and flutter. Although flutter and such advanced structure analysis is well beyond the scope of this design report, precaution was taken by advancing the tip motor's bulk mass forward a little bit till its center of mass is exactly parallel to the wing's quarter chord. Additionally, the propellers were extended further behind the wing to clear trailing edge vortices. Finally, ailerons and control surfaces are shifted inward the wing to clear from the props influence and gain full surface control.

The V-tail choice is known to be aerodynamically superior to conventional or T-tails due to the reduction in the number of surfaces and consequently reduction in interference and total drag. The only set back of that tail is the analysis complexity. For the scope of this report and this design stage, some approximations and reduction models are presented during the analysis in this report that reduce the analysis complexity with proved high accuracy.

Another great advantage of this configuration is the compactness of the main engine and motor compartment. As will be illustrated in later sections, this compartment contains the ICE along with the generator and the nose motor. The positioning of such a system at the nose of the aircraft give the advantage of augmenting the cooling mechanism as well as distributing the masses along the plane structure.

6.7 Mission Profile and Scenario

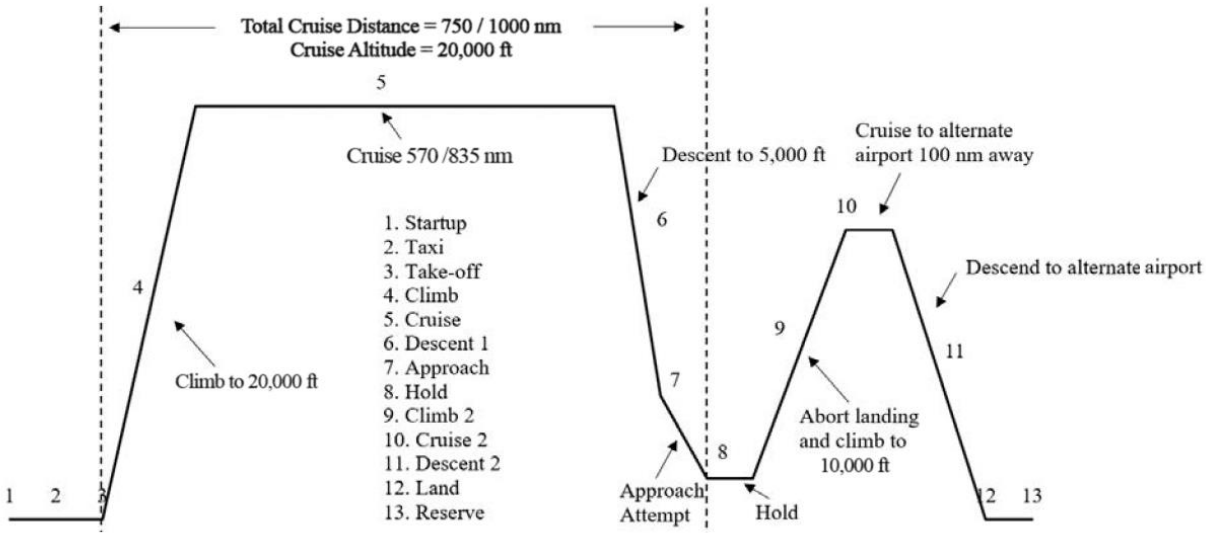

Figure 19: Mission profile

The mission profile for both aircraft is shown in Figure (22). Through performing trade analysis, described in a later chapter, cruise altitude was selected to be 20,000 ft and alternate cruise segment will be on 10,000 ft altitude.

6.8 Propulsion Sizing and Optimization

With the energy crisis looming, electric propulsion systems will help reduce operational costs, emissions and noise associated with fossil fuel engines. Today several all-electric aircraft exist which proves that electric propulsion is possible. However, each one of them is limited by the energy storage capability which limits the endurance and range; For example, Pipistrel Alpha Electro Figure (23-right) which has a full electric propulsion system with just +60 mins endurance at 122.5 kg of batteries in comparison with Cessna172 with +340 mins at 174 kg of fuel[3]

Figure 20: Example hybrid and electric aircraft

In order not to sacrifice the endurance and performance of current ICE powered aircraft, electrically assisted hybrids could be the key step toward full electrification.

The hybrid electric powertrain is available in many architectures such as serial, parallel and serial-parallel one Figure (24) [5].

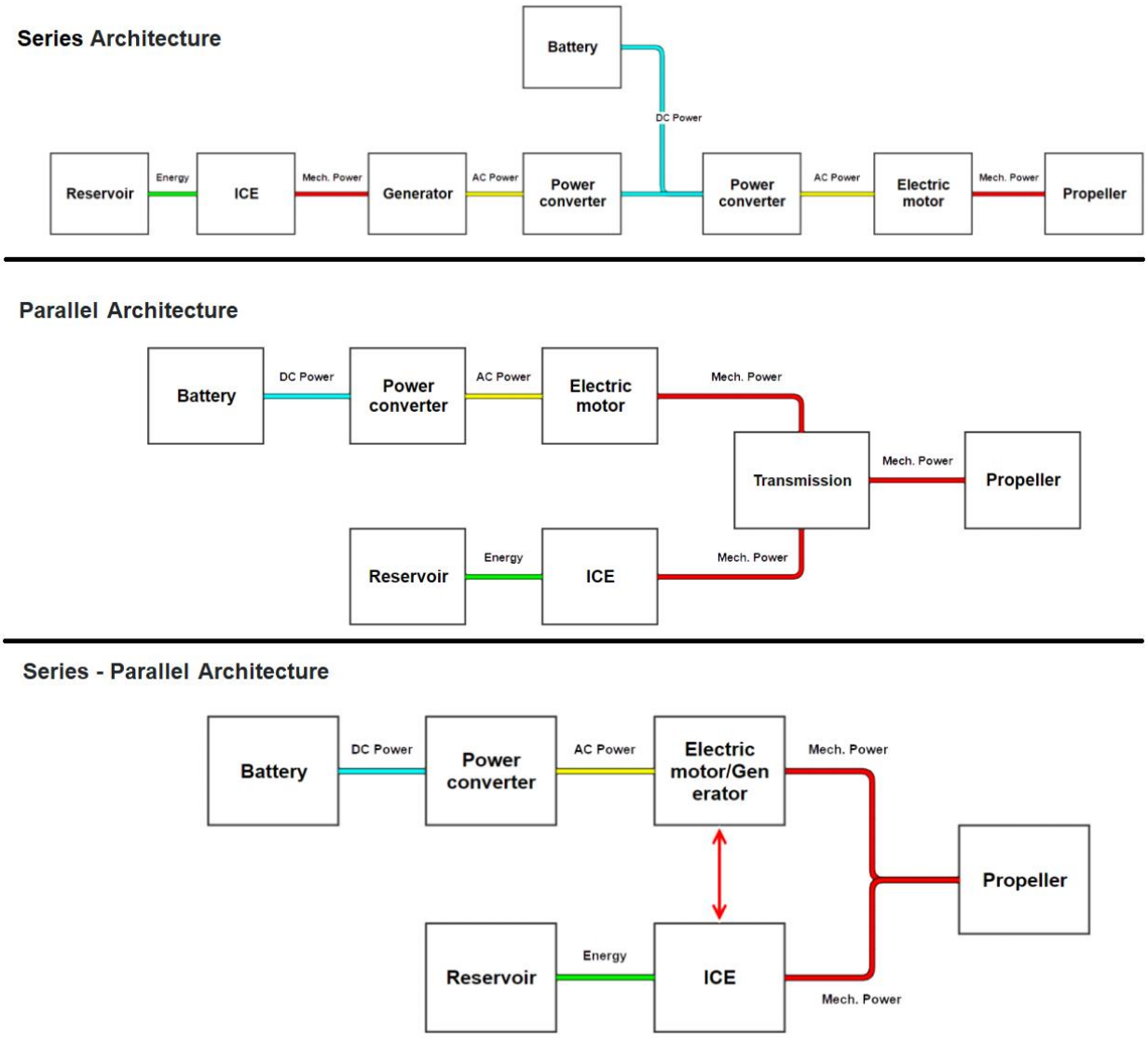

Figure 21: Hybrid power train architectures

The pros and cons of each architecture is discussed in Table (9) [5].

Table 9: Power train pros and cons

	PROS	CONS
Series	– ICE always operates at its peak efficiency RPM; – Efficiency loss can be reduced thanks to fewer gear pairs and absence of transmission; – Control system is relatively simple; – Possible to have DEP.	– Overall efficiency suffers at high speed; – Electric motor must be sized for maximum power, increasing its cost, weight and volume; – Necessity for an additional electric generator.
Parallel	– Higher overall efficiency in cruise; – Smaller electric motor required; – Large design flexibility.	– Necessity for a complex mechanical transmission; – ICE does not always operate at its peak efficiency RPM.
Series-Parallel	– Maximum power flow management flexibility; – Smaller and more efficient ICE.	– High complexity; – Efficiency of the electrical path is lower.

The team decided to use the series configuration which will allow highest efficiency for the engine. The most challenging part is to establish an accurate conceptual design strategy that can reasonably estimate the propulsive power needed from multiple sources to satisfy discrete performance criteria. The idea of having multiple energy sources for the propulsion system made the traditional conceptual design approach more complex. Typically, aircraft lose weight during each flight segment due to fuel burn which is not the case using batteries because of their weight doesn't change according to the mission segment weight fraction calculations.

6.8.1 Literature Review:

Georgia Institute of Technology have published methods for initial sizing of aircraft using multiple energy sources. They identified individual power paths whether they were consumable or non-consumable energy for each mission segment and assuming a specific mission scenario, the analysis will yield the initial size and weight estimation [18]. This approach will optimize the power needed to complete a specific mission.

Researchers from Delft University of Technology attempted to improve the fuel consumption of existing airframes using hybrid-electric technology by incorporating a smaller engine. The example was Boeing 737-800 assuming a specific energy of 750 Wh/kg, a 10.4% fuel saving was computed on a 2 hrs. mission and this comes at the expense of an increase in aircraft weight of approximately 10,000 kg. They found that the performance of these airplanes will suffer a lot because of the current battery power density is much lower than the fuel power density (285 Wh/kg vs 12,194 Wh/kg respectively) and this causes a significant increase in the weight of the airplane. They concluded that the Hybrid-electric propulsion systems is not feasible for regional aircraft above 70 passengers until the battery power density exceeds 750 Wh/kg in the future [7].

Researches from UNSW Sydney university examined the possibility of employing a hybrid powertrain for light aircraft which depends on internal combustion engines (ICEs). They showed many advantages of the proposed powertrain such as downsizing the ICE as a motor is directly connected to the propeller, the extra power required for climbing can be provided by this motor assisting the ICE which can lead to a significant downsizing of the ICE [14]. They suggested that using hybrid powertrain for the small and light aircraft that regularly climb and descent will be feasible with slightly increase in fuel consumption for small aircraft that operate continually in straight and level cruise.

A thesis titles “Sizing Analysis for Aircraft Utilizing Hybrid-Electric Propulsion Systems” published by Air Force Institute of Technology at Ohio (AFIT) discussed the sizing and analysis of the mild hybrid-electric propulsion system for general aviation single-engine aircraft and remotely-piloted aircraft [6]. The engines in most single-engine aircraft were oversized to satisfy takeoff and climb segments. At cruise, only 55% of the engine maximum power is needed [11]. The mild hybrid design needs the electric motors to assist at the takeoff, climb, and possibly landing conditions. The engine would satisfy the cruise segment because the cruise is the longest mission segment in a typical general aviation platform. After optimizing the engine at the cruise condition, all the needed additional power would come from the electric motors.

6.8.2 Methodology:

After surveying the previous approaches, it was decided to follow the AFIT approach of sizing the ICE engine to provide the required power for cruise and have the additional batteries to provide the extra power needed to take-off and climb. The way to do so is to use a software such as FLOPS and NPSS developed by NASA side by side with AAA (Advanced Aircraft Analysis) developed by DAR Corporation. Having no access to these softwares made it even more challenging. Consequently, we had to build our own tool that combines weight estimation, geometry, power sizing and optimization for our proposed aircraft models using MATLAB and Simulink software. The main algorithm is explained in the following flowchart.

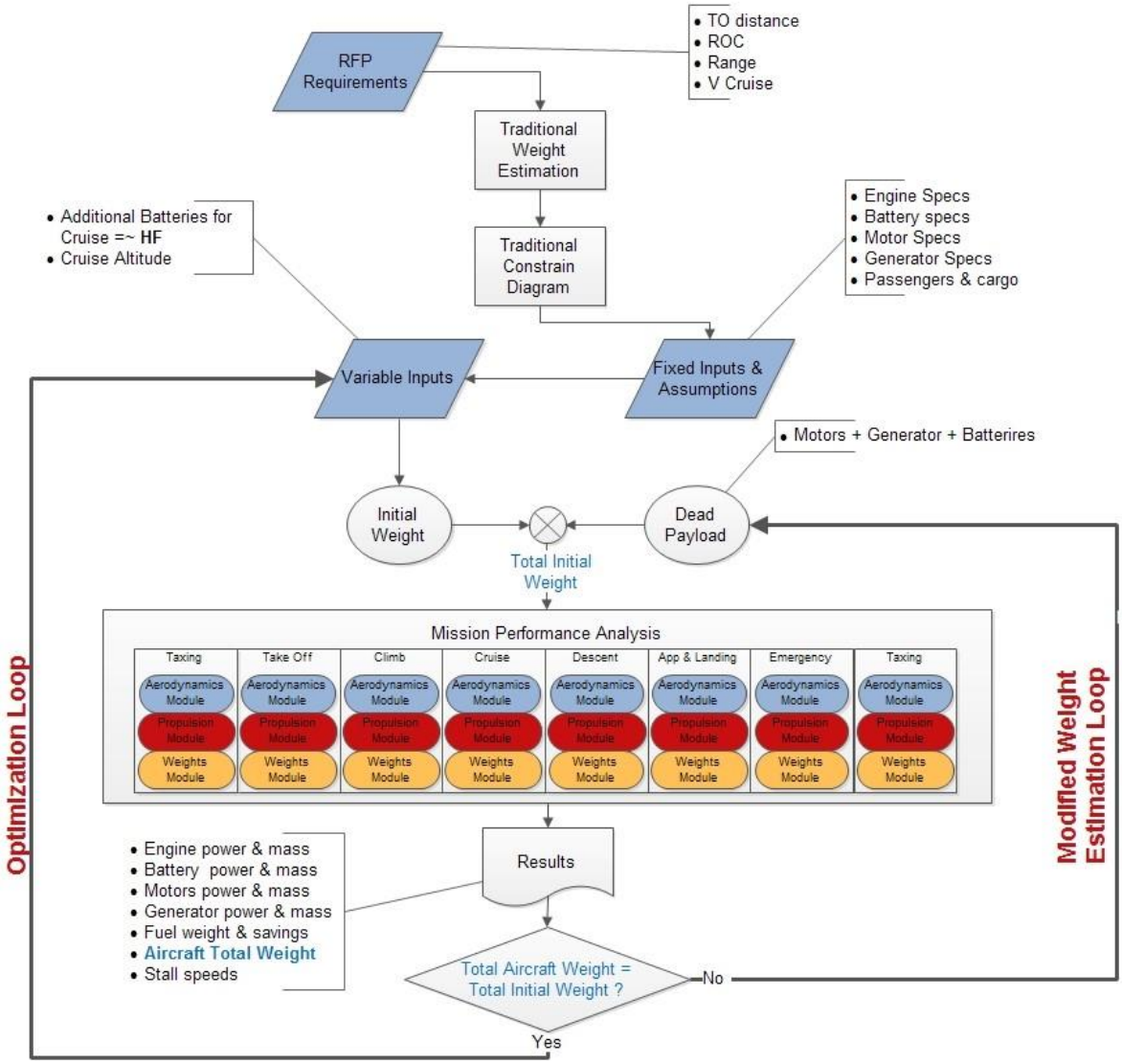

Figure 22: hyBIRD design tool algorithm

The algorithm starts by entering the request for proposal requirements such as takeoff distance, rate of climb, range, V cruise, passengers and cargo weight. Conventional weight estimation and constraint diagram is made based on the procedure defined by Roskam which will result in a conventional aircraft weight estimate, power requirements and wing area. The next stage will need to define fixed inputs (Engine, Motor, Generator and Batteries specs) then variable inputs (additional batteries for cruise segment* and cruise altitude) that will be varied to minimize the cost function which is the total fuel weight.

Initial weight of conventional airplane previously estimated is added to the assumed dead payload weight (the hybrid added components) and the total initial weight is used to analyze the mission performance analysis using the Aerodynamics, performance and weights modules which were coded using the flight dynamics equation in [13]. The results consist of engine, motor, generator, batteries power and masses; stall speeds(to be checked against RFP requirements), wing area, fuel weight and savings (compared with the reference aircraft) and total aircraft weight. If total aircraft weight doesn't equal the total initial weight, the assumed dead payload will be modified accordingly until convergence. Then the optimizer alternates the variable inputs to achieve the cost function and final sizing results is reported.

* Additional batteries for cruise segment is the input variable that will reflect into and change the HF value indirectly because the HF is a fixed output in takeoff, climb and descent due to our mission profile choice for a given aircraft weight and a variable output if we decided not to depend on the ICE completely in the cruise. So, if we want to sweep the HF value to get the optimum hybrid design, we can change the additional batteries for cruise segment by a value and the conventional weight estimation by the same value approximately to have a fully defined inputs to solve.

6.8.3 Results

> "Make sure to conduct trade studies to identify the most balanced and optimum design point "
>
> Marwan Dessouki, PhD student kansas State University

The optimizer was used to perform a multivariate trade studies to ensure the optimum design point is achieved. The results for the 4-seater and 6-seater aircraft shows that the optimum design point is achieved when zero batteries used in the cruise and depend completely on the ICE as shown in the Figure (26).

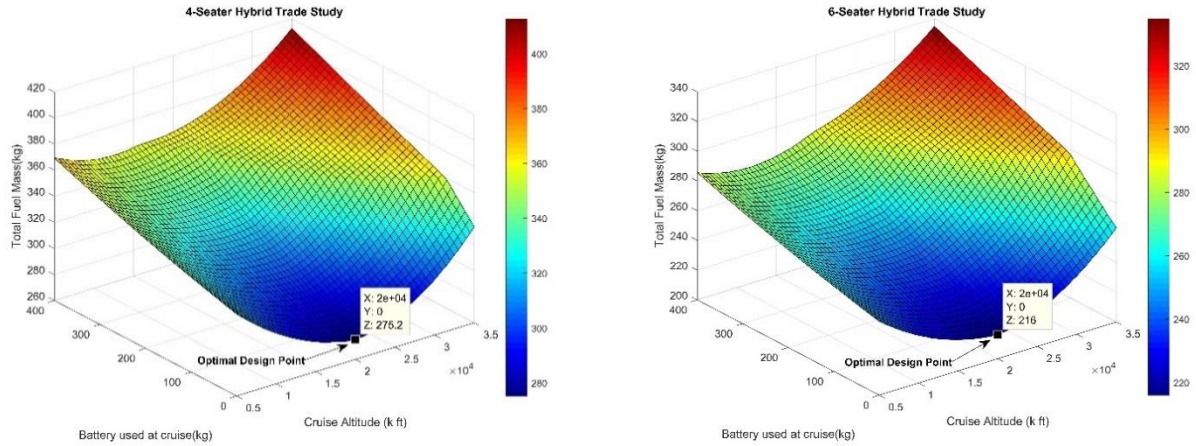

Figure 24: Trade studies results

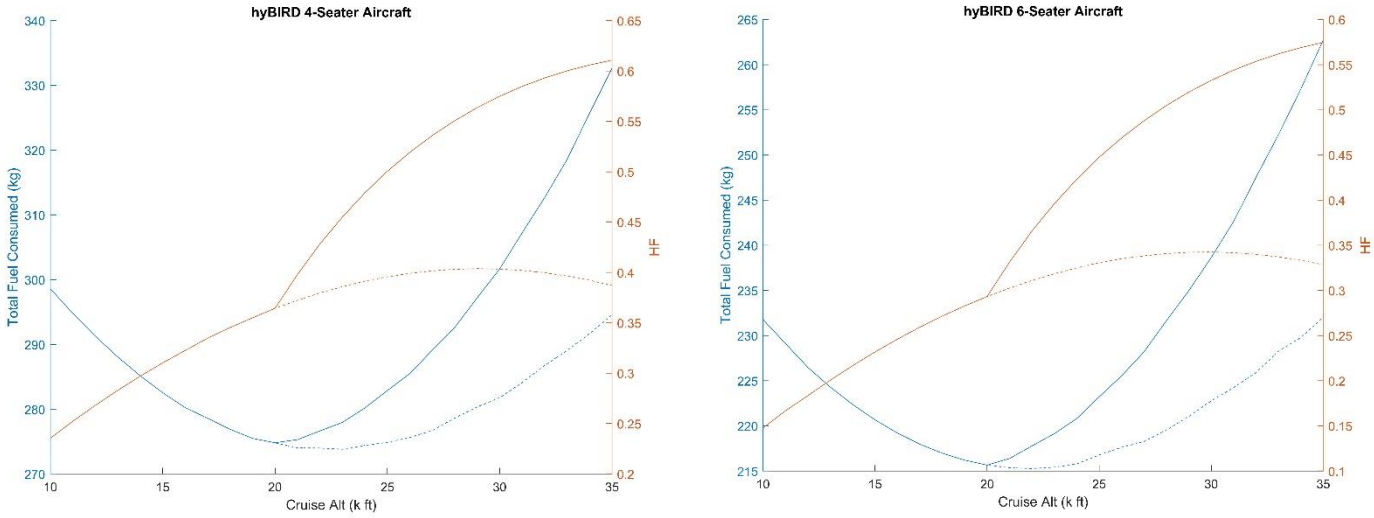

Figure 23: Cruise altitude trade studies

Regarding the choice of cruise altitude, it was decided to use a turbo-normalized engine which will be discussed later in this report. This engine has a performance drop after FL200 which increases the specific fuel consumption

(dotted curves). Considering this limitation in the analysis with zero batteries in cruise, FL200 cruise altitude was the optimum cruise altitude for both versions Figure (27).

To meet the FAR23 regulations and passenger comfort, it was decided to pressurize the aircraft and therefore the doors will be just two located besides passengers 3 and 4 to minimize the cutouts in the fuselage.

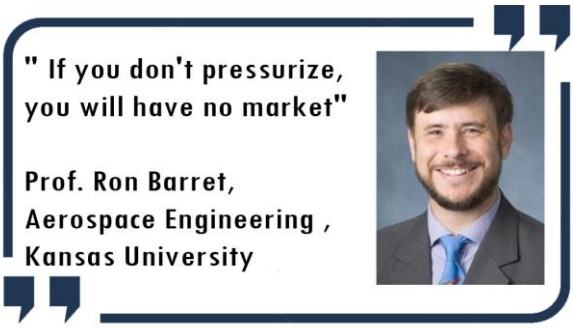

The results for both 4-seater and 6-seater are shown in the Table below.

Table 10: Design specs

Performance Specs		hB400	hB600	
Range		1000	750	nm
Cruise Speed		200	200	Knots
Stall Speed		61	61	Knots
Cruise Stall Speed		103	103	Knots
Takeoff Power		207	165	hp
Climb Power		409	361	hp
Cruise Power		222	220	hp
Fuel Savings		25.5	41.5	%
Hybridization Factor		38.2	31.2	%
Propulsion Specs				
Engine	Power	253	248	hp
	Weight	127	125	kg
Motor	Power	409	361	hp
	Weight	61	54	kg
Generator	Power	253	248	hp
	Weight	37.6	37	kg
Batteries	Weight	202	156	kg
Weights				
Gross Weight		2296	2367	kg
Empty Weight		1185	1173	kg
Fuel Weight		283	223	kg
Payload Weight		400	600	kg

The results show a great similarity between both airplanes in the weights and many components specs. The commonality between them is decided to have the same airframe and the propulsion system which means oversizing the 4-seater a little. This was referred to the following reasons:

- The space of the removed 2 seats will be 73 cm long, which is only 8 % of the 6-seater fuselage length.
- The aerodynamic shape of the fuselage later in this chapter will require the cabin to have a variable height which results in no constant diameter section to be removed from the 6-seater version and connect the other sections together without modifying them. In other words, the whole fuselage would be changed.
- From business point of view, the history shows that airplanes always almost increase their weight in response to the desire of adding new capabilities by time. For this reason, it was recommended for the main design driving systems (airframe, propulsion and landing gear) to be able to accommodate for an increase of growth weight by 25%. This can be achieved easily in the hyBIRD 4-seater version.

The propulsion system efficiency is expected by the survey to be 87%. The figure below shows its configuration.

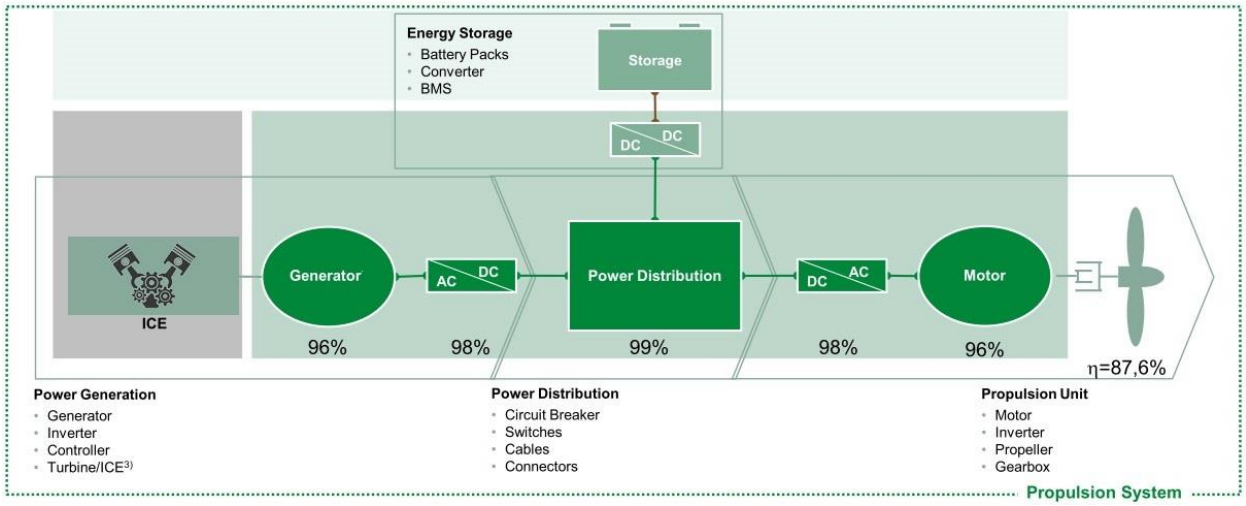

6.9 Mission Power Profile

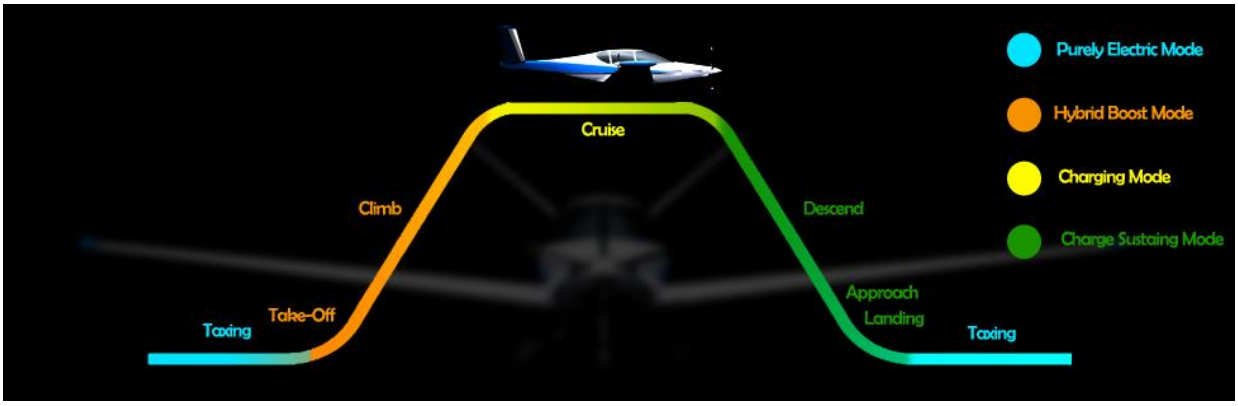

Figure 25: Mission power profile

The power profile for the hyBIRD aircraft is shown in the figure above. The Taxiing segment will be in the **electric mode** and the power will be delivered to the motors by the batteries. Takeoff and climb are the extensive power consuming segments which will be driven by the ICE in full power mode assisted by the batteries until reaching the cruise altitude **(Hybrid Boost mode)**. The cruise segment will be driven by the ICE providing the required cruise power and charging the batteries **(Charging mode)** to assist in any possible emergency climb or for the aircraft to be ready for the next flight without recharging. The descend segment is a **charge sustaining mode,** which means the power generated by the ICE is just to sustain the aircraft operation power. The final approach and landing will be purely in the **electric mode** with the ICE engine running at idle to enhance the aircraft safety and easily take control should any emergency situation happen.

6.10 Fuselage Configuration and Sizing

Fuselage configuration is one of the key design elements of the aircraft design process. Location and fixation of the lifting surfaces, engines, and the landing gears need to be well-designed and mounted on the fuselage. The openings in the fuselage (landing gear, doors, windows, baggage area and wing attachment area) have to be precisely selected in a way that best utilize the structure design of the fuselage frame and minimize the materials and cost. Fuselage can take the shape of either frustum or tadpole or tubular but since tubular in only used for large commercial aircraft, we studied the pros and cons of both frustum and tadpole shapes, Table (11), and came up with a conclusion that tadpole shape would be the best fit for our aircraft.

Table 11:Comparison between Frustum and Tadpole shapes

	Tadpole	Frustum
Cost	Expensive if Aluminum	Much cheaper
Generated Drag	Less	More (around 45% more)
Manufacturing	Hard – Compound surfaces	Easier
Preferred material	Composite	Aluminum – Metal folding
Internal Volume	Less	More

As the history of the general aviation (GA) aircraft shows, tadpole shape for the fuselage proved to be the best choice especially for small GA aircraft that doesn't carry heavy payload. Tadpole has other advantages as the forward shape of tadpole can sustain laminar boundary layer and the empennage shape of the tadpole results in as much as 30-40% less wetted area which means less aerodynamic drag.

Table 12 - Fuselage specs

Parameter	Dimensions
Front Engine Length	1.2 m
Cabin Length	3.75 m
Baggage Volume	0.7 m^3
Cabin Height	1.35 m
Cabin Width	1.52 m
Fuselage Surface Area	29.2 m^2
Fineness Ratio (empennage length/diameter)	4.96

Our tadpole fuselage geometry consists of a paraboloid (1), cylinder (2), and two sets of frustums (3,4), featuring the dimensions shown in figure (29).

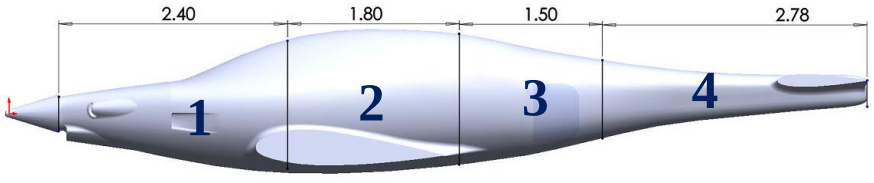

Figure 26 fuselage geometry

For millions of years, birds have been the perfect flying machines which inspire engineers to study and learn valuable lessons. The aerodynamic superiority of Cooper's Hawk, which has a speed of 88.5 km/h, helps to maximize

the endurance in the air searching for its prey using as little energy as possible. This natural aerodynamic body shape inspired the final shaping of the fuselage streamlines to yield a much more efficient design thanks to nature.

Figure 27: Fuselage geometry nature inspiration

When designing the cabin and, pilot visibility is a very important factor to consider. Pilot visibility for hyBIRD is shown in figure (31).

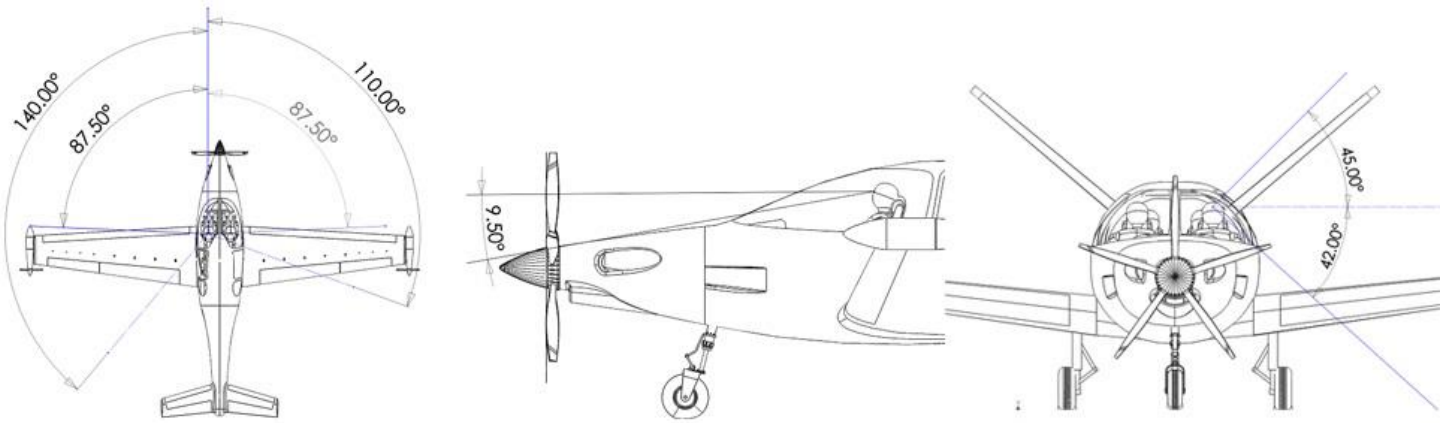

Figure 28 Pilot visibility

6.11 Wing sizing

The merit criteria for wing design is the performance. During the preliminary design, the choice of variables was made based on historical data and similar aircraft. The method mentioned in Roskam part (3) chapter (6) was followed to determine most of the variables. To start the wing sizing, wing area and the aspect ratio are needed. To get the wing area, maximum takeoff weight and the constrain diagram were used. Based on constrain diagram a wing loading of 71 psf was determined. Using the maximum takeoff weight, a wing area of 15.5 m^2 was chosen. The choice was based on the six-seater variant since the wing will be common between the two variants and to reduce the development cost. It was noted that using a larger wing for the smaller variant will have a negative effect on the stability and drag but it was assumed as an acceptable trade-off in terms of cost and performance.

To choose the aspect ratio, an equation was derived to predict the optimum aspect ratio for the minimum power consumption. The equation is based on some approximations as following:

$$Power_{min} \rightarrow \frac{C_l^{1.5}}{C_D}$$

And the limiting value is the $\left(\frac{L}{D}\right)_{max}$ which gives the following equation:

$$\sqrt{\frac{3 * \pi * e * AR}{16 * C_{d0}}} = \left(\frac{L}{D}\right)_{max}$$

Choosing the variables was based on historical data from Roskam's Airplane Design part I [15]. Solving this equation, the optimum aspect ratio was determined to be **7.6**.

Similar aircraft were studied to choose the structural configuration. A cantilevered wing was chosen in order to avoid any interference drag and the drag resulting from the strut arrangement. Also, the low wing configuration seems to be very common between aircraft of the same category. This configuration decreases the landing gear weight with some penalty on decreasing the cabin visibility.

To choose the sweep angle, we studied the available choices which are: zero or negligible, aft sweep, forward sweep and variable or oblique sweep. Two sweep angles are for advanced missions like having both supersonic and subsonic mission requirements which require variable sweep. Forward sweep is perfect for high maneuverability on low speed near the stall limit as it enhances stall performance of the wing. Aft sweep angles are good choice for high

speed missions. But for our mission a sweep angle of zero was chosen due to the low speed requirements which doesn't need sweeping. This was verified by studying similar aircraft which came to conclusion that zero-sweep angle is very common.

The thickness to weight ratio is a very important parameter that has a huge effect on the performance. If it was chosen to be greater than what's needed, it will result in a larger drag which contributes to the sizing of the aircraft. Also, small thickness to weight ratio will lower the fuel capacity inside the wing and lead to more complexity in the structure. Roskam part (2) illustrated those changes and by using the approximated Reynolds number and the chosen airfoil, we can approximate the t/c to be between 12% and 18%. In other words, 18% at the root section and 12% at the tip section as that region is noticed to have the maximum $C_{l\max}$ as shown in figure (32)..

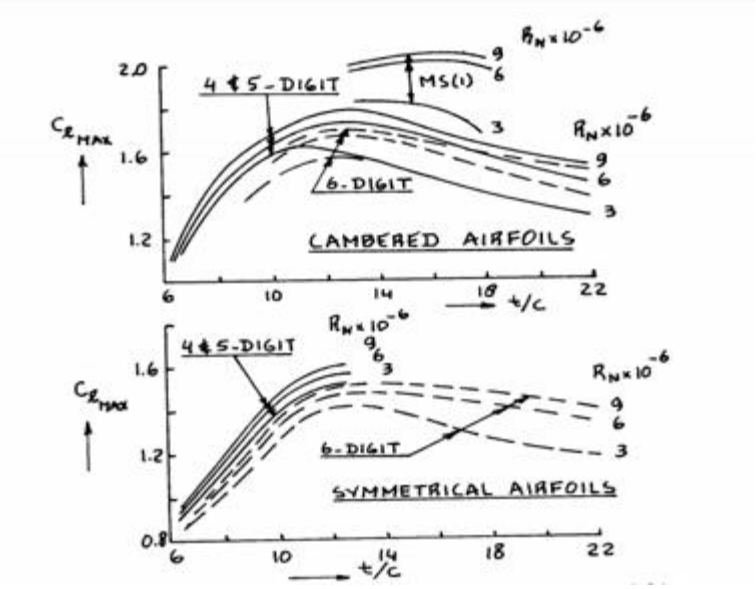

Figure 29: Effect of thickness ration and Reynolds number on section max lift coefficient [17]

Dihedral angle, incidence angle and tapering ratio were chosen based on the historical data collected from similar aircraft at Roskam's Airplane Design part II [18]. Twist was decided to be -1.5 from root to tip in order to enhance the ailerons performance. If the pilots sensed a stall sign, then probably the tips are still away from stall, which preserve the ability to control the aircraft out of that stall. On the other hand, from a structural point of view, the washout reduces the torsion near the tips.

Table 13 - Wing specs

AR	S	Wingspan	Dihedral	Root Inc	Twist	Sweep	Tapering Ratio
7.6	172	36.2	5	2	-1.5	0	0.45

When deciding on the airfoil to be used, many parameters must be studied like section drag, maximum lift coefficient and section moment are important to get the desired performance of the wing.

A 5- series airfoil was chosen which is suitable for piston powered aircraft. The variation of airfoils and their characteristics is very wide, so similar aircraft were studied to guarantee a well-chosen performance in a similar mission like ours. Cessna variants with the same range and shape are the closest to our aircraft. NACA-23018 airfoil was chosen to be used in hyBIRD wing root which also agrees with the chosen thickness over chord ratio. For the tip we chose NACA-23012.

Figure 30 NACA-23018 Airfoil

Ailerons to wing area ratio was determined based on historical data from Roskam part II [18] which contains ratios for similar aircraft. It's better at that stage of design to accept this method. The wing area will affect the response of control action, which can be determined in a later stage of the design process. The ailerons and high lift devices are drawn to scale with respect to the wing in the following Figure (34)

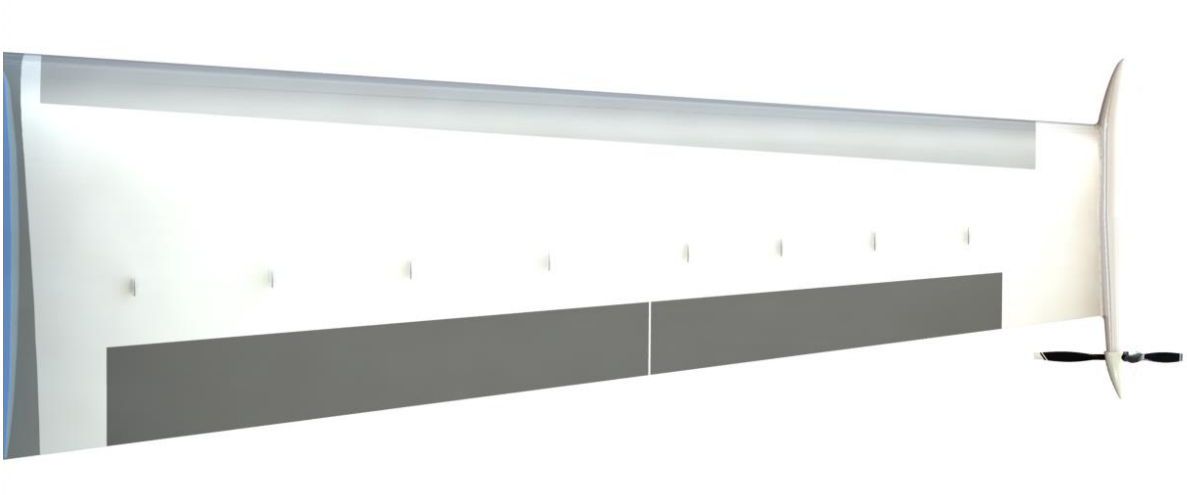

Figure 31 Top view of the wing and high-lift devices

6.12 High Lift Devices

It's been known in the aviation that to achieve high airspeeds, we need wings of small areas. The drag equation shows that the drag increases with increasing the wing area $D = \frac{1}{2} * \rho * V^2 * S * C_D$. And at the same time, we do need large wings area for low speed operations and landing and take-off since the large wing area means high lift force as per the lift equation $L = \frac{1}{2} * \rho * V^2 * S * C_L$. A solution for this is to reduce the wing area as much as possible to reduce the drag force and increase the lift forces by increasing the lift coefficient C_L. This solution was achieved through using mechanical devices called high lift devices that can be mounted on the wing to enhance the wing lift capabilities. So, we can summarize the purposes of enhancing the lift in four main points:

1. Enable the aircraft to fly at low airspeeds and, in turn, has access to shorter runways and more airports accordingly.
2. Improve the lift to drag ratio during the take-off.
3. Increase the drag forces during landing and make the landing easier.
4. Reduce the angle of attack near the maximum lift.

The purpose of the high lift devices is mainly to change the chamber of the wing airfoil and to delay the air separation. We are using passive trailing edge high lift devices only to increase the maximum lift coefficient and reduce the stall AOA too.

Among all the flap configurations, we chose to use Plain flaps for the following reasons:

1. Simple: works through rotation only without any translation.
2. Easiest to control
3. Easier and cheaper to manufacture

The plain flap causes a relatively low increase in the drag forces with deflection, especially for deflections in the $\pm$ 10 degrees range since it increases the airfoil camber and increases C_{Lmax} and reduced a_{stall} as a result.

The flap-to-cord ratio is 0.25. We oversized the flaps by 0.003.C. The main purpose of this oversizing is to help the air to stay attached to the airfoil surface and re-energize the boundary layer.

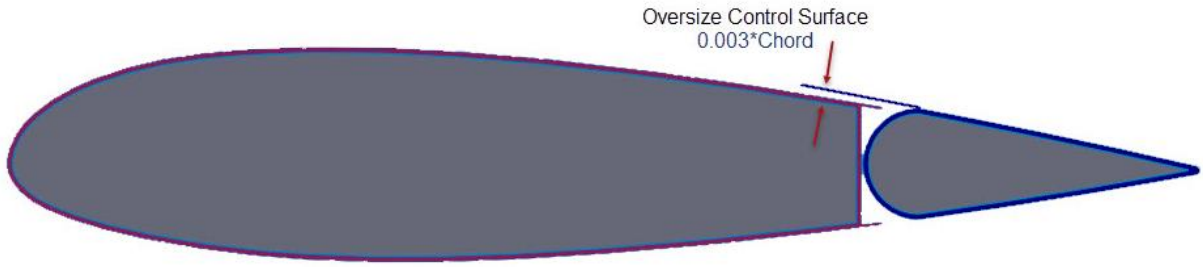

Figure 35 Oversized control surface/flap

The flaps have a maximum deflection angle of $\pm$ 40 degrees as shown in the following figure.

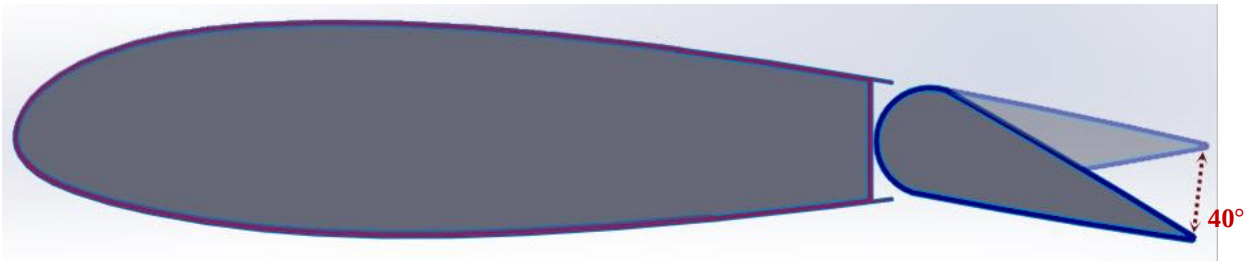

Figure 32 Maximum deflection flap angle

To test wether the increment of C_{Lmax} of the wing due to the flaps is sufficient to meet the required C_{Lmax} or not. From Roskam the required C_{Lmax} is **2.3** and the C_{Lmax} of the clean wing, without flaps, at take-off is **1.5**. The difference between those is what needed from the flaps (**=0.8**) which is achievable by our flap design.

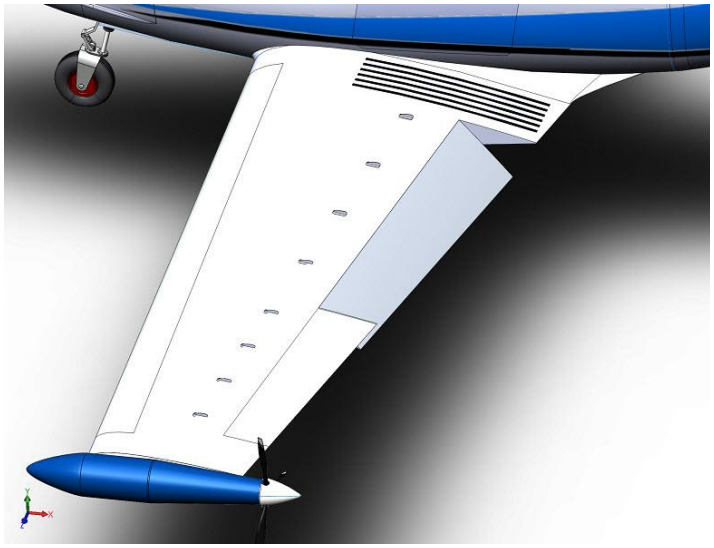

6.13 Empennage

The procedure suggested by Jan Roskam in his reference "Airplane Design", part II [18], chapter 8 for empennage sizing was adopted in our design. The configuration for the empennage for our design was already selected with the overall configuration down selection to be a V-Tail (Butterfly empennage). This was preferred for less drag as a result of less surfaces and also better placement of the control surfaces away from the aft stream of the motors. The method called "tail volume coefficient method" starts by determining the disposition of the empennage. That is the l_t or $X_{V,H}$, or namely, the empennage moment arm values calculated from the CG of the airplane. It's obvious that the larger the moment arm the better because this allows for less empennage area and hence less drag - assuming constant fuselage wet area.

The initial values of the empennage position are to be calculated from the general arrangement of the fuselage. In our design, these values are: $X_{V,H} =$ 5.13 m

The so-called the V-method then requires an initial value for the tail volume coefficient, which is defined as

$$V_h = x_h S_h / S\bar{c}$$

$$V_v = x_v S_v / Sb$$

For conventional tail configuration, suitable values for these coefficients can be found from historical data of similar airplanes. Using the twin-engine propeller-driven airplanes database provided in the same reference we can find a good average of these values to be $V_h = 0.786$ & $V_v = 0.0622$. Having determined the volume coefficients as well as the empennage positioning, the horizontal and vertical tails' areas can be calculated as $S_h = V_h S\bar{c}/x_h$

It should be noted though that the limiting case for vertical tail sizing is one engine out condition and for horizontal tail sizing is the trim at landing with full flaps deployed. In a later stage of the design, this limiting case was analyzed and found that our tail can only counter 15% of a tip-motor moment when the other motor is out. However, the main nose-motor will be able to satisfy FAR 23 EI requirements.

The results for S_h and S_v are 3.423 and 2.03 m^2 respectively.

Now migrating to the butterfly configuration, Roskam suggests that the resulting areas for the horizontal and vertical tails can be considered as projection areas for the V-tail and thus the area of the V-tail was calculated to be $S_v = 2\ m^2$. Furthermore, the tail dihedral angle can be calculated using the same principle as $\Gamma = \tan^{-1}(S_v/S_h) = 30.67°$

Finally, geometry characteristics including

a. Aspect ratio
b. Sweep angle
c. Tapering ratio
d. Airfoil
e. Incidence

Are to be initially estimated on the historical data of similar airplanes using the database provided in the main reference.

The aspect ratios of the horizontal tails of conventional twin-engine propeller-driven aircraft ranges between 3.7 and 7.7 with an average of 5.7. The vertical tails in turn have a range of 0.8 to 1.7 with an average of 1.25. For our V-tail a rough estimation can be obtained by further averaging these values to get **AR=3.5.** Using similar approach for the sweep angle for which the horizontal tail range 0-17 and average 8.5 degrees and for the vertical tail we have 18-45 range with 31.5 degrees of average. Thus, for our V-tail we choose **20 degrees sweep angle**.

Similarly, for the tapering ratio we have 0.48-1.0 of range for the horizontal tails of the same class of airplanes and 0.33-0.74 for the vertical tails. For the subject design we calculate **0.64 taper ratio.**

Tail airfoils are typically symmetric NACA airfoil in the range of 0009/0018. For our design, **NACA 0012** is chosen. Finally, a **zero incidence** is found to dominate the historical data and was adopted for initial value. Ruddervator sizing will follow the same procedure depending on the historical data which resulted in **40% of the tail area**.

6.14 Sizing Summary

The above initial estimates were adopted and were used to perform some performance and stability analyses iterations. These iterations were feeding back this initial sizing and modifying the values. After about three full iterations including several sub-iterations on some parameters only, the final empennage specs are summarized in the table below.

Table 14- tail detailed specs

Variable	Value	Unit
Area	1.8	m^2
Dihedral	40.0	degree
Aspect Ratio	3.0	-
Sweep Angle	10	degree
Taper Ratio	0.64	-
Airfoil	NACA 0012	-
Incidence	1.0	degree
Control surface area	40	%
Root Chord	0.945	m
Tip Chord	0.605	m
Span/2	2.32	m

7. Performance

7.1 Aerodynamics:

AVL: The aerodynamics analysis for the aircraft was done initially using AVL; which is a vortex lattice software that can quickly calculate lift and induced drag along any given wing-tail configuration. However, it is unable to simulate viscous or high Mach number flows. AVL results reported the values of the CD0, CD, CL, lift and drag forces. These results were used as initial values to validate our historical estimation and iterate and modify different configurations before performing the CFD analysis. AVL results will be discussed next in details.

Ansys Fluent: The CFD analysis of the aircraft was performed using Ansys Fluent. The analysis was performed on half the geometry of the aircraft to halve the calculation time. The flow field was an enclosure 7 times the length of the fuselage to capture the flow around the aircraft and the free stream conditions in the inlet. A tight mesh was generated taking into consideration the curvatures and the critical regions to fine the mesh at these positions. The boundary conditions were set up with cruise speed, static temperature and flow direction. The solver uses the energy equations with coupled implicit K-epsilon model with a stopping criteria of 1000 iterations. The analysis results are presented below.

Table 15: Aerodynamics results

M0	0.3228	CD	0.0453
Altitude	20,000 ft	CL	0.461
T0	248.5 K	L/D	10.176

The front and wing propellers were not included in the CFD therefore the tip motors' positive effects on aerodynamics are not included in these results. Consequently, the L/D is less than the expected value and the CD is larger due to the induced drag in this simplified configuration.

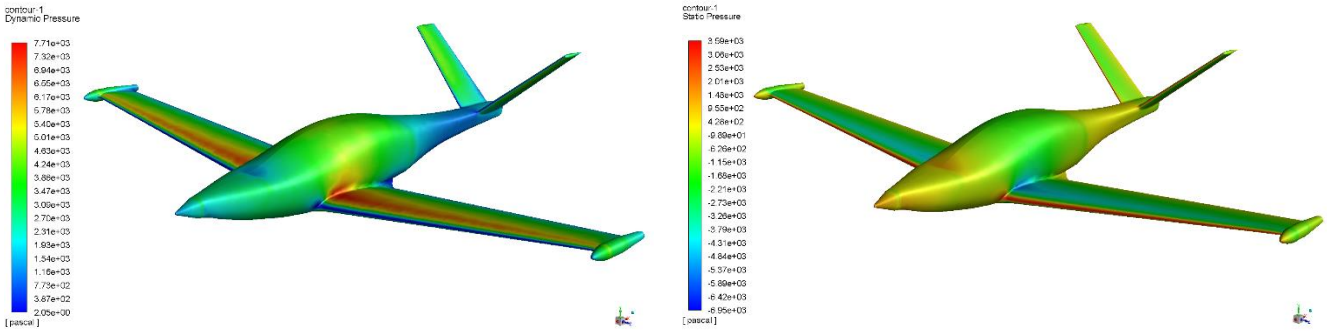

Figure 33: Dynamic and Static pressure distribution results respectively

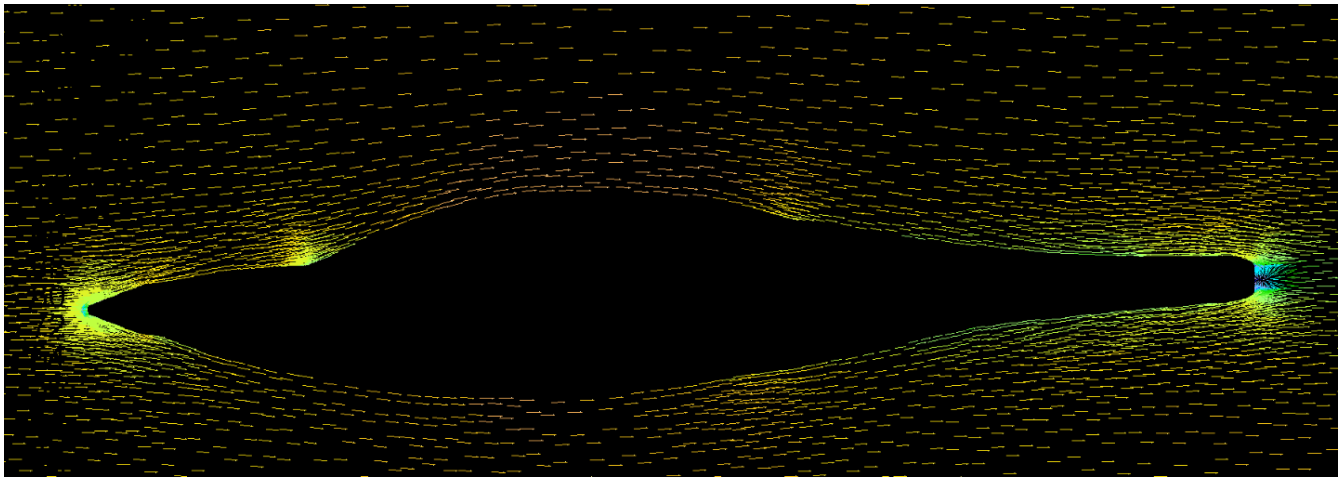

Figure 34: Fuselage cross-section velocity vectors

7.2 DRAG estimation:

The drag estimation for the hyBIRD aircraft was done by finding the individual drag increments of the aircraft components (Wing, V-tail, Fuselage and miscellaneous items). After considering the wing/fuselage interaction, skin friction coefficient, airfoil thickness location, thickness to chord ratio and wing exposed wetted area, the zero lift drag coefficient of the wing was found to be 0.0116. The vortex generator drag increment was calculated using Dr. Ron Barrett's thesis on vortex generator technology and the result shows that it would only contribute by 3 % of the zero lift drag coefficient of the wing because they are functioning mostly inside or near the boundary layer which don't significantly contribute to the drag.

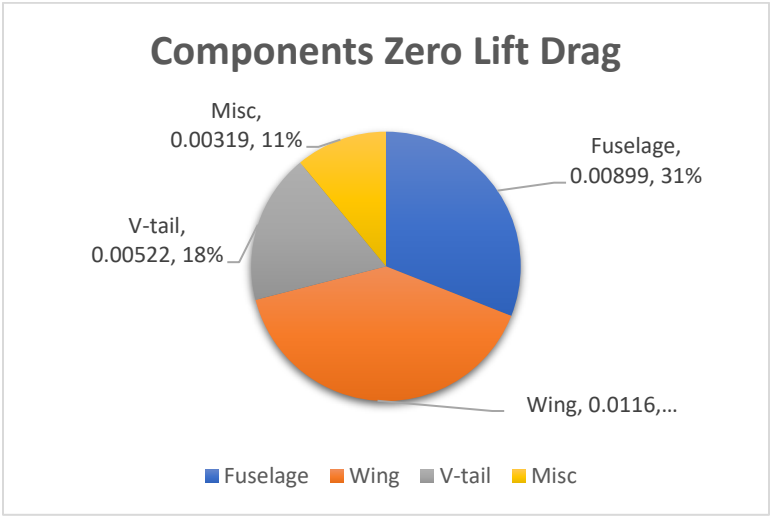

Figure 35: Component percentage contribution to drag coefficient

Following the drag estimation procedure for the fuselage, V-tail and utilizing the CAD geometry, their zero lift drag coefficient were found to be 0.00899 and 0.00522 respectively. Some other miscellaneous items such as fixed antennas, pitot tubes, ventral fins etc. were estimated to contribute with 11% to the total aircraft zero lift drag coefficient. Given that the total C_{D0} value was 0.029, Oswald efficiency factor was determined to be 0.85 and the aspect ratio was previously calculated to be 7.63, then the drag polar is calculated using the following equation.

$$C_D = C_{D0} + \frac{{C_L}^2}{\pi\, e\, AR}$$

Extending the flaps by 15 degrees and with the landing gear deployed in takeoff would increase the total drag coefficient by 0.0316 and extending to max position which is 40 degrees in landing will add another 0.0421. Using the previous values, the drag polar curve is plotted in Figure (39).

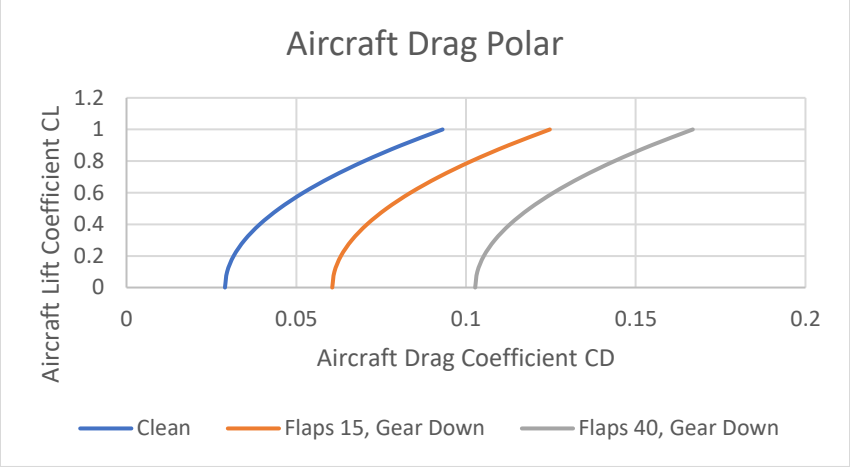

Figure 36: Drag polar

7.3 Take-off and Landing Performance:

The RFP requested the aircraft 4-seater and 6-seater versions to have maximum takeoff and landing field lengths of 1,500 ft and 1800 respectively over a 50 ft obstacle to a runway with dry pavement. Take off performance was calculated using the following equation from [17].

$$S_{Takeoff} = \frac{1.44\, W^2}{\rho\, g\, S_{wing}\, C_{L\,max}\, [\, T - (D + \mu_{Static}(W - L)_{average}]}$$

The value of the rolling friction was changed to simulate different runway conditions and max takeoff weight was used with $V_{Takeoff} = 1.2\, V_{stall}$ to generate the following graph.

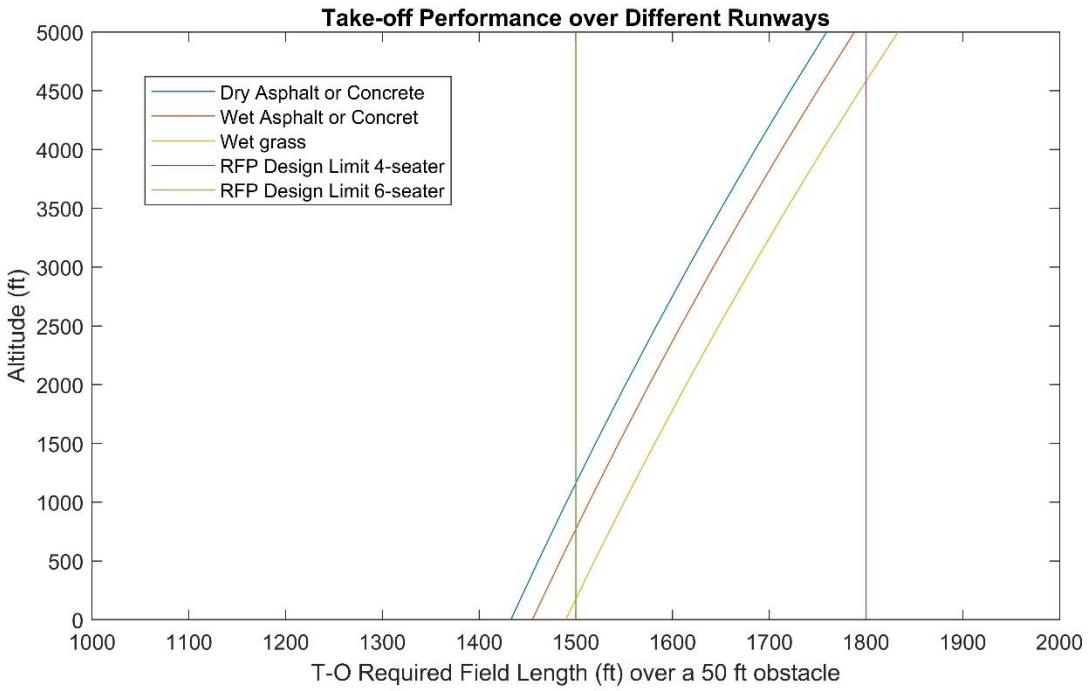

Figure 37: Takeoff performance

The aircraft was performing well for all versions and the performance exceeded what was required by the RFP. The landing performance was evaluated assuming brakes would be applied, $V_{Landing} = 1.3\, V_{stall}$, rolling friction altered and the landing distance was calculated using the following equation from [17].

$$S_{Landing} = \frac{1.69\, W^2}{\rho\, g\, S_{wing}\, C_{L\,max}\, [\, D + \mu_{Dynamic}(W - L)_{average} + 0.25\, T_{max}]}$$

The electric motors on wing tips can be used as a thrust reverse in order to enhance the landing distance of the aircraft and accommodate for any yawing moment caused by crosswind with the guidence of the control augmentation system. The term $0.25\, T_{max}$ was used to express using 25% thrust reverse in the previous equation.

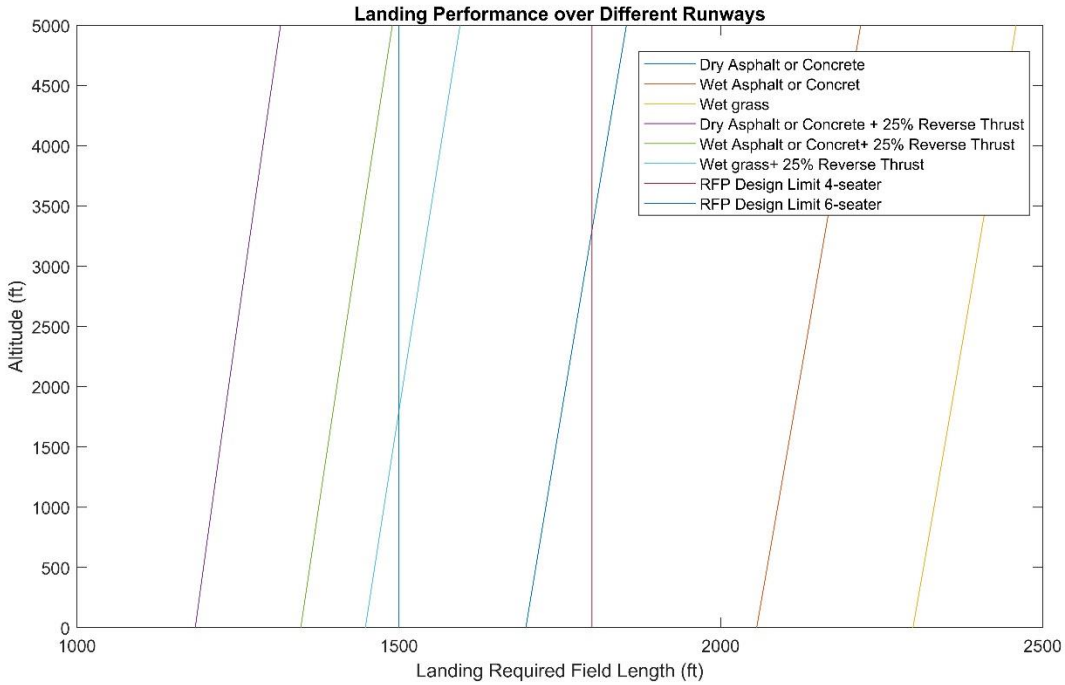

Figure 38: Landing performance

7.4 Climb Performance:

Climb performance was evaluated using the following equation from [17].

$$ROC = \frac{P_{available} - P_{required}}{W}$$

Both aircraft climb performance was verified and tabulated in the following table:

Table 16: Climb performance

	Verified Climb Rate	RFP requirements
hyBIRD 4-seater Aircraft	1629 ft/min	> 1500 ft/min
hyBIRD 6-seater Aircraft	1573 ft/min	> 1300 ft/min

The results showed that the RFP requirements were exceeded for the 4-seater and 6-seater aircraft.

7.5 Range:

The RFP requested the aircraft's 4-seater and 6-seater versions to have 1000 and 750 nm respectively as an IFR range profile. This requirement was met by both aircraft. Using Breguet equation, the payload-range diagrams for both aircraft as well as the extended range version were generated.

- **hB600:**

A) Point A is defined by operating the aircraft with max payload of 6 passengers and their baggage as required by the RFP with no fuel onboard and zero range.

B) Point B is defined by having 551 lb fuel onboard with maximum payload and harmonic range of 750 nm as declared in the RFP while achieving maximum takeoff weight.

C) In point C, the payload of 324 lb is traded for fuel until maximum fuel capacity of 877 lb is reached. 1550 nm is reached while achieving maximum takeoff weight.

D) In point D, the payload of 804 lb is removed (the 5 passengers were completely removed by this step) without more increase in fuel and a range of 1900 nm is achieved.

E) In Point E, the pilot payload is removed and no more gain in range is achieved (ferry range)

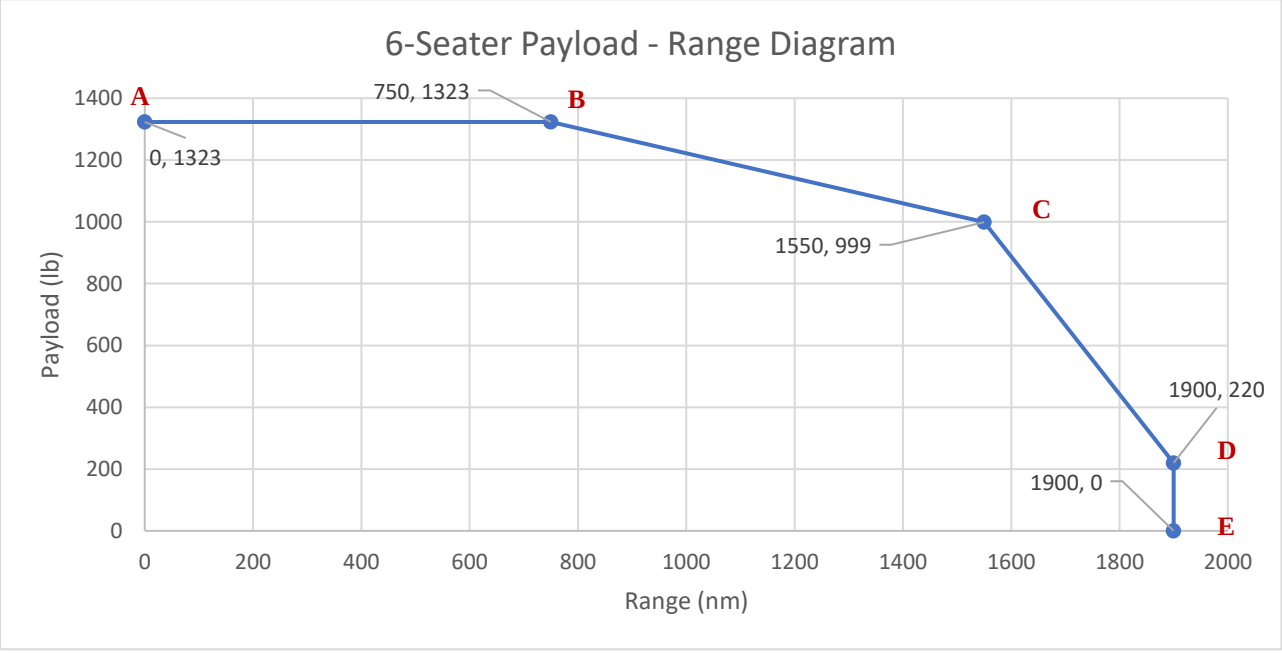

Figure 39 - 6-Seater Payload Range Diagram

- **hB400:**

A) Point A is defined by operating the aircraft with max payload of 4 passengers and their baggage as required by the RFP with no fuel onboard and zero range.

B) Point B is defined by having 705 lb fuel onboard with maximum payload and harmonic range of 1000 nm is achieved as required by the RFP while not reaching maximum takeoff weight.

C) In point C, the maximum takeoff weight is reached by having 100 lb more fuel in the wing tanks and this achieves a range of 1200 nm.

D) In point D, the payload of 172 lb is traded for fuel until maximum fuel capacity of 877 lb is reached. 1600 nm is reached while achieving maximum takeoff weight.

E) In point D, the payload of 488 lb is removed (the 3 passengers were completely removed by this step) without more increase in fuel and a range of 1900 nm is achieved.

F) In Point E, the pilot payload is removed and no more gain in range is achieved (ferry range)

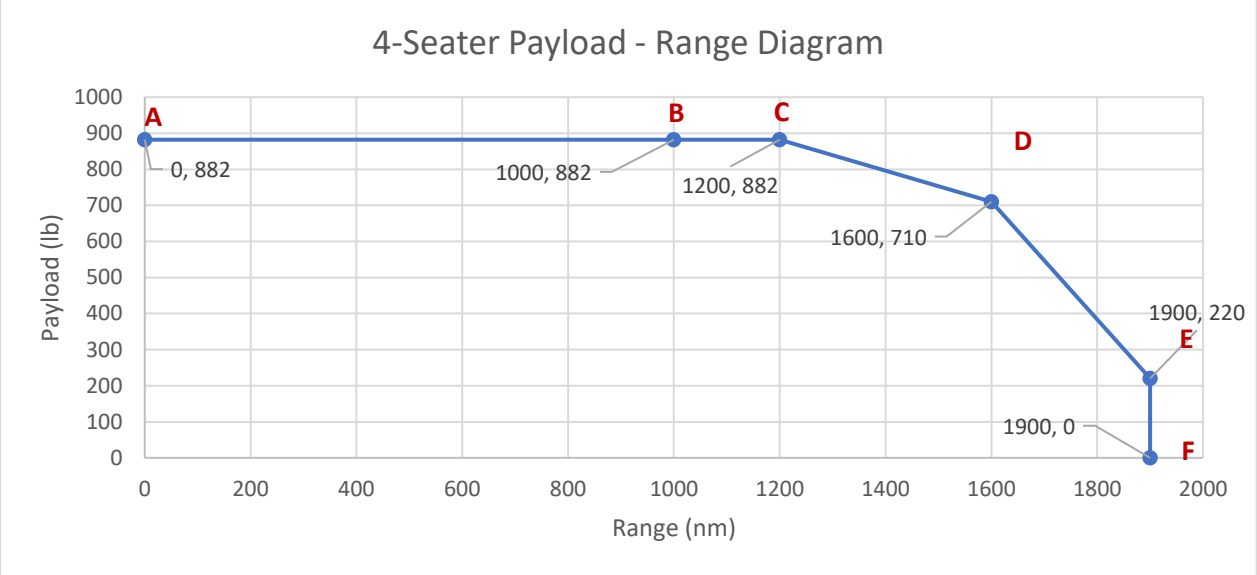

Figure 40 4-Seater Payload Range Diagram

- **hB400-ER:**

A) Point A is defined by operating the aircraft with max payload of 4 passengers and their baggage with no fuel onboard and zero range.

B) Point B is defined by having 705 lb fuel onboard with maximum payload and harmonic range of 1000 nm is achieved as required by the RFP while not reaching maximum takeoff weight.

C) In point C, the maximum takeoff weight is reached by having 100 lb more fuel in the wing tanks and this achieves a range of 1200 nm and reaching maximum takeoff weight.

D) In point D, the payload of 677 lb (3 passengers were completely removed by this step) is traded for fuel until maximum fuel capacity of 1486 lb is reached (874 lb in wing tanks and 608 lb in the fuselage auxiliary tank). 3200 nm is reached while achieving maximum takeoff weight.

E) In Point E, the pilot payload is removed and no more gain in range is achieved (ferry range)

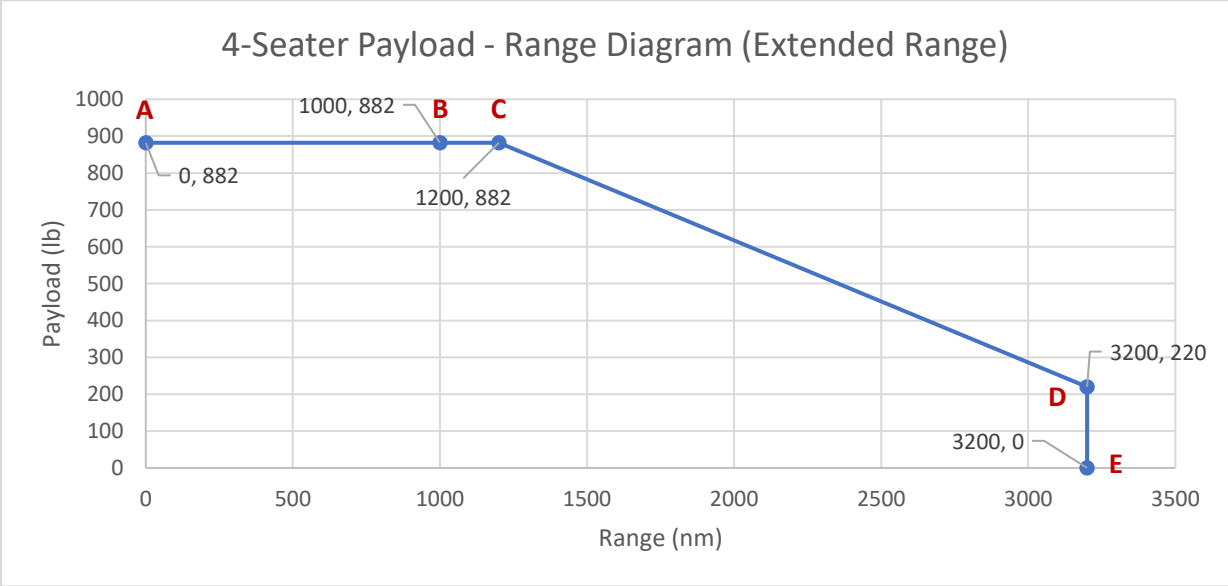

Figure 41 - 4-Seater ER Payload Range Diagram

To ensure compliance with the RFP, the cargo space for both aircraft was designed to exceed the requirement of 0.68 m^3.

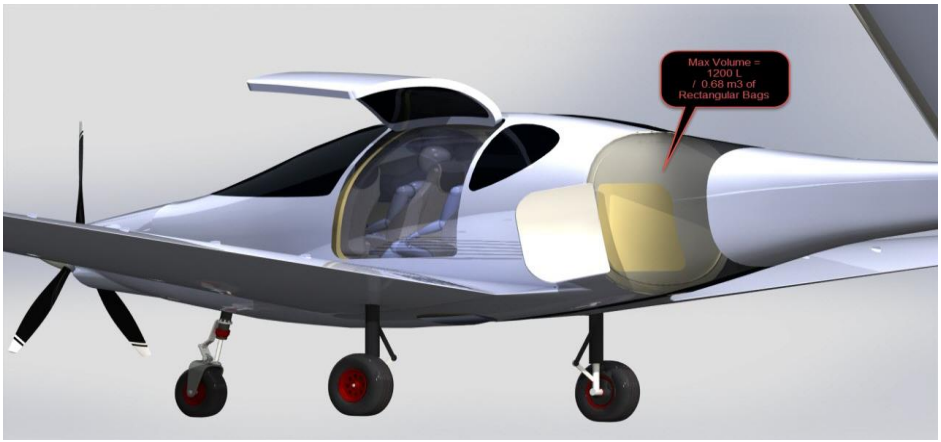

Figure 42: Cargo capacity

7.6 V-N Diagram

Aircraft is subjected to different types of loads. The major load is the inertial load which the aircraft must be able to endure. A V-n diagram was constructed according to the FAR 23 requirements. Roskam's methodology in "Airplane Design" part V was followed [15]. The gust wind speed is put at cruise speed of 174 knots and dive speed of nearly 244 knots at both sea level and flight level 200. The diagram was constructed based on the six-seater variant, which guarantees the structural integrity of the lighter variant as the wing is used in common. It shows the operational constraints on the two variants in terms of loading.

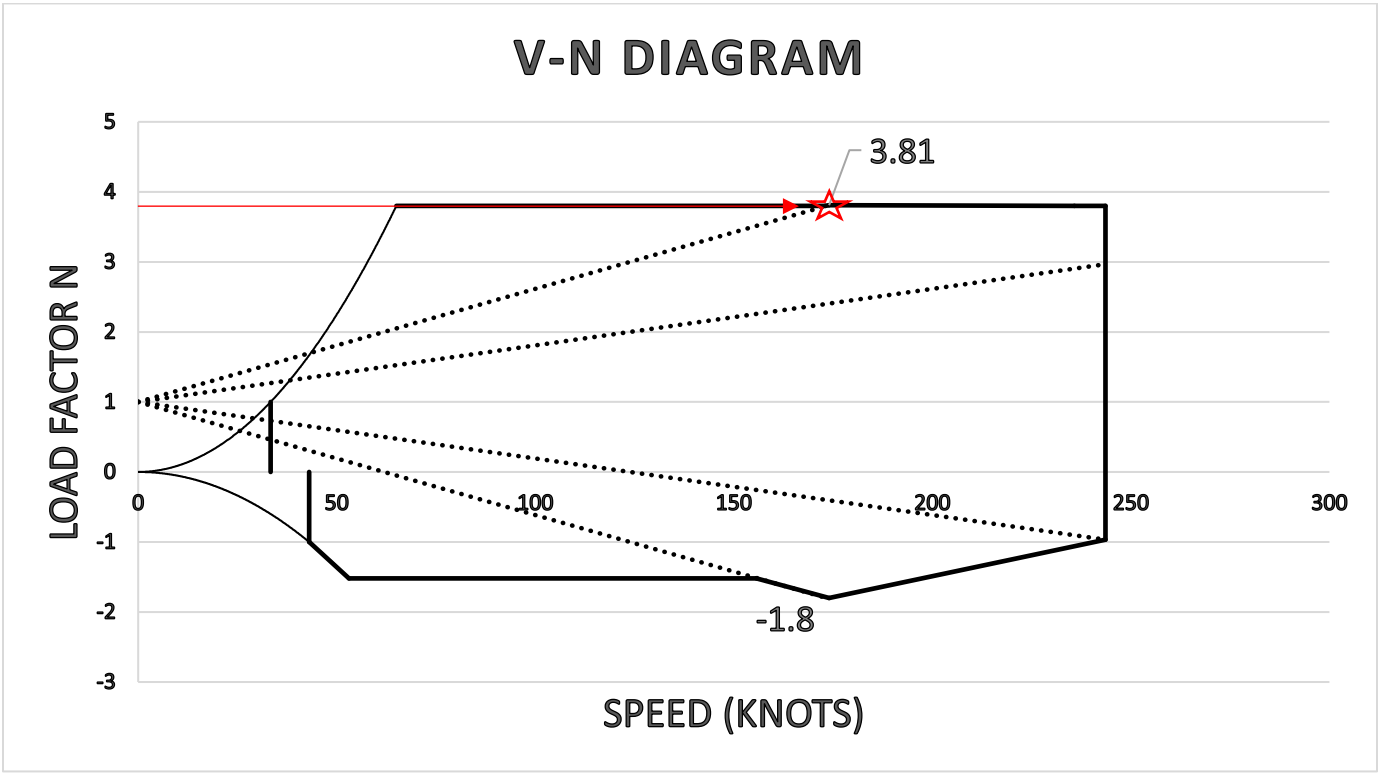

Figure 43 – VN diagram

8. Structure and Materials

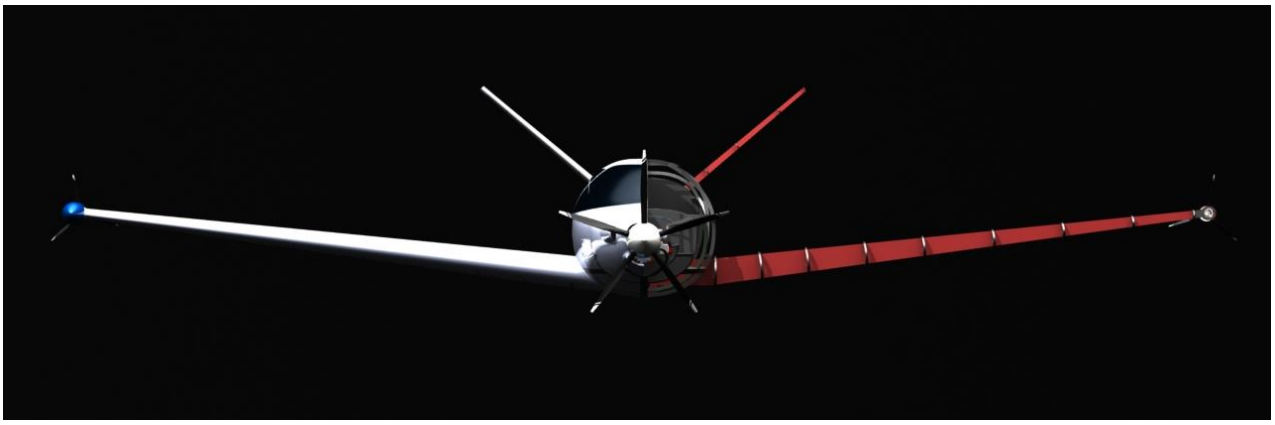

8.1 Material Selection

When it comes to aircraft design, important decisions are made in that early stage of planning. Those decisions will change the route of thinking for some design aspects. Material selection is one of those decisions. A hybrid aircraft target is to minimize the power consumption and reduce emissions. So, using composite materials were considered which allows having the same performance with much less weight. The disadvantage of composites, however, is the high manufacturing and maintenance cost.

The aircraft is divided into four main parts, fuselage, wings, empennage and undercarriage. Fuselage is the largest part spatially and in weight perspective. Thus, it should need fewer component changes and maintenance alterations in the future. Which makes it perfect for the usage of composite materials to enhance the total aircraft performance. A carbon fiber reinforced polymer composite with epoxy resin was chosen. A sandwich structure will form the stiffeners, rings and skin panels. It is highly resistive to rupture, have good fatigue strength and small specific mass.

Wings and empennage are carrying huge load aerodynamically and structurally. They need to be optimized carefully to endure these loads. Conventional metallic structures have a huge weight penalty compared to composites. High technology is used to make carbon fiber sheets and assemble them into layers which enhance their strength and capabilities. The structure will be optimized side by side with the manufacturing of each part of the wing and empennage. This will make use of the orthotropic nature of carbon fiber allowing for variable stiffness in different directions. Loads will be determined, and the manufacturing will be optimized to carry these loads with the minimum

weight penalty. A core material would be used in some structures like ribs and spars to enhance the materials. Generally, the addition of core with carbon fiber increases material stiffness on the expense of manufacturing flexibility. However, only rips and spars, which are simple structures with few curves and complexity, are chosen to be sandwiches.

The landing gears, on a different level, experience extremely high impact loads in short times. It must carry the entire weight of the aircraft during on land and taxiing while minimizing their size and weight. It requires a material with high toughness and strength. A survey was done to find the best material to use. The result was a special alloy of steel and titanium. So, the landing gears would be made of steel 300M alloy which can handle such stresses.

8.2 Wing Structure and Analysis:

We decided to use cantilevered low wing due to advantages regarding maintenance and ground operations, accommodating maximum cabin space for passenger comfort, and incorporating dihedral to increase stability. It also has the advantage of avoiding interference drag resulting from using external structural elements as braces or struts. The wing must handle the bending moment and shear forces resulting from the distribution of force on the airfoil and wing span. Double spar arrangement is used with a C-beam cross section which is commonly used in such applications. Beams are designed and specially made to totally fit the wing angles, namely; dihedral, sweep and twist. While using composite structures in most of the wing metallic reinforcements are necessary at spar ends to make the wing-fuselage attachment. Each spar is fixed to a ring using titanium bolts in a way that guarantees the right load transmission. Spar locations are 20% and 75% of the chord. The main spar is put at 20% to handle the tremendous lift load which act on the wing near quarter chord position. The secondary spar at 75% is determined by the control surfaces limitation. The control surfaces, and their actuation systems, are linked to that secondary spar as well. The wing structural layout can be seen on figure (47).

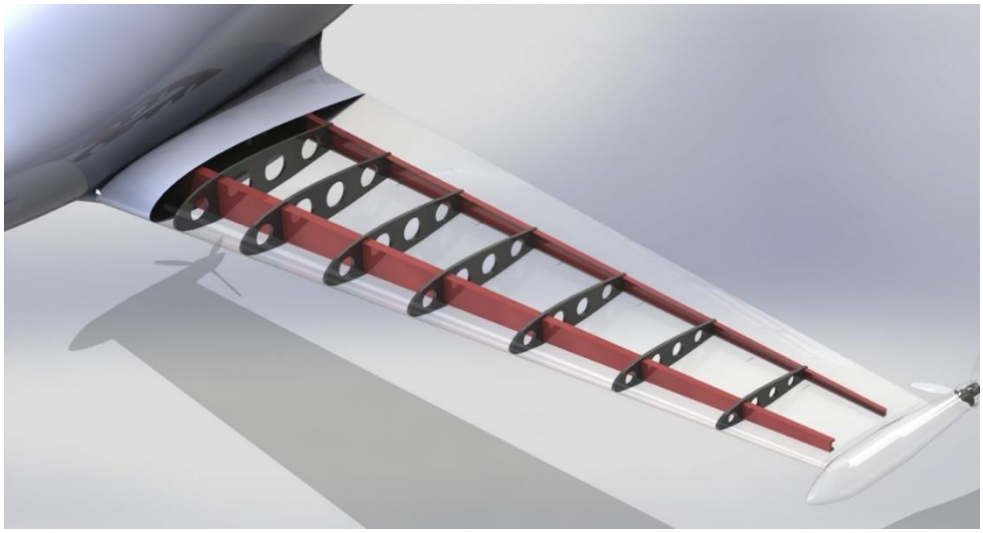

Figure 44:Wing structure

Skin is made of multiple layers of carbon fibers to handle the aerodynamic load acting on it. The skin must maintain the aerodynamic shape all over the V-n diagram margin. Also, the buckling criteria in case of going above the allowed load must be a fail-safe scenario. Ribs are made with thicker core material of foam and carbon. They must handle the shear stress coming from torsion and transmit the loads from skin to spars which are the real load carrying elements. Ribs conserve the aerodynamic shape of the skin as well. Their spacing is determined upon history and opinions of industry engineers and experts. The spacing was variable between different regions of the wing as inboard spacing is less than outboard spacing. The spacing data can be found on table (17):

Table 17

Wing structural layout	
Inboard rib spacing	20 inches
Middle board rib spacing	25 inches
Outboard rib spacing	30 inches
Front spar location	20 % chord
Rear spar location	75 % chord

Wing is treated as one body structure and put under the test using ANSYS Composite ACP and static structural and buckling modules. The maximum load that can happen is when the wing reaches maximum loading factor which is equal to 3.8 times the weight of the aircraft. Wing loads, including fuel, batteries and wing weights, as well as tip

motors thrust loads, are approximated and put as a concentrated load acting on fixation points. To guarantee accurate results the load is taken from a CFD analysis on the wing on a higher speed to get the same load as the loading factor. Then results are put as an input to the static analysis. Fixations are defined at the end plates of the spar roots as if it's fixed to the fuselage already.

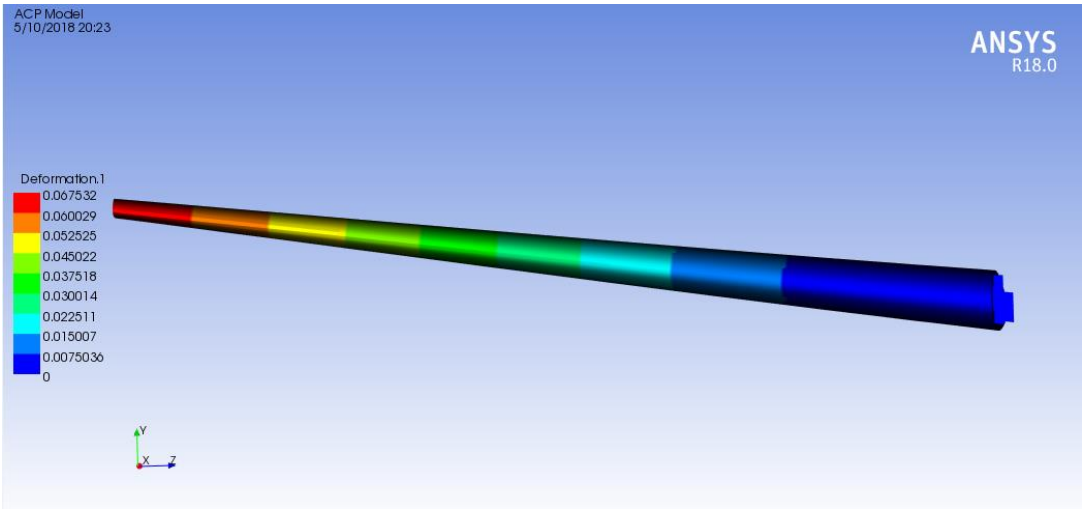

Figure 45: Structure deflection

The results were promising as the deformations were small and acceptable for this class of aircraft as shown in figure (48) . Several failure criteria, such as core failure and Tsai-Wu failure, were tested using ANSYS ACP. Tsai-Wu failure criteria was used to evaluate the possible failures of the structure such as crack, core failure and delamination. The results showed a minimum safety factor of 2 in the outer carbon ply which is a critical layer. Figure (49) describes the failure safety:

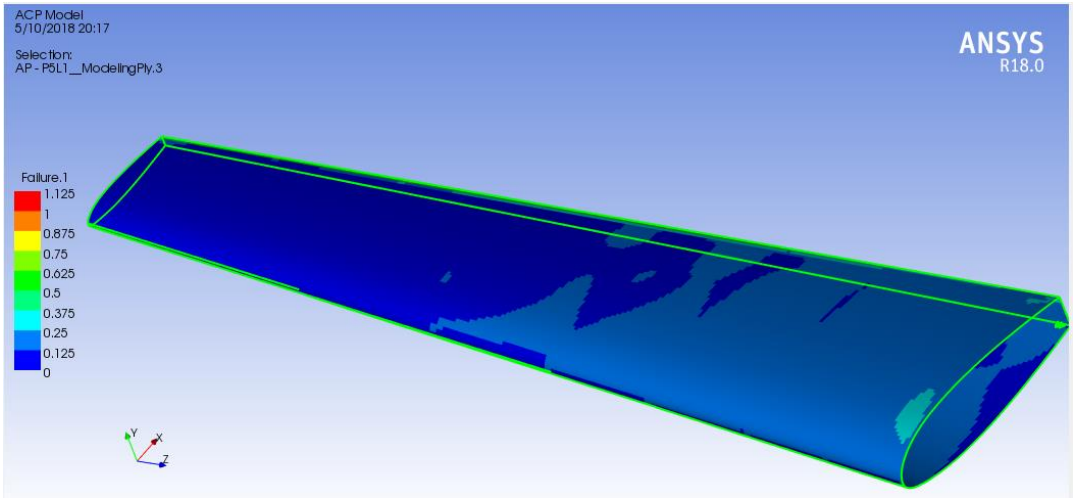

Figure 46: Tsai-Wu Failure test results

Maximum stress is found to be way below the allowable stress for the carbon fibers and sandwich structures for both normal stress and shear stress. Figures (50 & 51) show the maximum shear and equivalent stresses simulated by ANSYS.

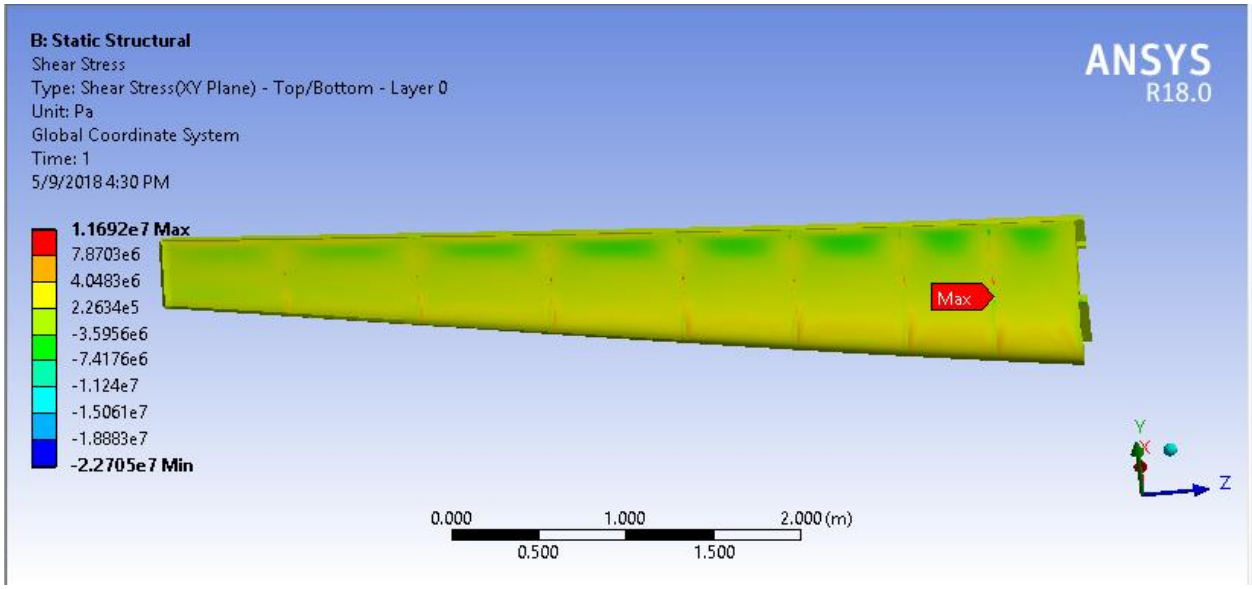

Figure 47: Shear stress

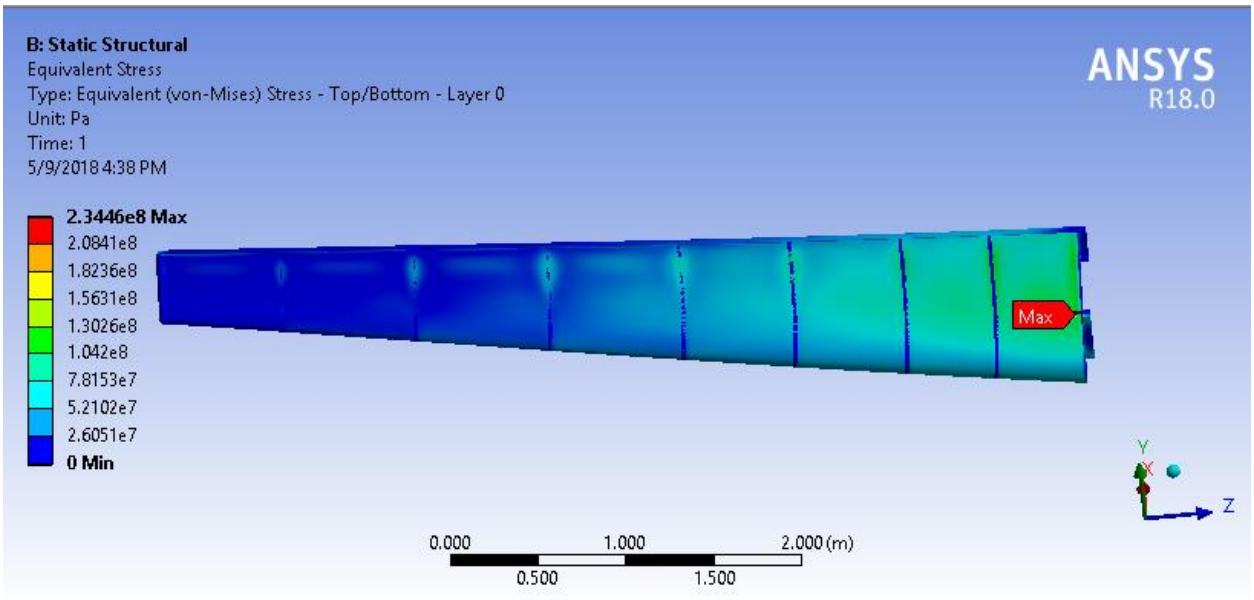

Figure 48: Equivalent stresses

Table (15) summarizes epoxy carbon fiber woven (395 GPa) prepreg properties to compare and ensure the safety of the wing structure. The properties are aligned with the stacking directions:

Table 18: Epoxy carbon fiber properties

Young's modulus X, Z directions	92000 MPa
Shear modulus XZ	19500 MPa
Tensile strength X direction	829 MPa
Tensile strength Z direction	829 MPa
Compressive strength X direction	-439 MPa
compressive strength Z direction	-439 MPa
Shear strength XZ	120 MPa
Shear strength YZ, XZ	50 MPa

*hy*BIRD empennage is chosen to be a V-tail configuration which makes the structural design very similar to the wing structural. The tail is made of the same materials with less thickness as the loads on the tail are less. The initial values for rib spacing are taken from historical data for similar aircraft. Table (19) describes the structural layout of the tail:

Table 19

V tail structural layout	
Inboard rib spacing	12 inches
Middle board rib spacing	18 inches
Outboard rib spacing	25 inches
Front spar location	20 % chord
Rear spar location	60 % chord

8.3 Fuselage Structure

The structural design of fuselage starts with the understanding of the applied loads. The limiting case of maximum loading come from pressurization. Two bulkheads are installed at both ends of the cabin to make the empty space in between similar in shape to a cylinder. Rings and longerons are arranged with a spacing which can contain the pressurization load on the walls. Wing attachment is reinforced with stronger rings which are connected to the main spars.

the material we decided to use is carbon fiber-based structures with titanium alloy bolts and blind rivets. Stiffeners are made from honeycomb core with unidirectional carbon fibers which enhance the limit load and buckling behavior resulting in less members compared to metal passed structures. Skin panels consists of several woven carbon fiber layers stacked in different directions. This will contain the pressurization and enhance the structural integrity of the fuselage. *hy*BIRD fuselage contains high curvatures with several windows which reduces the space for stiffening elements. This made the design closer to a space frame chassis in which the spacing between elements vary widely as shown in figure (52):

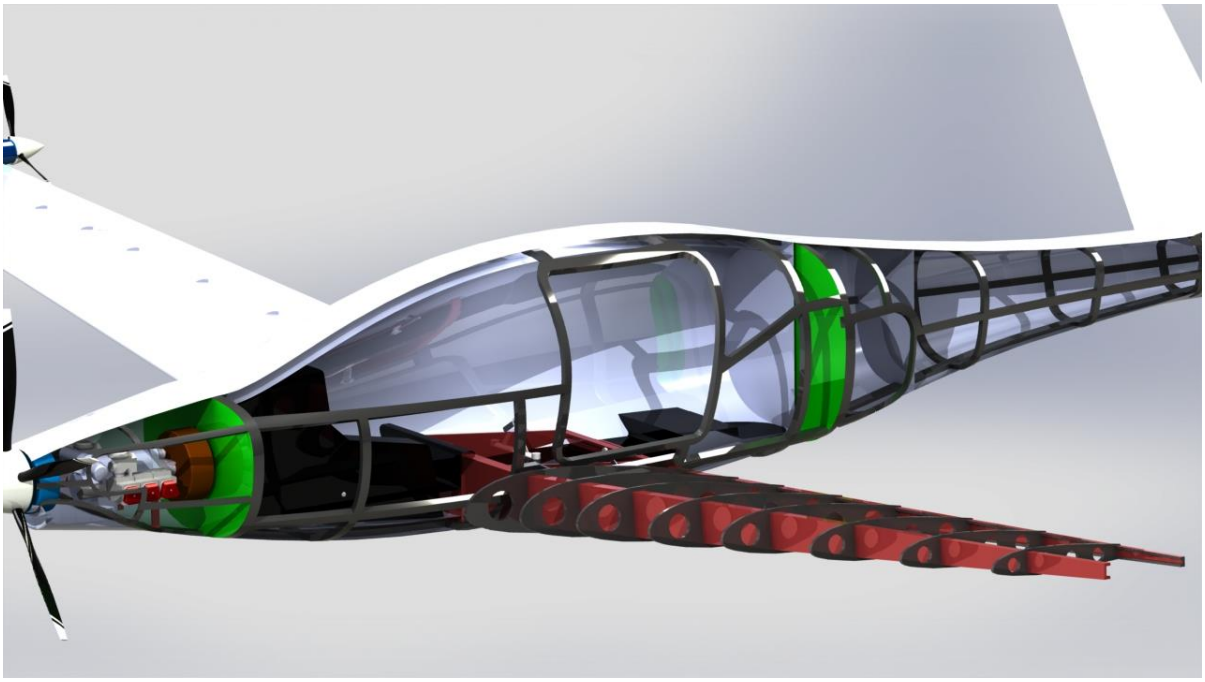

Figure 49: Fuselage and wing structure

Manufacturing an aircraft fuselage is not an easy task. To reduce the complexity and accessibility of fuselage it was decided to divide the fuselage into three parts, the engine front part, middle cabin and the tail boom. Those three

parts are manufactured separately and then assembled together at the last stage of the assembly line. That will enhance the ability to alter the common parts between variants. In other words, a single fuselage could be used for the four-seater or six-seater.

8.4 Landing Gear

In order to save cost and solve complexity issues, we designed the landing gear system to fit for the 6-seater version of our aircraft family since it's heavier which results in higher landing loads and, by default, this will work for the 4-seater version too which would increase the commonality. Tricycle and taildragger are the most common two landing gear arrangements (both are used in 99.5% of all aircraft). Each of these two arrangements has its pros and cons. The comparison between both arrangements is summarized in Table (20).

Table 20 Comparison between Tricycle and Taildragger arrangements

Tricycle (hyBIRD)	Taildragger
Dynamically stable, easier to maneuver	Dynamically unstable, harder to maneuver
Good ground control in crosswinds	Poor directional control with strong crosswinds
Good forward visibility because of low deck angle	Poor forward visibility because of high deck angle
Easier to land	Harder to land
Propeller is protected from ground strike	Propeller strike is possible
Good acceleration during T-O due to lower AOA	Slower acceleration during T-O due to higher AOA

We decided to use the tricycle configuration for our landing gear. Tricycle still has some cons that we considered when designing the gears. Table (21) shows those cons and how we approached them.

Table 21 Tricycle cons and our solutions to them

Problem	Solution
Requires minimum airspeed before T-O rotation	hyBIRD goes faster than that minimum airspeed
Higher structural weight and cruise drag	5s retraction time and 8s deployment time (electric actuation)
Nosewheel shimmy	Added a shimmy absorber
High dynamic ground loads	Considered nose-wheel design
Complex steering mechanism	Actuation through electric motors makes it easier

The actuation mechanism, doors, and support structure are designed so that the actuation can work at gross weight and at 1.15 of the cruise speed (200 knots). The nose landing gear is positioned so it can carry about 18% of the aircraft weight when the CG is at the forward limit, and about 9% when the CG is at the aft limit. We are using also disc brakes in the main wheels since they are lighter and easier to maintain than drum brakes and will be electrically actuated. We considered all the common possible landing gears issues like Shimmy, Whistling, and non-linear loads when selecting and designing its components.

We are using solid rubber tires, forged aluminum wheels as they are less expensive and have better corrosion resistance. The inflation pressure of the landing tires is selected based on the aircraft weight, number of tires and the bearing capability as shown in Table (22). After surveying all the possible vendors for the landing gears, we chose Aircraft Spruce, Grove, Wicks Aircraft as the possible vendors to purchase the whole custom landing gear system.

Table 22 Landing gear tire information

	Tire Type	Inflation Pressure	Main Tire Size
Nose Wheel	Three Part Type	80 psi	12.5.00-4.5 in
Main Wheel	Three Part Type	265 psi	20.00-5.5 in

The position of the main landing gear was determined through the following methodology shown in figure (53)

50. Positioning of the Main Landing Gear

The main landing gear is a two-wheel suspension system. Each wheel has one tire per strut with an oleo shock absorber and a trailing link which makes the main gear perfect for paved and unpaved surfaces as shown in Figure (55). While the nose wheel consists of a single wheel with single tire and an oleo shock absorber as shown in the same

figure. The main landing gears retract to the fuselage body then the doors close so that only the tires are not covered as shown in figure (54) where the nose wheel retracts to the nose body.

Figure 51: Landing gear design

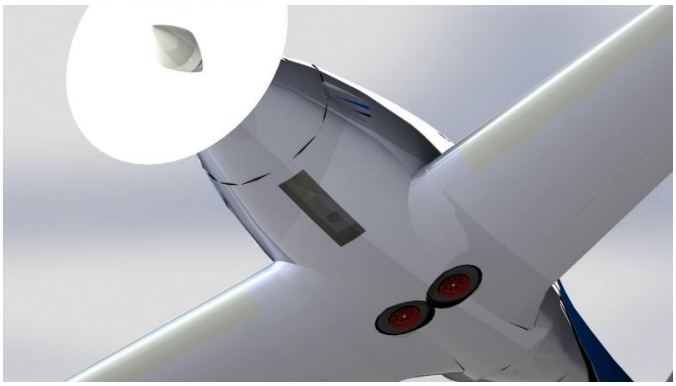

Figure 52: Retracted gear

9. Manufacturing

Manufacturing process is one of the most important stages in aircraft industry. It affects the final cost and quality of the product. Since the manufacturing is the last step before realizing the final product, it's expected to be around the year 2025 or later. Advancements of manufacturing technologies and methods can be expected to be available. Costs of current manufacturing processes are also expected be reduced. In this design, composites structures and materials are used frequently to reduce weight and increase the reliability. So much so, the complexity and cost penalties of such design decision are to be reduced by future projection of the manufacturing time.

The manufacturing process will consist of several steps from the raw material to a ready to fly unit. The following few steps summarize the process:

1. Manufacturing separate components from raw materials (sheets, beams and cut sections)
2. Fuselage, wing and empennage assembly from sub components.
3. Final assembly of the main parts.

4. Quality check and control.
5. Finishing and testing.

Manufacturing process will include two main types, inhouse manufacturing and out-sourcing. Out-sources will be used for equipment, tools and special technology manufacturing techniques. For example, wing and empennage require special methods to get the best surface finish and quality without compromising their structural stiffness. Those specialized tasks would be distracting and draining for the aircraft manufacturer man power and resources. It is much more suitable to our-source such parts with quality assurance supervision on the supplier.

The wing will be assembled as one part. Starting with the ribs and spars which are more like a chassis for the aerodynamical load carrying skin. Spars and ribs are made as a sandwich structure with a PVC foam core and few layers of high stiffness carbon fibers. They are cured together to get the maximum bonding stiffness. Upper skin is made afterwards and cured to the assembly. Then the wing is sealed and equipped with the fuel tanks and connections. Afterwards, the lower skin will be cured after to the whole assembly taking into consideration accessibility, inspection and service windows to continue installing the needed equipment like de-icing devices and actuators. The last steps for the wing is installing the main gear, applying the electrically conducting coating layer on the carbon fiber skin, then performing inspection and testing. The wing manufacturing process is summarized in the chart of figure (56).

The fuselage will be manufactured inhouse to reduce the cost and assure quality. This also allows for the release and testing of different model and features. It will be assembled from three main sections. Those sections are made from composite materials. A core material like PVC foam of honeycomb will be used with few layers of carbon fibers to build fundamental parts. The thickness of layers will differ between skin, longerons and rings. High quality alloys like aluminum 7075 will be used to make the doors and windows fittings. A special structure will be made from the same alloy to enhance motor fixation stability and isolation. After front part, cabin and the boom are finished they will be mated together with proper fixations of titanium bolts and fittings to make service easier. Cabin is sealed due to pressurization and in order to increase safety. Bulkheads on the cabin ends are made of sandwich structures with a metal core material of aluminum 7075 to handle large shock loadings. Doors, windows, chairs and avionics are assembled to the full fuselage. The last step is to test and inspect to ensure acceptable quality. Figure (57) and (58) describe fuselage manufacturing.

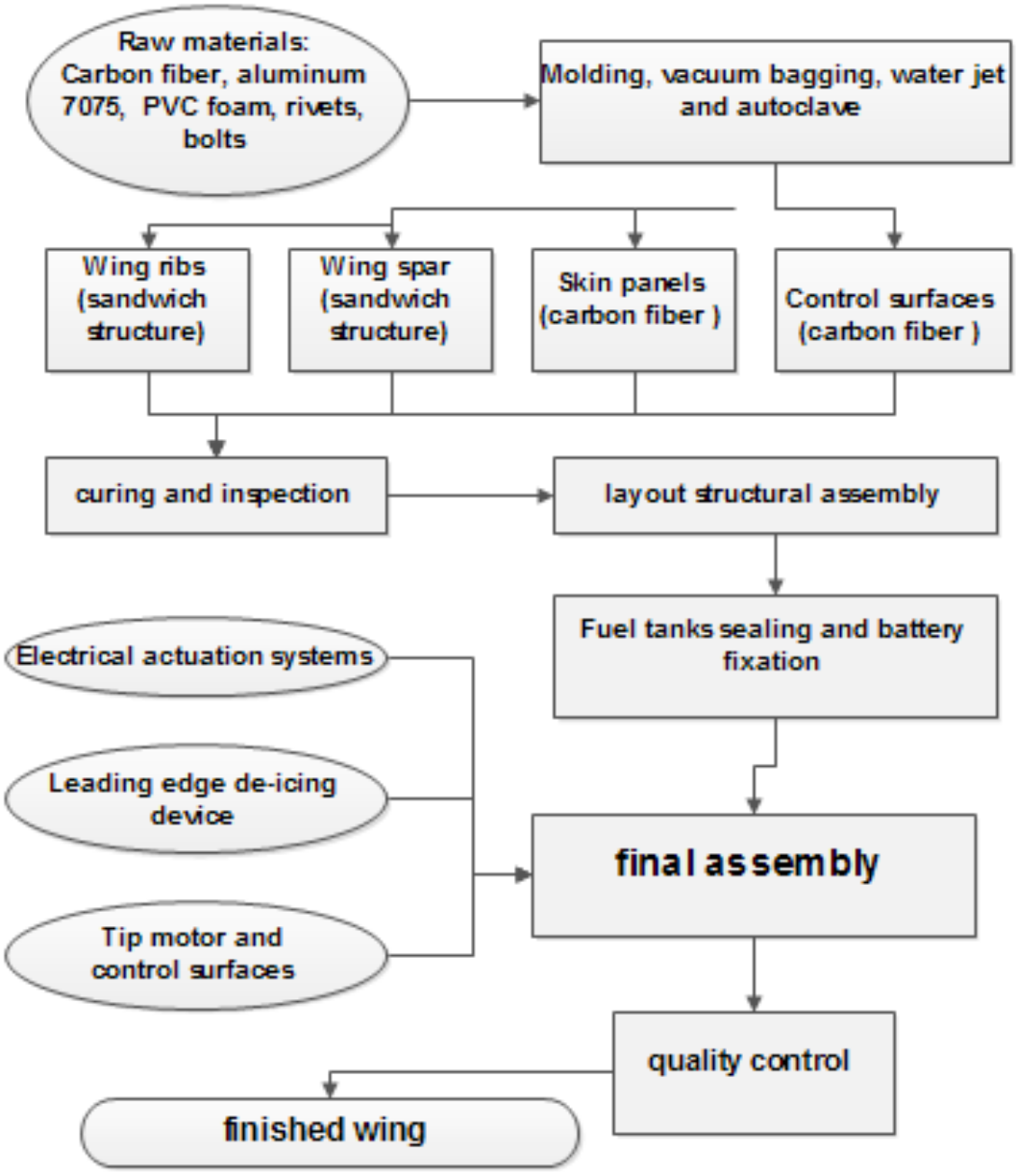

Figure 53:Wing manufacturing scheme

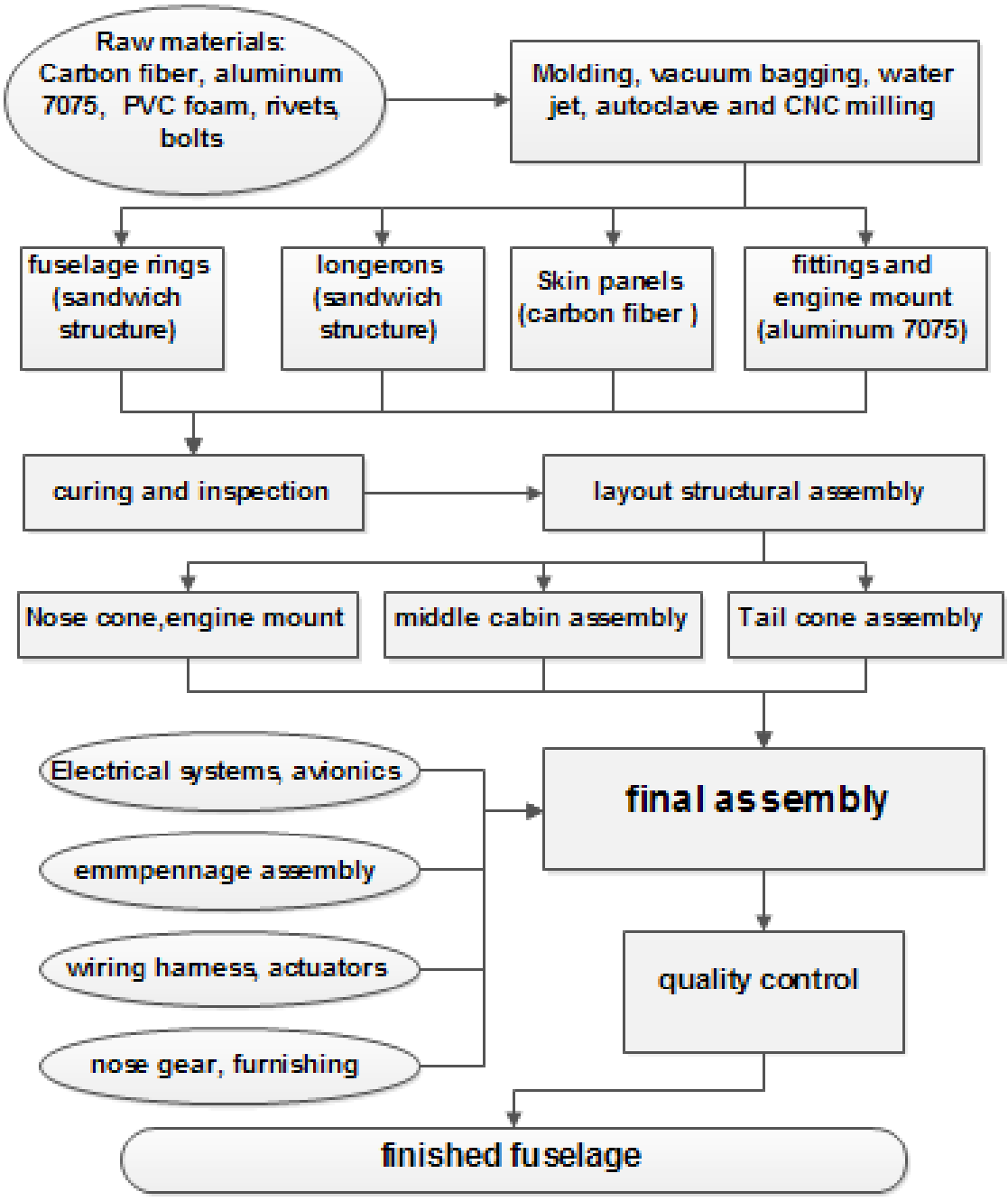

Figure 54: Fuselage manufacturing scheme

The assembly process continues after that with the attachment of both wings under the fuselage using attachment points that secure the spars to fuselage reinforced rings. Nickel alloys and high-quality steel will be used to manufacture the attachment bolts. Engine will be secured to the frame inside the nose compartment. When final assembly is complete the aircraft is transferred to testing facility where careful inspections are done to insure ultimate quality and safety. Ground testing is done to make certain of the reliability of every system and the correct integration between them. Afterwards the skin is fully fixed, painted and polished to get the perfect surface finish. The interior furniture is the last thing to be installed in cooperation with the customer who can customize his aircraft.

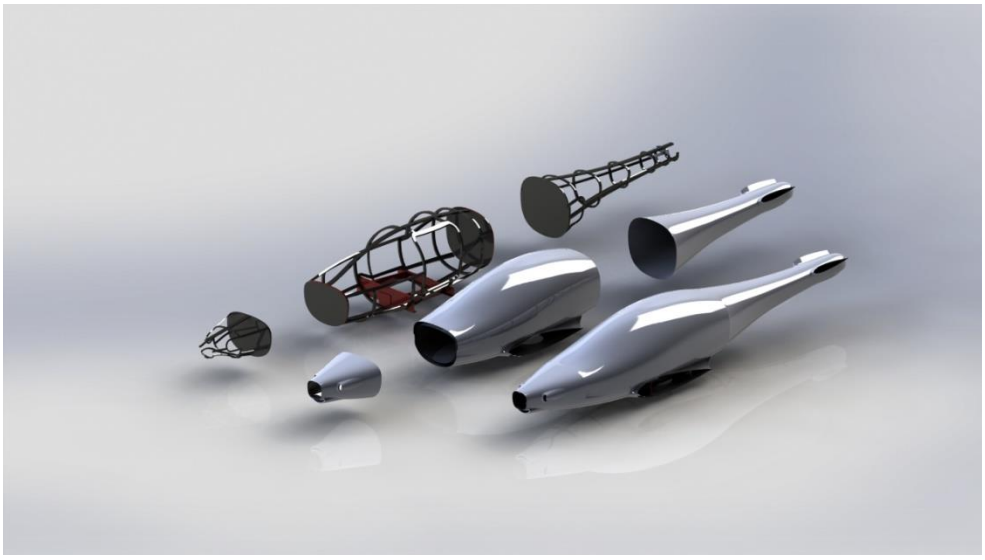

Figure 55: Fuselage manufacturing

10. Weight Sizing Class II

A detailed weight and balance analysis was performed for the final design iteration on the aircraft. The equations used were taken from Roskam's Aircraft Design Series Part V, Section 5. Cessna, USAF and Torenbeek methods were used and the most reasonable value was chosen. The results are shown in Table (23).

Table 23: Weight sizing class II

No	Component	Four-Seater	Six-Seater
1	Wing	295	295
2	V-tail	81	81
3	Fuselage	238	238
4	Landing Gear		
	Main	76	76
	Nose	22	22
5	Engine	184	184
	Propellers	23	23
	Fuel System	45	45
6	Motors		
	Nose	31	31
	Tips	2x16	2x16
7	Generator	38	38
8	Batteries	202	158
9	Fixed Equipment		
	Flight Controls	157	157
	Electrical System / Avionics	118	118
	Air Conditioning and Anti-ice	30	30
	Furnishings	81	81
10	Fuel	283	223
11	Passengers	344	516
12	Cargo	55	82
	TOTAL	2335	2398

Based on the detailed component weights shown in the previous table, the values were added to the CAD model by placing components such as cargo and systems where it can facilitate the weight and balance analysis. For each configuration, the CG was adjusted along with wing placement to achieve the best cruise static margin shown in figure (59). Different load cases were considered and CG excursion diagram was developed and trim analysis was performed. The details of these steps are the next section.

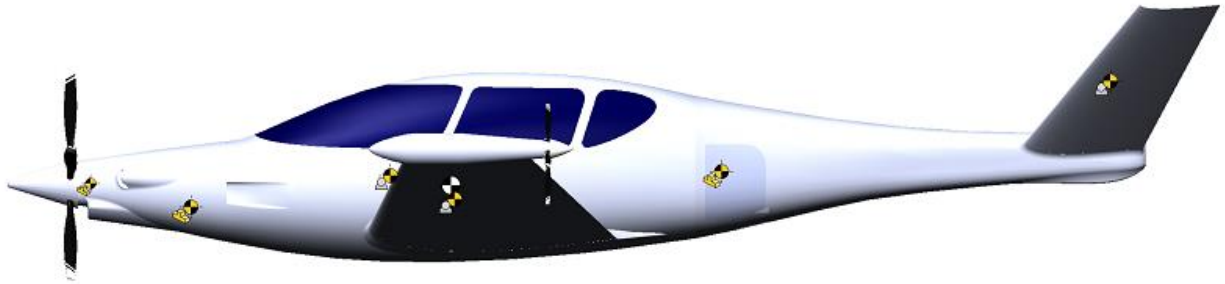

Figure 56: Aircraft CG and component placement

11. Stability and Control

Stability analysis is a pivoting step in the aircraft design process as it confirms and feeds back the sizing placement of all the components and surfaces. The results of this process determine what design parameters to be fixed and what to be changed. It is the check condition of the design loop.

The following analyses are performed on the main two variants of the *hy*BIRD family, the hB600 and hB400, at cruise conditions. The third variant, hB400-Extended range, was found to always exhibit characteristics falling between the other two members. Although, more critical conditions might take place during flight segments other than cruise, cruise analysis is thought to suffice for the scoop of this report. Other flight segments could be tested for stability following the same approaches as the following cruise analyses.

11.1 Static Stability

For our category of aircraft, inherent stability is required without reliance on a feedback control system. To achieve this, a Static Margin (SM) must ensure that the aircraft's Neutral Point NP is well aft the Centre of Gravity CG position in the X-direction along the aircraft's symmetry axis. A minimum value for the SM of 10% is required at all loading cases according to Roskam for our class. Before calculating the SM, a CG-travel diagram was calculated and plotted for different loading conditions Figure (60).

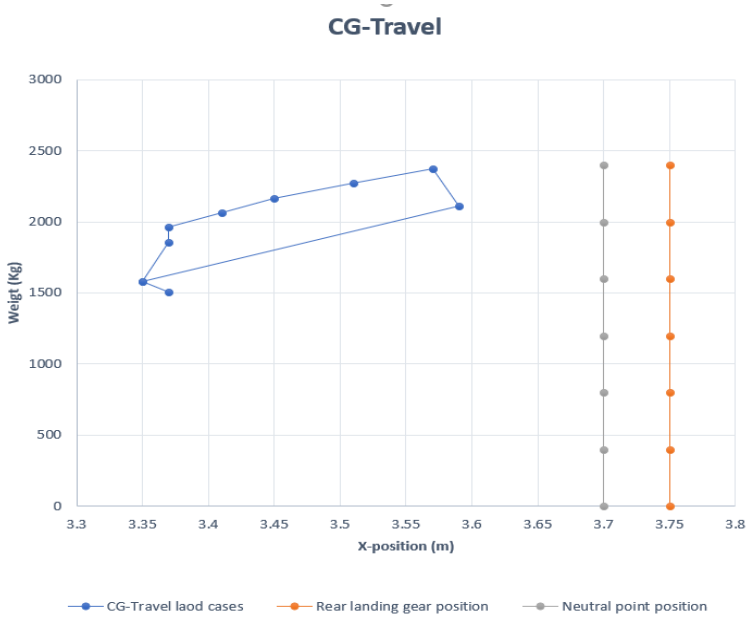

Figure 57: CG excursion diagram

The position of the main landing gear was adjusted according to the maximum aft CG position so that the CG falls always between the front and rear gears.

To calculate the NP position, Mark Drela's open source vortex lattice software, AVL, was used. The geometry of aircraft's wing and tail including the control surfaces was input. The aircraft total mass and CG position was provided as well. The NP was calculated and the SM was found to be 10.5% and 17.2% for hB600 and hB400 respectively. This means the 4-seater variant is more longitudinally stable. But both SM's are adequate for this class of aircraft. It's not so small that the aircraft is susceptible to instability and not too stable to be smoothly controlled.

11.2 Trim Analysis

The same software was used for trim analysis in cruise case. AVL calculates the required C_L at cruise from weight, which is equal to the lift at cruise, and the cruise speed. The Angle of Attack AOA required to achieve that C_L is obtained as well as the elevator deflection required to ensure zero Pitching Moment PM. The results were 1.78 and -0.13 degrees for alpha and delta respectively for hB600. The small trim angles are thanks to the incidence angles of these surfaces which were optimized for the airplane to fly on minimum drag configuration during cruise. An incidence of one degree at the tail and 0.5 at the wing are offset. The trim angles for hB400 are 1.67 and -0.52 degrees for alpha and delta respectively.

Figure (61) demonstrates the lift force per local chord generated in the lifting surfaces.

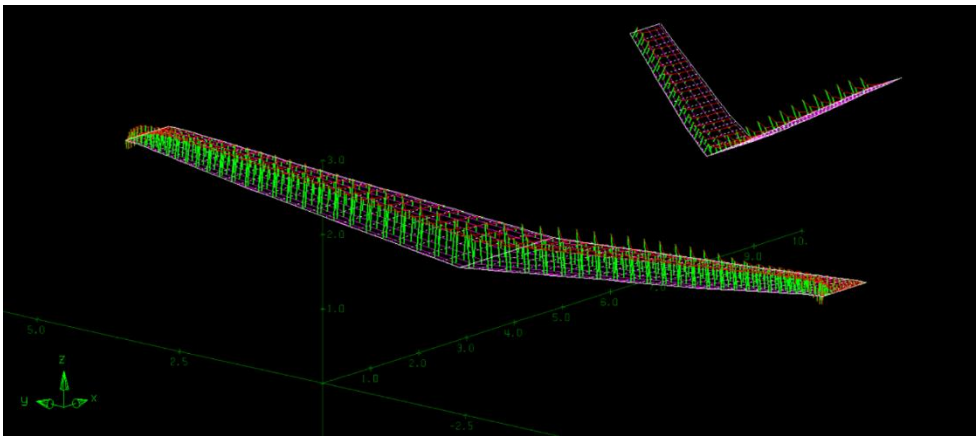

Figure 58: Wing and tail loading at cruise for hB600

Trefftz plot in Figure (62) shows the coefficient of lift distribution and downwash as a function of the span.

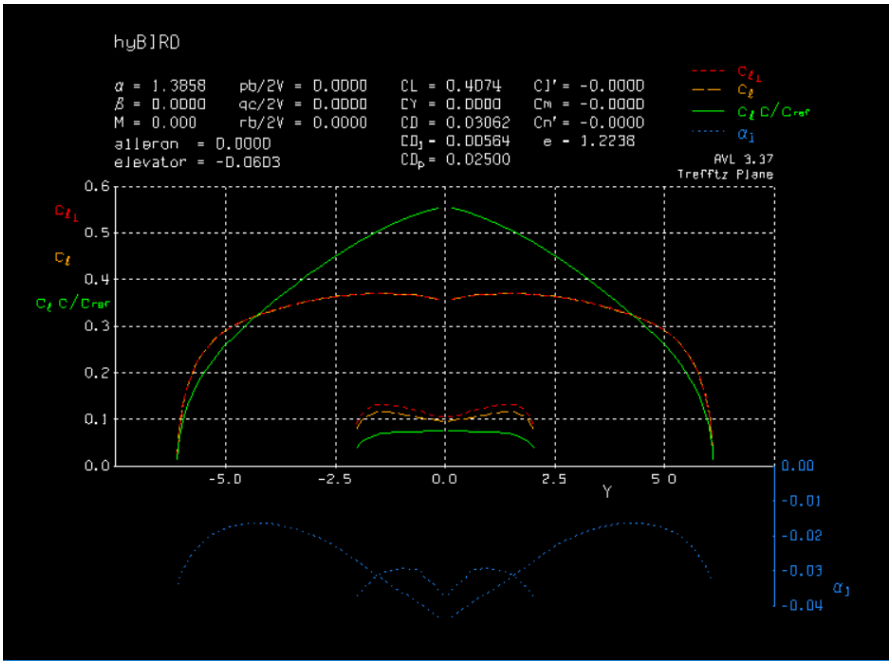

Figure 59: Trefftz plot for cruise condition for hB600

11.3 Longitudinal Stability

As demonstrated by the center of gravity excursion diagram and the stated static margins, the aircraft is longitudinally stable under all load cases possible. AVL was used for calculating the stability derivatives as well. Table (24) indicates the values of the critical longitudinal derivatives as well as their desired values for stability. The analysis was done for the two variants; the four and six-seater during cruise.

Table 24: Longitudinal stability derivatives

Stability derivative	hB600	hB400	Requirement
$C_{L\,\alpha}$	6.0	5.983	(around 2*pi)
$C_{m\,\alpha}$	-0.613	-1.00	-0.6 < $C_{m\,\alpha}$ < -1.0 for GA aircraft
$C_{L\,q}$	9.15	10.38	-
$C_{m\,q}$	-16.6	-18.52	-
$C_{L\,\delta_e}$	0.773	0.687	-
$C_{m\,\delta_e}$	-2.46	-2.23	-

It is desired that the aircraft attain Level I handling qualities - defined on the Cooper-Harper scale as, "excellent, highly desirable," with pilot compensation not a factor for desired performance. The requirements to achieve this for

long and short-period longitudinal motion are shown in Table (25 & 26). These values are the values required for our class of aircraft and category of missions.

Table 25: Phugoid Mode flying qualities

Phugoid Mode (Long Period)	
Level 1	$\zeta > 0.04$
Level 2	$\zeta > 0$
Level 3	Unstable, Time-to-double $T_2 > 55$ seconds

Table 26 : SP Mode flying qualities

Short period Mode	
Level 1	$0.3 < \zeta < 2.0$
Level 2	$0.2 < \zeta < 2.0$
Level 3	$0.15 < \zeta$

AVL introduced a challenge in defining the V-tail and the Ruddervator control surface. The software couldn't use the same control surface (Ruddervator) to trim the Pitch and Yaw Moment at the same time. To overcome this problem, the area projection approach, introduced before in Roskam [15], was used to convert the V-tail into conventional horizontal and vertical surfaces. The same goes for the control surfaces. This approach was verified to be correct by comparing the results of both configurations in longitudinal stability derivatives and found to produce the exactly the same output with error less than 0.7% in all stability and control derivatives. The methodology was also reviewed and confirmed by professor Haitham Taha, professor of flight mechanics and control at UCLA.

The results of the eigenmode analysis in the longitudinal plane along with their respective flying quality level are tabulated in Tables (27 & 28).

Table 27: Phugoid eigenmode results

Phugoid Mode (Long Period)		
Variant	ζ	Level
hB600	0.0063	2
hB400	0.027	$2 \rightarrow 1$

Table 28: SP eigenmode results

Short period Mode		
Variant	ζ	Level
hB600	0.62	1
hB400	0.53	1

The longitudinal dynamics consist of the short-period and the phugoid or long period mode. The phugoid mode is a lightly damped, long-period oscillation in pitch of the aircraft that results in the vehicle constantly exchanging airspeed for altitude (alternatively, potential energy for kinetic) and then altitude for airspeed. On the other hand, the short-period mode is typically a highly damped, short period oscillation in angle of attack in response to a sudden pitch input or perturbation. The results of the eigenvalues show that both variants meet the level 1 flying qualities

criteria in the short period mode while the phugoid mode is down to level 2. hB400 show better damping for long period mode though, almost approaching level 1 flying quality.

11.4 Lateral Stability

Lateral stability derivatives for both airplanes during cruise are presented in Table (29).

Table 29: Lateral stability derivatives

Stability derivative	hB600	hB400	Requirement
$C_{Y\,\beta}$	-0.466	-0.465	-
$C_{L\beta}$	-0.183	-0.182	<0
$C_{N\beta}$	0.175	0.178	>0
C_{Yp}	-0.182	-0.185	-
C_{Lp}	-0.723	-0.724	-
C_{Np}	-0.026	-0.022	-
C_{Yr}	0.433	0.440	-
CL_r	0.170	0.170	>0
C_{Nr}	-0.179	-0.186	<0
$C_{Y\,\delta\,aileron}$	-0.057	-0.057	-
$C_{L\,\delta\,aileron}$	-0.286	-0.286	-
$C_{N\,\delta\,aileron}$	0.0046	-0.0034	-
$C_{Y\,\delta\,rudder}$	-0.343	-0.343	-
$C_{L\,\delta\,rudder}$	-0.0476	-0.0458	-
$C_{N\,\delta\,rudder}$	0.160	0.172	-

The three modes to look for in lateral analysis are the Roll, Spiral and Dutch Roll modes. The roll mode presents the system's short-term response to the pilot's roll command or aileron deflection. If the damping ration for that mode is high, this indicates abrupt and sudden response while lower damping means smoother transition, which is preferred by passengers for comfort. Like the phugoid mode capturing the long-term response due to pitch angle, spiral mode is the long-term response for a bank angle. Most aircraft trimmed for straight-and-level flight, if flown stick-fixed, will eventually develop a tightening spiral-dive, which means the wings will return to a level bank angle if displaced or disturbed. Otherwise, the bank angle will diverge away into a higher and higher bank angle.

Finally, Dutch roll may be described as a yaw and roll to the right, followed by a recovery towards the equilibrium condition, then an overshooting of this condition and a yaw and roll to the left, and so on. This undesirable motion causes passengers discomfort and nausea. Due the coupling between roll and yaw, this mode is common to be found naturally unstable and thus most aircraft install special-purpose automatic pilot that damps out any yawing oscillation by applying rudder corrections. The flying quality levels and requirements for these modes are shown below in Table (30). Table 30: Lateral modes flying qualities

Roll Mode Time Constant			
Level 1	<1.4 s		
Level 2	<3 s		
Level 3	<10 s		
Spiral Mode Time to Double			
Level 1	>20 s		
Level 2	>12 s		
Level 3	>4 s		
Dutch Roll Mode			
	ζ_{min}	$(\zeta\omega_n)_{min}$	$\omega_{n_{min}}$
Level 1	0.08	0.15	0.4
Level 2	0.02	0.05	0.4
Level 3	0.02	-	0.4

The results of the two hyBIRD family members in cruise condition show level 1 for roll and spiral stability qualities and level 2 for the dutch roll. Although the stability caracteristics of both variants are very close to each other, the 4-seater show slightly better damping and higher stability performance in most of the dynamic modes.

Table 31: Lateral eigenmodes results

Roll Mode Time Constant				
Variants	Time const		Level	
hB600	0.55		1	
hB400	0.58		1	
Spiral Mode Time to Double				
Variant	Time to Double		Level	
hB600	131		1	
hB400	154		1	
Dutch Roll Mode				
Variants	ζ	$(\zeta\omega_n)$	ω_n	Level
hB600	0.03	0.05	1.583	2
hB400	0.0333	0.0054	1.627	2

11.5 Stability Augmentation System (SAS)

Although many airplanes have level two flying qualities specially for these two modes; Dutch Roll and Phugoid, and although designing a controller fro the aircraft is beyond the scoop of this report, a stability augmentation system was designed to enhance the flying qualities at all flying modes to become level 1 and to further mature the design and take it more step closer to implementation.

To design a stability augmentation system for these two modes, an approximation for the state space at these modes is used. A two by two system matrix ("A" matrix) for each state is obtained from the elements of the original full nine by nine system matrix. These selected elements and these resulting system matrices were found to be dominent at each of these modes and were found to well represent the behavioural flight dynamics of the aircraft with acceptable accuracy. These approximations result from first decoupling the full nine by nine system into a four by four longitudenal system and a five by five lateral system and then further decoupling or approximating each of these systems to get a two by two system for each flying mode. This analysis and these decoupled matrices can be found in [27] and are presented below.

For the phugoid or long period mode, the approximated state space matrices are

$$\begin{pmatrix} \Delta\dot{u} \\ \dot{\theta} \end{pmatrix} = \underbrace{\begin{bmatrix} X_u & -g \\ -\frac{Z_u}{u_0} & 0 \end{bmatrix}}_{\boldsymbol{A}_{lp}} \begin{pmatrix} \Delta u \\ \theta \end{pmatrix} + \underbrace{\begin{bmatrix} X_{\delta_e} & X_{\delta_T} \\ -\frac{Z_{\delta_e}}{u_0} & -\frac{Z_{\delta_T}}{u_0} \end{bmatrix}}_{\boldsymbol{B}_{lp}} \begin{pmatrix} \Delta\delta_e \\ \Delta\delta_T \end{pmatrix}$$

For our system, the numerical values for these matrices were obtained (using AVL) and presented below.

```
A_ph = [-0.0108 -9.81; 0.0015 0];
B_ph = [-0.001429; -0.2652];
```

Note that the second column of the B matrix was ignored since the given steady-state flight condition at cruise does not require the determination of the control derivatives with respect to a thrust input.

Now the desired values for $\boldsymbol{\zeta}$ and $\boldsymbol{\omega_n}$ that ensure level one flying quality were calculated. A reasonable safety factor was implemented to account for the error in the state space approximations above. In other words, the min $\boldsymbol{\zeta}$ required for achieving a level 1 flying quality at the Phugoid mode for instance is 0.04, but in our design, we shoot

for a 0.5 damping ratio. This is chosen carefully to account for the error in the state space approximation as mentioned before, which could be as high as 20% for this mode, and also not so high to cause stiffness or decrease performance or controlability.

Using this analysis, the state feedback control law was designed and the resulting gains are tabulated below.

K_α	**-4.866e-4**
K_q	-0.4155

These valuse for the gains indicate that the system is near the desired state and only such small gains are required to ensure better flying qualities. They also indicate that the pitch rate feedback gain is much more important in this case than the AOA gain, in fact, the pitch rate gain might be sufficient for conrolling this mode.

Similarly for the Dutch Roll mode, the state space is;

$$\begin{pmatrix} \dot{v} \\ \dot{r} \end{pmatrix} = \underbrace{\begin{bmatrix} Y_v & Y_r - u_0 \\ N'_v & N'_r \end{bmatrix}}_{\boldsymbol{A}_{DR}} \begin{pmatrix} v \\ r \end{pmatrix} + \underbrace{\begin{bmatrix} Y_{\delta_a} & Y_{\delta_r} \\ N'_{\delta_a} & N'_{\delta_r} \end{bmatrix}}_{\boldsymbol{B}_{DR}} \begin{pmatrix} \delta_a \\ \delta_r \end{pmatrix}$$

And the numerical valuse for our design were;

```
A_DR = [-0.1012 -101.4062; 0.0203 -0.115];
B_DR = [-0.1377; 0.03445];
```

Finally the resulting gains are presented below.

K_β	**0.5566**
K_r	18.59

This analysis and control augmentation system preliminary designs were performed for the 6-seater variant aircraft only, which was found to be the less stable one as well. The same analysis could be easily done for the 4-seater and even smaller gain values would be expected.

12. Subsystems Design

The *hy*BIRD family was designed to incorporate both hybrid-electric propulsion and electric subsystems to result in a more efficient and eco-friendly aircraft. Moreover, all the subsystems of *hy*BIRD are electrically driven, which means there's no on-board hydraulic system. This was found to reduce weight, maintenance, and eliminate contamination problems as recommended by the reference [26] and this was also proven through Boeing 787 Dreamliner.

12.1 Electrical System

The electrical system has a general scheme as shown is figure (63).

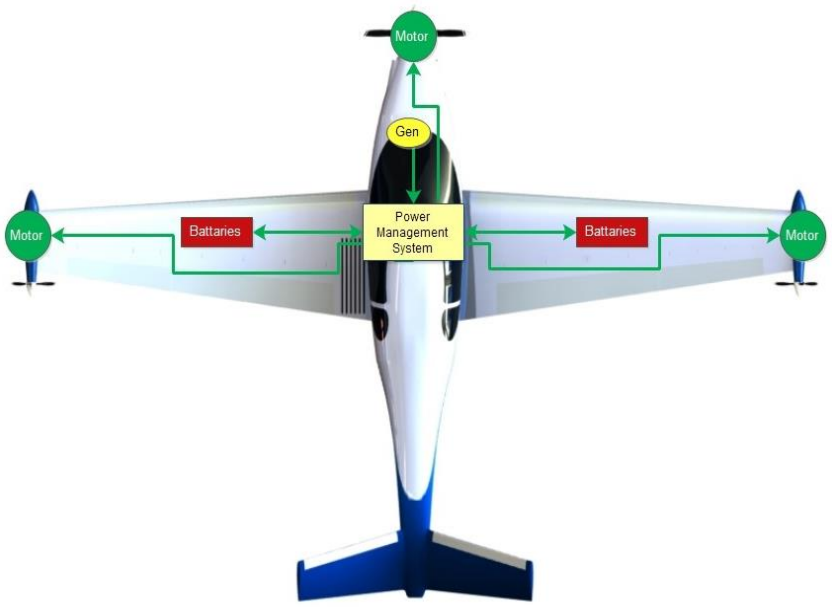

Figure 60:Electrical System General Scheme

Power management system is responsible for managing the power between batteries, the generator and the electrical loads of the aircraft including motors, actuators and flight instrumentations. Based on the future forecast of the LIB technology mentioned above, we will need a battery pack with the following properties:

Table 32 - Battery Specs

Property	Value		Unit
	4-Seater	6-Seater	
Capacity	62,400	80,800	Wh
Density	2.75		Kg/L
Volume	0.05673	0.07345	m^3

The battery pack is divided into modules that are parallelly connected to increase the redundancy of the system.

12.2 Thermal Management System (TMS)

Battery Thermal Management System: If the temperature of the LIB goes too high, this can lead to loss of battery capacity, power fade and thermal runaway in some extreme cases. On the other hand, if it's too cold, this results in higher resistance, lower efficiency and decreased available capacity and can also cause lithium plating which can cause accelerated degradation and failure of the cell. Thermal management system provides a balance between degradation and performance and ensures safe operations. We are using cylindrical LIB since they are easy to manufacture and has better mechanical stability. We are using surface cooling to keep the temperature of the LIB controlled since tap cooling is more expensive and more complex to manufacture. Cooling happens through the flow of the liquid of water glycol through a pipe that goes in between the battery cells as shown in figure (64).

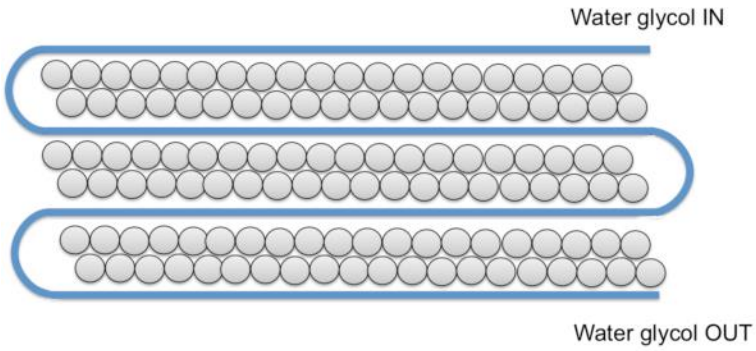

Figure 61: Battery cooling system

ICE Engine and Electric Motor Thermal Management: Heat dissipation from the three electric motors (main and tip-motors) is achieved through two ways; conductive cooling and forced air cooling. The latter is done by utilizing the accelerating air flow to cool the motors, where the first is achieved through a mounting interface between the electric motor and the machine structure so that the heat can dissipate into the machine structure through that mounting interface. Cooling of the ICE engine is achieved through forced air cooling too. The aircraft nose was designed to force the cooling air to flow inside the engine cowl and cool both the ICE engine and the e-motor as illustrated in the following figure.

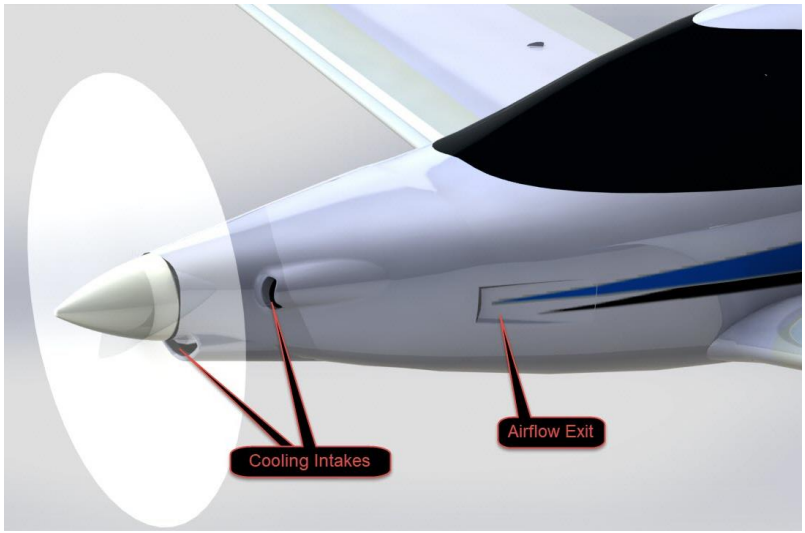

Figure 62: Engine compartment cooling mechanism

12.3 Environmental Control System

The environmental control system comprises temperature, humidity, oxygen level control of the cabin and the anti/de-icing systems.

The temperature and humidity control are provided through a fully-automatic climate control system. Conditioned air is supplied by a vapor cycle air conditioning system which utilizes an engine-driven compressor, in conjunction with condenser and evaporator units installed inside the tail cone. The control unit has temperature, humidity and oxygen sensors side by side with a control panel in the cockpit allowing the pilot to select the desired cabin temperature which will be automatically maintained. If the system detects a low level of oxygen in the cabin, the onboard pressurized oxygen tanks will supply the air with enough oxygen to maintain the comfort of the passengers.

In order to combat the ice buildup during flights, the wings and tail will need a de-icing system. For a piston engine aircraft, neither bleed air can be extracted from the engine operation such as the jet engine nor the piston engine exhaust will be sufficient for the wing and tail leading edge warming up. The thermal heaters will extensively consume power which will be against the MOI of the aircraft subsystems. Instead, the aircraft will use Electro-Expulsive Separation System (EESS) system for the wings and tail leading edges. The EESS uses electrical current to generate opposing magnetic fields to accelerate two layers of elastomers apart which would break any layer of ice. According

to Leonard Haslim of NASA's Ames; "it can remove layers of ice thin as frost or thick as an inch of glaze. The ice, shredded into small particles, is too small to harm aircraft components, including jet engines. It uses one-thousandth the power and is one-tenth the weight of Electro-Thermal Ice Removal Systems used to-day". A diagram showing how the EESS works can be seen in the figure below.

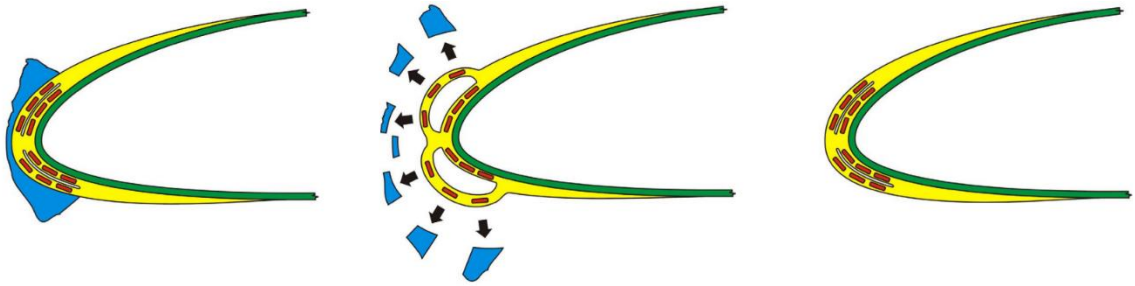

Figure 63: Electro-Thermal Ice Removal System work principle

The aircraft propeller ice buildup at low RPMs produces distortion to the airfoil shape, unbalance in the props and destructive vibrations. The inner and the middle third parts of the airfoil need to be de-iced by using thermal heaters because of the smaller volume available and the ease of fitting without affecting the airfoil shape of the propeller which will decrease the efficiency.

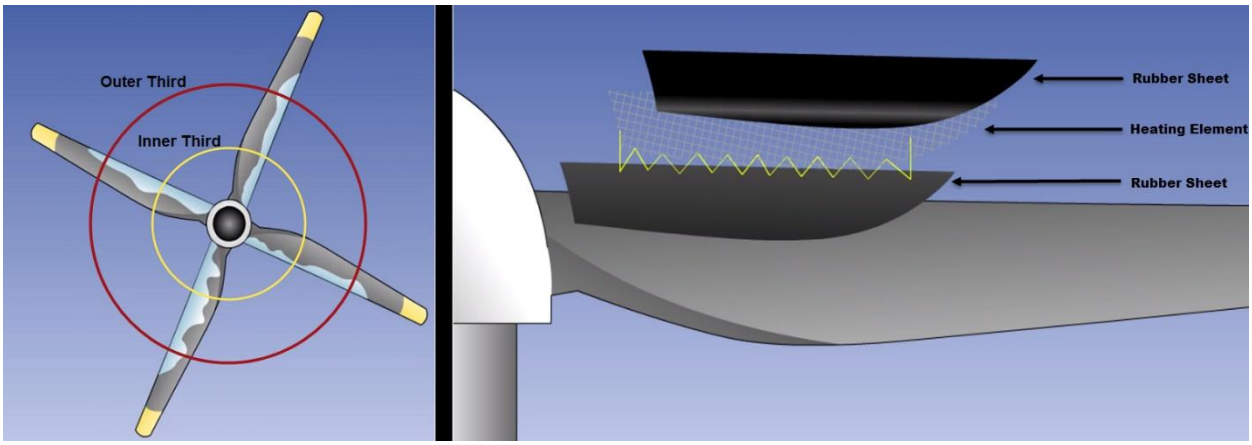

Figure 64: Thermal heaters for props de-icing

12.4 Fuel System

The fuel system has the objectives of fuel storage, delivery to the engine and altering the CG for the aircraft in flight. Both aircraft have wing integral tanks of capacity of 240 liters each and a central fuel hopper allowing the crossflow between tanks to help adjust the center of gravity in flight. The hB400 is equipped with aft cabin fuel tank to accommodate for the 60 liters increase in the fuel quantity needed for the extended range. A high-level overview

of the fuel subsystem is presented in figure (68). The fuel lines shall be located away from the easily damaged regions and shut off valves must be provided to increase the safety. Reliability is achieved through redundancy by having a backup pump in case of any failure of the main pump in each tank. For refueling, gravity refueling ports are located on top of each wing to directly fill the wing tanks and if the pressure is available, the central tank will be refueled in hB400; if not, the central fuel hopper will push enough fuel to the aft cabin tank during refueling procedure.

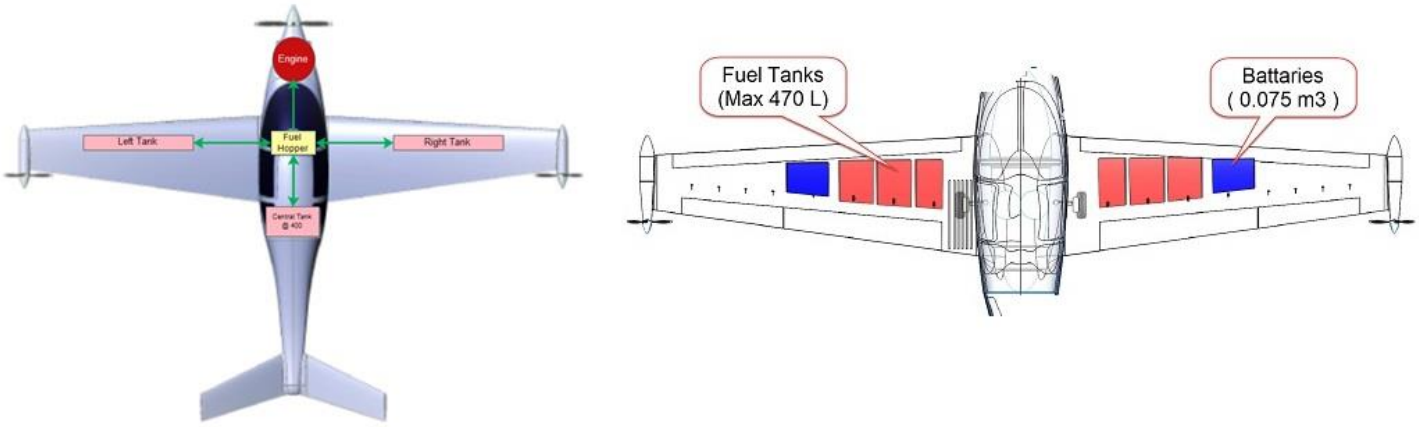

Figure 65: Fuel subsystem

12.5 Safety

Special attention has been paid to the safety of our aircraft, the *hy*BIRD aircraft family features a full-airframe parachute rescue system, which is specially developed so it can be deployed at both low and high speeds as well as low altitudes. The parachute is part of standard equipment; the set of features and equipment available for all *hy*BIRD variants. It is anchored to the fuselage in four points, engine compartment main frame, aft cabin and both wings-fuselage connections, which helps the airplane to descend at the neutral attitude once the parachute is deployed. The parachute can be deployed by using the emergency handle available in the back of the upper head panel which allows the pilot to trigger it easily in case of mid-air collision, water landing or emergency landing in rough terrain.

Figure 66: Parachute deployed

The parachute straps are completely hidden inside the bracing roll bar to keep the aerodynamic efficiency as high as possible and is designed to be repairable and not to cause any harm to the main structure of the airplane. The right-side emergency door contributes to the safety of the aircraft by providing additional exit for the four passengers in the aft cabin section to ease the evacuation procedure in case of emergency landing.

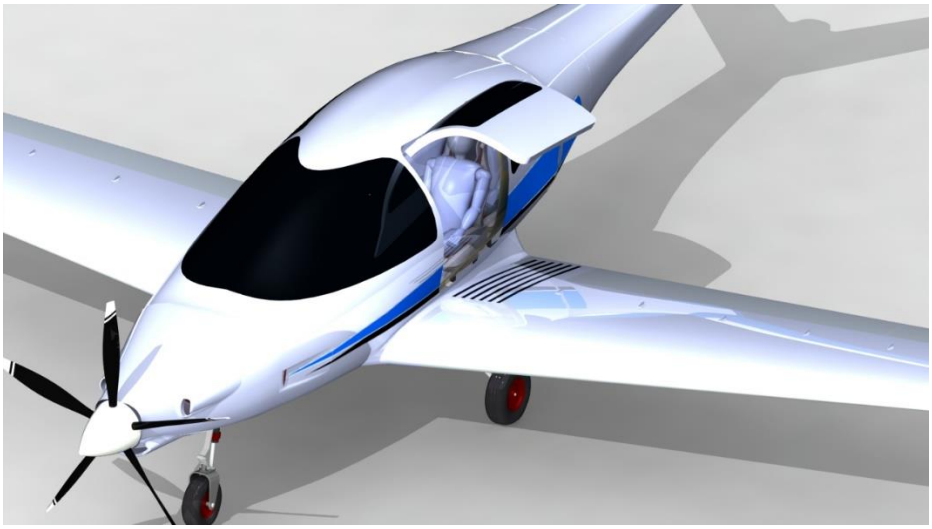

Figure 67: Side door

Another safety feature is present in the redundancy of the propulsion system which can be shown in the following figure.

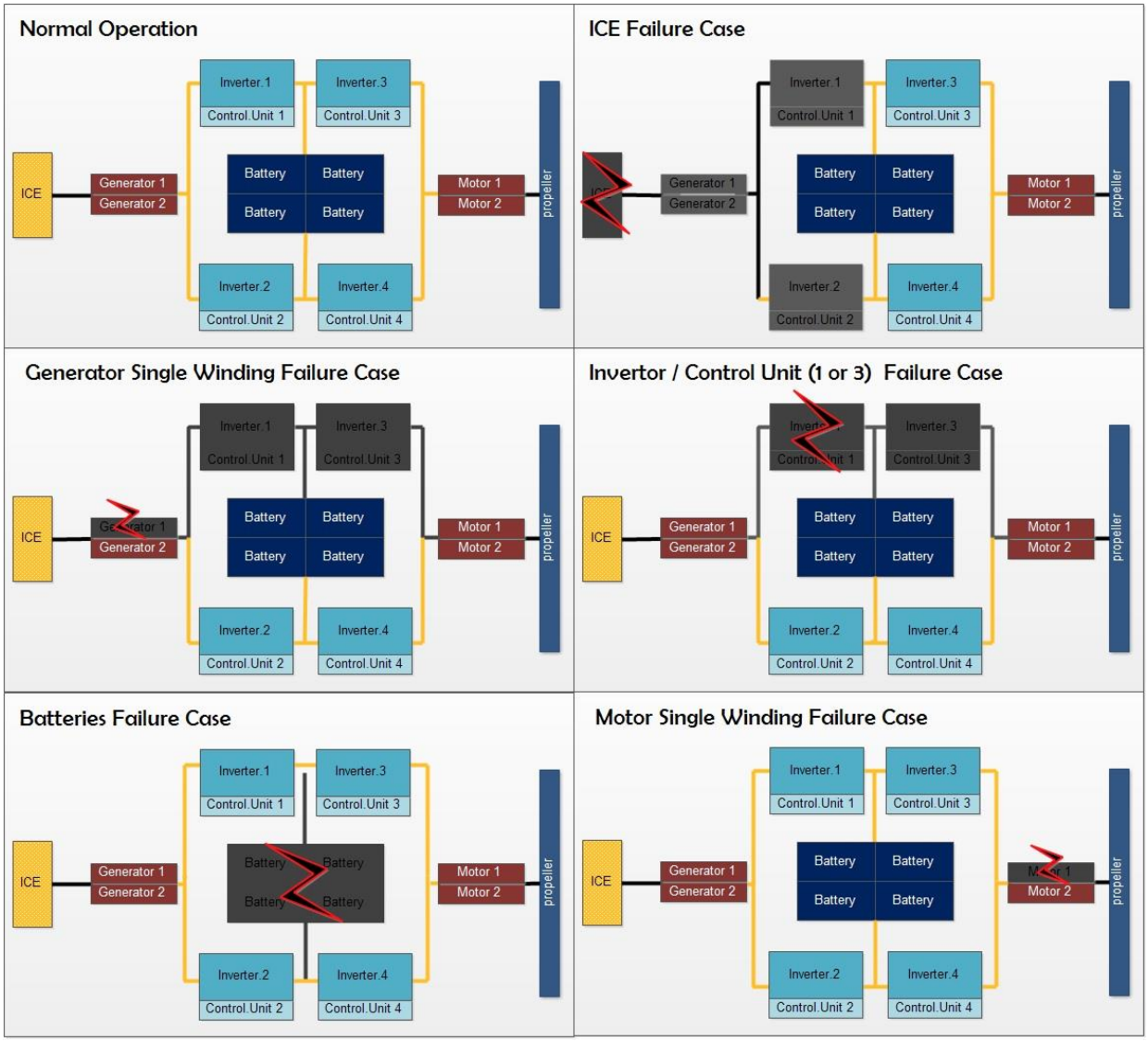

Figure 68: Propulsion system redundancy and safety scheme

The malfunctioning of any component of the powertrain system can by overcome and the operation of the aircraft will continue safely until landing.

In case of primary and auxiliary power subsystems failure, commercial aircraft uses the ram air turbine RAT which generates power from the airstream by the ram pressure due to the speed of the aircraft. This approach lacks the reliability, efficiency and is expensive to maintain. This is replaced in the *hy*BIRD aircraft by using the variable pitch tip motors as generators in case of emergency which can be led by the variable pitch of the propellers and wing vortices which drives the generators side by side with the ram pressure of air stream.

The exterior lights of *hy*BIRD aircraft will be outfitted with position, anti-collision, taxi, and landing lights. These lights will be arranged and operated in accordance with 14 CFR 91.209. A general layout of the required lights for the aircraft can be seen in the below figure and a rendering of the hB600 with the lights can be seen in figure (72)

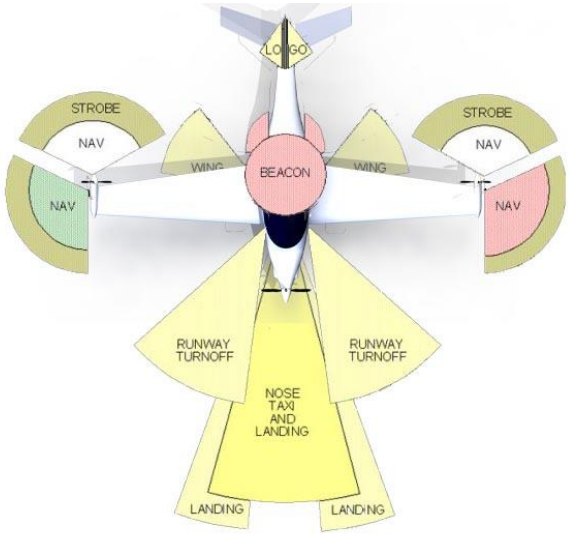

Figure 69: Aircraft lighting layout

13. Interior Design

13.1 Cockpit/Flight Deck Design

The ultimate sensation, simplicity and outside visibility is the design goal of the instrumental panel of the *hy*BIRD family. The cockpit was designed with emphasis on following FAR 23 pilot visibility and enhancing the outside view more by using only one central pillar between the pilots. In this way, the visibility forward and sideward is free of obstacles which greatly increases the safety of the flight.

The IFR Instrumental panel consists of three different functional areas, the upper back-up area, the PFD/MFD area and the communication stack. The avionics were selected to be Garmin G500 series PFD/MFD synthetic vision screen with GTN series touch-screen Flight Management System.

The Garmin GHD 2100 head up display will be used to provide critical flight information, including synthetic vision, from taxi to landing while also allowing pilots to keep their eyes outside the aircraft. Moreover, the fully integrated modular cockpit provides all traffic, weather alerts, transponder and 3D audio-panel which took the polit's attention via different audio and visual alarms (terrain, stall, overspeed, engine issues, etc.). All these systems are integrated to enhance the pilot's experience and ensure the highest level of safety on board

Figure 70: The Garmin GHD 2100 Display

Figure 71: hyBIRD Cockpit Design and CAD model


Headup Display
PFD
Backup Instruments
Autopilot
SFD
Speakers
Landing Gear
Environment Control
Aircraft systems
Displays Control
Lights Panel
Side Sticks
Communications
Rudder Pedals
Engines Control
Throttle
Flaps

13.2 Cabin Options

We offer five different options for *hy*BIRD 400, normal and extended range versions, interior design.

1. **Basic Economy Layout:** it's the basic layout for both hB400 and hB600. It has four forward-facing seats including the pilot's seat and enough convenient ample legroom. It has leather seats and each screen has its LED TV screen and outlet to be used by passengers to power their personal electronic devices.

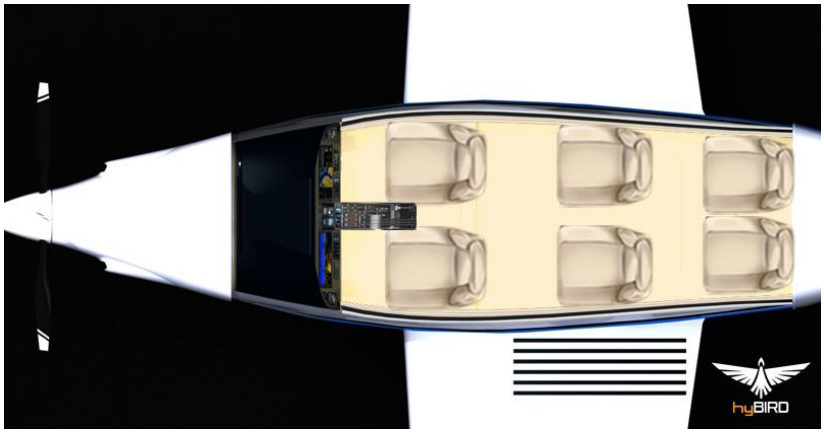

Figure 72: Basic Economic Layout

2. **Executive Layout:** we have an executive version only for hB400. It has four seats; two cabin seats and the other two seats are almost facing each other, one at each side of the cabin so we have enough space to add some luxurious features like wider LED TV screens and a small projector screen at one side of the cabin.

Figure 73: Executive Layout

3. **Medical Layout:** it features almost the same base as the utility layout with more tie-downs, built-in cabinets and counter space for the medical equipment and more importantly a built-in medical cot for patient transport.

Figure 74: Medical Layout

4. **Utility Layout:** this can be customized as per the request and the application. It can be used for fast delivery in urgent situations, etc.

Figure 75: Utility Layout


hyBIRD

14. Cost Analysis

We used the Eastlake model developed by Professor Charles Eastlake at the Embry-Riddle Aeronautical University which is a modified version of the development and procurement co*sts of aircraft known as DAPCA-IV [20] developed by RAND corporation to fit the GA aircraft. DAPCA-IV is a method that uses only some basic information about the aircraft like its empty weight and maximum airspeed to establish some special cost estimating relationships (CERs). Assuming we will be able to produce and deliver an average of 40 airplanes per year based on the historical data provided in the 2016 General Aviation Statistical Outlook by the General Aviation Manufacturers Association (GAMA) [21]. It is worth mentioning that the Eastlake model for calculating the development and operational costs takes into account some factors like the certification program, the complexity of the flap system, the ratio of the of the composite to non-composite materials in the aircraft, the pressurization, the wing tapering and the average labor rate and its projected consumer price index (CPI) in 2028 as the entry in service (EIS).

14.1 Development Costs

The Eastlake model utilizes the knowledge of only two main basic parameters; the empty weight of the aircraft and the maximum airspeed along with applying correction factors such as the certification factor, complex flap, composites, etc. And another important parameter called the Quantity Discount Factor (QDF) which depends on the experience effectiveness adjustment factor. If the experience increases that means the productivity of the engineer and the technician would increase too. QDF can be calculated using the following formula: $QDF = (F_{EXP})^{1.447*lnN}$

Which means that the development costs decrease exponentially with increasing the QDF. Where F_{EXP} is the experience effectiveness and was assumed to be 95% as per the Eastlake model and N is the number of units produced in a specific period which we took to be 5 years. Another challenge we faced is that the Eastlake model was first developed in 1986 and to project the resulted costs on 2028, we had to apply the consumer price index (CPI) which we took to be 1.4 as per the Bureau of Labor Statistics. The development costs mainly include the cost to certify the aircraft which is the fixed part and the cost of manufacturing and quality control which is the variable part. The costs to certify the aircraft include the costs of engineering, development support, flight test operations and tooling.

$$C_{CERT} = C_{ENG} + C_{DEV} + C_{FT} + C_{TOOL}$$

Where the variables costs include the costs of manufacturing labor, quality control, materials, power plant and the avionics.

$$C_{VAR} = C_{MFG} + C_{QC} + C_{MAT} + C_{PP} + C_{AV}$$

The total development cost of the aircraft then becomes:

$$C_{TOT} = C_{CERT} + C_{VAR} + C_{INS}$$

Where, C_{INS} is the manufacturer's liability insurance cost. *hy*BIRD will need to deliver a total of 119 units either from the 6-seater or the 4-seater model to reach the break-even point and start making profit which means the revenue is more than the total expenses. That means we will be making profit after around two years and 10 months.

$$N_{BE} = \frac{total\ fixed\ cost}{unit\ sales\ price - unit\ variable\ cost} = 209\ (4\ seater)\ or\ 212\ (6\ seater)$$

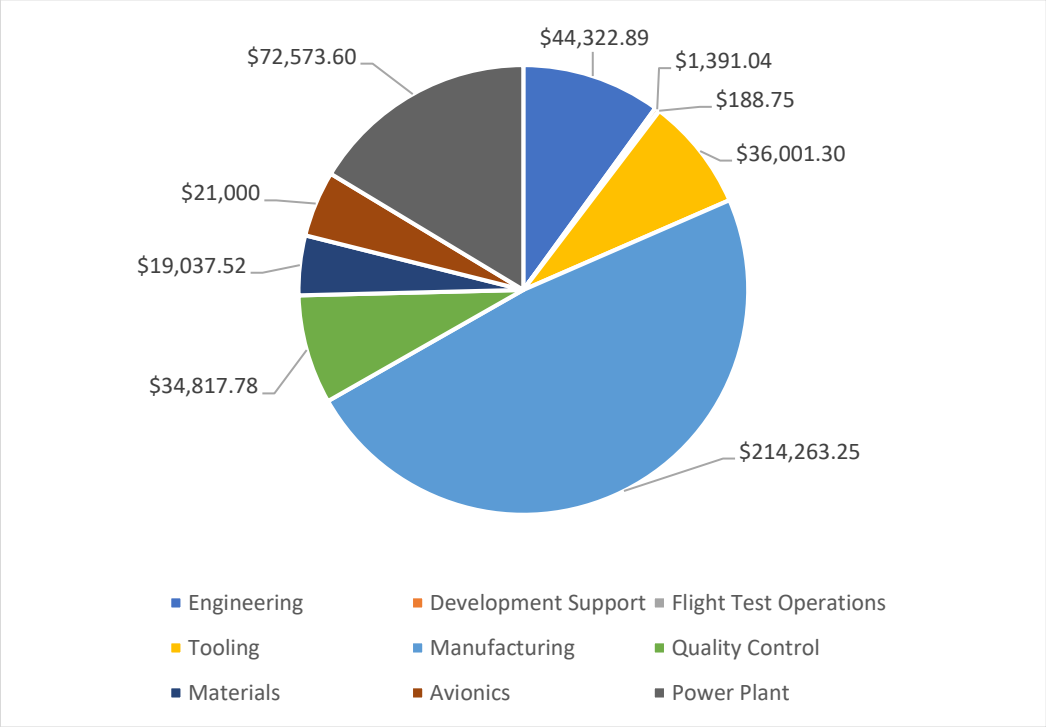

Figure 76:hyBIRD Development Cost

Table 33 - hyBIRD Development Cost

Description	Parameter	Value		Unit
		4 Seats	6 Seats	
Number of planned aircraft produced over 5 years	N	480	480	units
Engineering Man-hours	Heng	43,067	46,230	hrs.
Number of Tooling Man-hours	HTOOL	55,787	59,740	hrs.
Number of Manufacturing Labor Man-hours	HMFG	434,967	464,789	hrs.
Average time to manufacture a single unit	tAC	906	968	hrs.
Number of engineers to develop the aircraft over a year	NENG	22	24	
Total Cost of Engineering	CENG	11,631,449	12,485,847	$
Total Cost of Development Support	CDEV	288,145	311,592	$
Total Cost of Flight Test Operations	CFT	34,024	37,751	$
Total Cost of Tooling	CTOOL	9,990,047	10,697,959	$
Total Cost to Certify (fixed cost)	CCERT	21,943,664	23,533,149	$
Total Cost of Manufacturing	CMFG	67,676,476	72,316,451	$
Total Cost of Quality Control	CQC	12,317,119	13,161,594	$
Total Cost of Materials	CMAT	7,160,662	7,616,716	$
Cost of Avionics	Cavio	10,080,000	10,080,000	$
Cost of Power Plant (engines, propellers)	CPP	3,9062,208	39,062,208	$
Total cost to produce per aircraft	Caircraft	329,667	345,354	$
Manufacturing Liability Insurance	12%.Caircrat	59,340	64,164	$
Minimum selling price of the unit		390,000	410,000	$

The price of the aircraft decreases with the increase in the number of units being produced. It's expected that, in case that *hy*BIRD 400 success in the market, the production rate will increase gradually with years so that after 5 years the cost of the aircraft would decrease from $330,000 to around $287,000 which means the profit will increase from 18% in the first production year to 36% in the fifth production year, assuming that the production rate would be increasing by one airplane per month starting from the second production year.

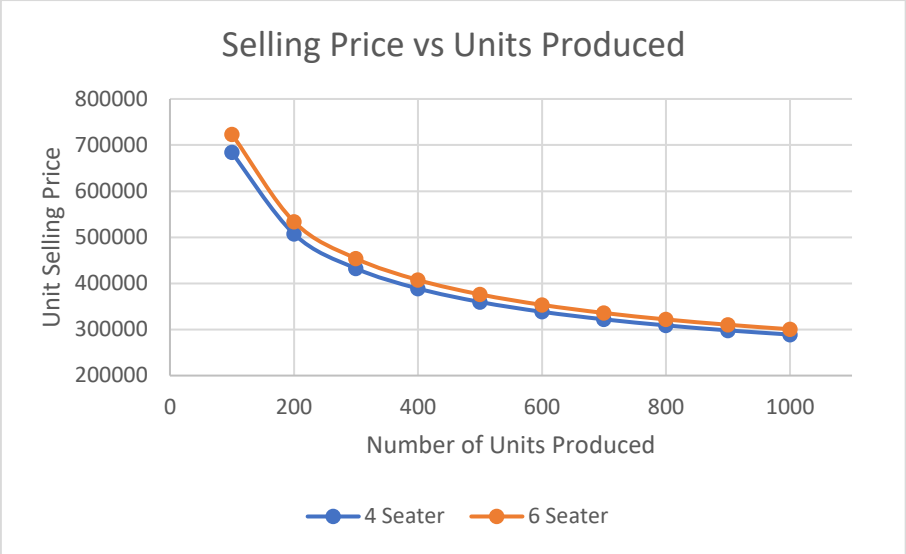

Figure 77: Selling Price vs Units Produced

14.2 Operational Cost

Attracting customers to pick our aircraft from all the other available choices in the market requires us to market the point that we are not only producing an aircraft that is cheaper and more efficient than its competitive of the same category, but it can also be shown that *hy*BIRD has lower operational cost than most of the other GA aircraft. Calculating the cost of ownership which is the amount of money that's required to own and operate the aircraft, it can be shown that *hy*BIRD is a wise and smart choice. The operational cost is calculated based on some primary inputs like the total flight hours per year, projected cost of fuel and the amount of insurance coverage. Assuming that the owner is a pilot which in turn doesn't incur any additional cost for a flight crew. Operational costs include the storage cost, annual inspections cost and the cost on the engine overhaul bank. It's important to note that the operational costs are calculated based on the fact that the buyer of the aircraft didn't acquire any loan to buy our aircraft, so he doesn't have to make a pay a monthly installment to pay back the loan. In case of loans, the operational cost of the airplane would double.

Table. 34 hyBIRD Operational Cost

Description	Parameter	Value		Unit
		4 Seats	6 Seats	
Number of flight hours per year	Q_{FLGT}	300	300	hrs.
Annual Maintenance Cost	C_{AP}	12,600	12,600	$/year
Annual Storage Cost	C_{STOR}	4,200	4,200	$/year
Annual Fuel Cost	C_{FUEL}	21,504	21,504	$/year
Annual Insurance Cost	C_{INS}	8,669	9,058	$/year
Engine Overhaul Fund	C_{OVER}	2,100	2,100	$/year
Annual Inspection Cost	C_{INSP}	700	700	$/year
Annual Loan Payment	C_{LOAN}	0	0	$/year
Total Yearly Cost per aircraft	C_{YEAR}	49,264	49,617	$/year
Cost per Flight Hour	C_{HR}	164.2	165.4	$

As shown from Table (34) that the operational cost of both *hy*BIRD 400 and *hy*BIRD 600 is almost the same and that's due to the commonality of the aircraft assuming that both aircraft fly 300 hours per year which is a reasonable number of hours as per the history of GA. As shown in figure.7, most of the operational cost will still go to the fuel which is supposed to decrease dramatically with the degree of hybridization as long as the cost of kWh of the batteries decreases.

.

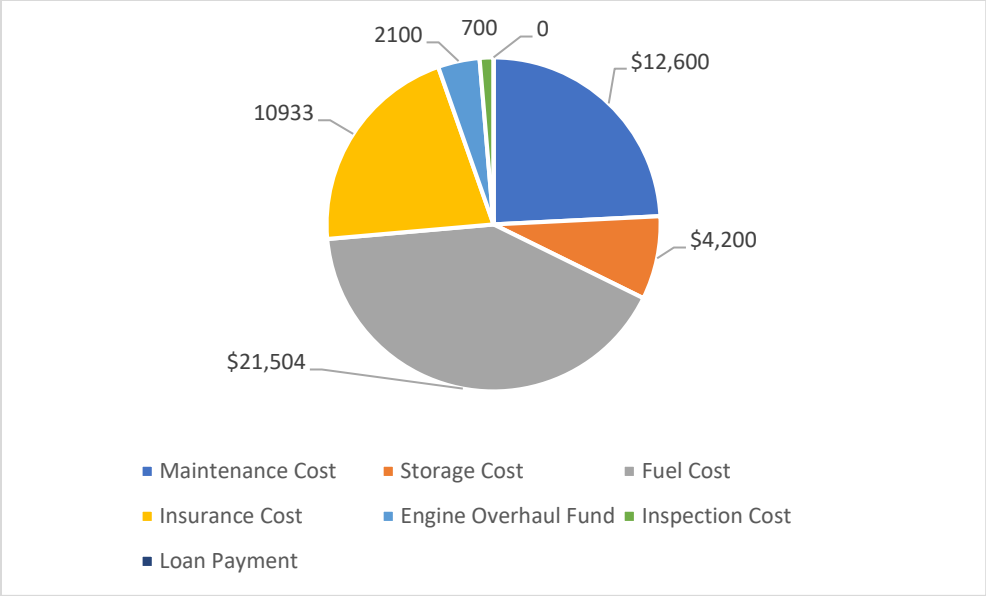

78. hyBIRD Operational Cost Analysis

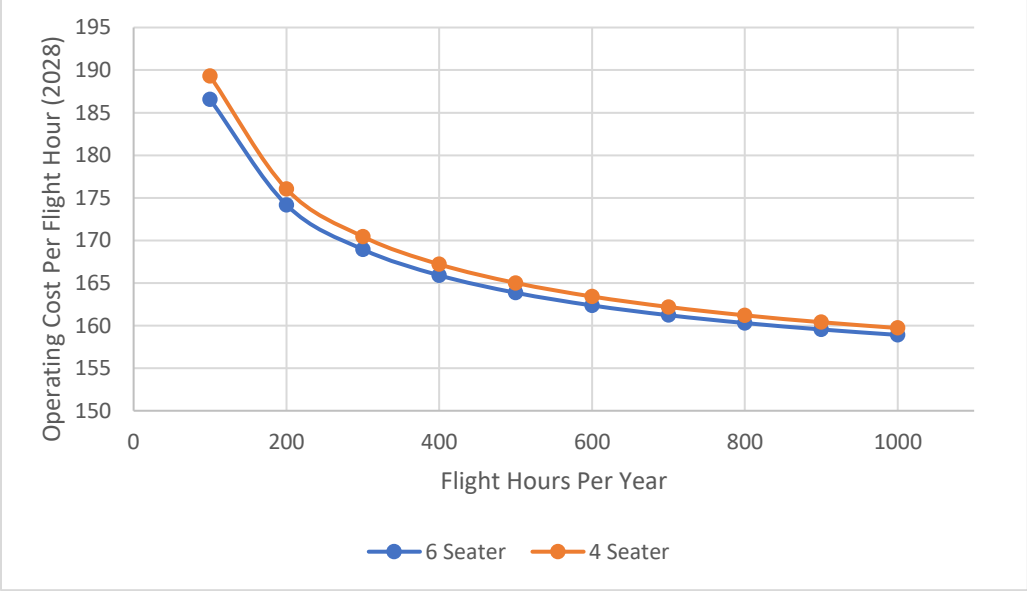

79. hyBIRD Operational Cost over Years

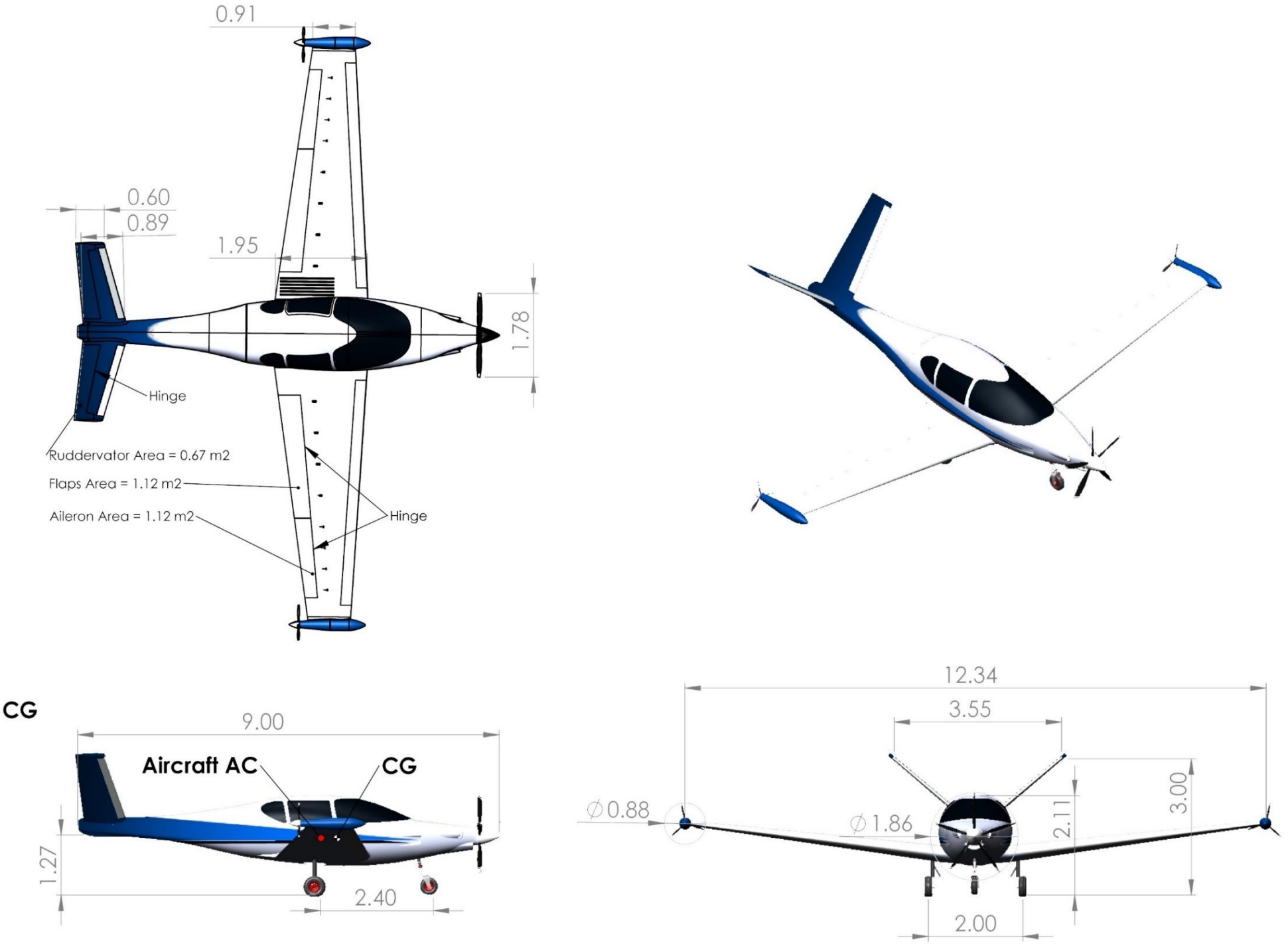

Figure 80 - hyBIRD 3-views drawing

15. References

1) Abdel-Hafez, A. (2012). Power Generation and Distribution System for a More Electric Aircraft - A Review . Recent Advances in Aircraft Technology.

2) (2016). Alpha Electro Technical Data. Pipistrel.si.

3) Barrett, R. (19933). An Experimental Evaluation of Smart Tetrahedral Vortex Generators,. Lawrence KS: University of Kansas.

4) Concept of Modular Architecture for Hybrid Electric Propulsion of Aircraft. (2017). Retrieved from mahepa: https://mahepa.eu/wp-content/uploads/2017/12/D1.1-Concept-of-Modular-Architecture-fro-Hybrid-Electric-Propulsion-of-Aircraft.pdf

5) G.Rippl, M. (2012). Sizing Analysis for Aircraft Hybrid Electric Propulsion Systems. Department of The Air Force Air University .

6) Glassock, R., Galea, M., Williams, W., & Glesk, T. (2017). Hybrid Electric Aircraft Propulsion Case Study for Skydiving Mission. Aerospace 2017, 4(3), 45.

7) Goraj, Z. (2004). An Overview of the De-Icing and Anti-Icing Technologies With Prospects for The Future. Warsaw: Warsaw University of Technology.

8) Jr, A., & D, J. (New York). 'Elements of Airplane Performance' Introduction to Flight, 7 th ed . McGraw Hill.

9) Masson, P. J., Tixader, P., & Luongo, C. A. (n.d.).

10) Masson, P. J., Tixador, P., & Loungo, C. A. (2007). Saftey Torque Generation in HTS Propulsion Motor for General Aviation Aircraft. IEEE Transaction on Applies superconductivity , Vol.17, no. . 1619-1622.

11) Nelson, R. C. (1989). Flight Stability and Automatic Control. McGraw-Hill: General aviation book.

12) Olsen, J., & Page, J. (2014). Hybrid Powertrain for Light Aircraft. International Journal of Sustainable Aviation (IJSA).

13) Paerson, J. (1987). Evaluation of Installed Performance of a Wingtip Mountented Pusher Turpoprop. Hampton: NASA Reseach Center.

14) Roskam, J. (1985). Airplane Design Part I: Preliminary Sizing of Aircraf. Lawrence KS: DARcorporation.

15) Roskam, J. (1985). Airplane Design Part V: Component Weight Estimation. Lawrence KS: DARcorporation.

16) T. Nam, D. S. (2005 Paper 2005-818). Power Based Sizing Method for Aircraft Consuming Unconventional Energy. AIAA.

17) Torenbeek, E. (2013). Advanced Aircraft Analysis: Conceptual design, Analysis and Optimization of Subsonic Civil Airplanes. Delft: A John Wiley & Sons, Ltd.

18) Turbo Normalizing. (n.d.). Retrieved from westernskyways: http://www.westernskyways.com/turbonormalized_cessna.asp

19) Wyczisk, H., & Zeumer, C. (2016). Hypstair - Aystem Architecture, Certifiability and Safety Sspects. Stuttgart: Siemens.

20) Hess, R. W., and H. P. Romanoff. Aircraft Airframe Cost Estimating Relationships. R-3255-AF, RAND Corporation, December 1987.

21) 2016 General Aviation Statistical Databook & 2017 Industry Outlook. (2016). Washington DC: General Aviation Manufacturers Association (GAMA).

22) "Undergraduate Team Aircraft Design – Hybrid-Electric General Aviation Aircraft (HEGAA)." AIAA: The American Institute of Aeronautics and Astronautics, [www.aiaa.org/2018UndergradTeamAircraftDesign–HEGAA/]

23) HYPSTAIR – System Architecture, Certifiability and Safety Aspects, Symposium E²-Fliegen 2016, Stuttgart

24) "Bloomberg New Energy Finance | Bloomberg Impact Report." Bloomberg.com, Bloomberg, www.bloomberg.com/impact/impact/bloomberg-new-energy-finance/.

25) "Cessna 310R Specifications, Cabin Dimensions, Speed - Cessna." GlobalAir.com, www.globalair.com/aircraft-for-sale/Specifications?specid=1133.

26) A. Abdel-Hafez, "Power Generation and Distribution System for a More Electric Aircraft - A Review," Recent Advances in Aircraft Technology, vol. InTech, no. ISBN: 978-965-51-0150-5, 2012.

27) R. C. Nelson. Flight Stability and Automatic Control. McGraw-Hill, 1989.

28) The Handbook of Lithium-Ion Battery Pack Design: Chemistry, Components, Types and Terminology. Chapter 16. Page 212

ABOUT THIS WORK

With the recent development of battery technology and electric motors, many industries are shifting towards depending more on the renewable energy resources. As we see most of the automotive manufacturers are electrifying their vehicles, aircraft manufacturers are also following up and developping their electric airplanes nowadays. This report presents a design concept of a Hybrid - Electric general aviation family of aircraft in response to the mission requirements of the AIAA international design competition 2018 and as a fulfillment for the senior year capstone project of the Aerospace Engineering major at the University of Science and Technology at Zewail city - Egypt.

AUTHORS

AHMED A. HASHEM
AHMED S. ELBERMBALI
AMR M. MOUSA
WESSAM A. ZEID